



Universiteit Gent  
Faculteit Wetenschappen  
Vakgroep Fysica en Sterrenkunde

<sup>2</sup> No title yet

<sup>3</sup> No sub-title neither, obviously...

---

<sup>4</sup> Alexis Fagot

5



Thesis to obtain the degree of  
Doctor of Philosophy in Physics  
Academic years 2012-2017





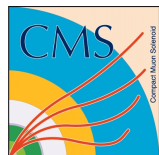


Universiteit Gent  
Faculteit Wetenschappen  
Vakgroep Fysica en Sterrenkunde

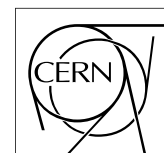
Promotoren: Dr. Michael Tytgat  
Prof. Dr. Dirk Ryckbosch

Universiteit Gent  
Faculteit Wetenschappen  
Vakgroep Fysica en Sterrenkunde  
Proeftuinstraat 86, B-9000 Gent, België  
Tel.: +32 9 264.65.28  
Fax.: +32 9 264.66.97

17



Thesis to obtain the degree of  
Doctor of Philosophy in Physics  
Academic years 2012-2017





## Acknowledgements

<sup>19</sup> Ici on remerciera tous les gens que j'ai pu croiser durant cette aventure et qui m'ont permis de passer  
<sup>20</sup> un bon moment

<sup>21</sup> *Gent, ici la super date de la mort qui tue de la fin d'écriture*  
<sup>22</sup> *Alexis Fagot*



# Table of Contents

24	<b>Acknowledgements</b>	i
25	<b>Nederlandse samenvatting</b>	xvii
26	<b>English summary</b>	xix
27	<b>1 Introduction</b>	1-1
28	1.1 A story of High Energy Physics . . . . .	1-1
29	1.2 Organisation of this study . . . . .	1-1
30	<b>2 Investigating the TeV scale</b>	2-1
31	2.1 The Standard Model of Particle Physics . . . . .	2-1
32	2.2 The Large Hadron Collider and the Compact Muon Solenoid . . . . .	2-1
33	2.3 Muon Phase-II Upgrade . . . . .	2-1
34	<b>3 Amplification processes in gaseous detectors</b>	3-1
35	3.1 Signal formation . . . . .	3-1
36	3.2 Gas transport parameters . . . . .	3-1
37	<b>4 Resistive Plate Chambers</b>	4-1
38	4.1 Principle . . . . .	4-1
39	4.2 Rate capability of Resistive Plate Chambers . . . . .	4-1
40	4.3 High time resolution . . . . .	4-1
41	4.4 Resistive Plate Chambers at CMS . . . . .	4-1
42	4.4.1 Overview . . . . .	4-1
43	4.4.2 The present RPC system . . . . .	4-2
44	4.4.3 Pulse processing of CMS RPCs . . . . .	4-3
45	<b>5 Longevity studies and Consolidation of the present CMS RPC subsystem</b>	5-1
46	5.1 Testing detectors under extreme conditions . . . . .	5-1
47	5.1.1 The Gamma Irradiation Facilities . . . . .	5-3
48	5.1.1.1 GIF . . . . .	5-3
49	5.1.1.2 GIF++ . . . . .	5-5
50	5.2 Preliminary tests at GIF . . . . .	5-7
51	5.2.1 Resistive Plate Chamber test setup . . . . .	5-7
52	5.2.2 Data Acquisition . . . . .	5-9
53	5.2.3 Geometrical acceptance of the setup layout to cosmic muons . . . . .	5-9
54	5.2.3.1 Description of the simulation layout . . . . .	5-10
55	5.2.3.2 Simulation procedure . . . . .	5-12
56	5.2.3.3 Results . . . . .	5-13
57	5.2.4 Photon flux at GIF . . . . .	5-13

---

58	5.2.4.1	Expectations from simulations . . . . .	5-13
59	5.2.4.2	Dose measurements . . . . .	5-18
60	5.2.5	Results and discussions . . . . .	5-19
61	5.3	Longevity tests at GIF++ . . . . .	5-20
62	5.3.1	Description of the Data Acquisition . . . . .	5-23
63	5.3.2	RPC current, environmental and operation parameter monitoring . . . . .	5-24
64	5.3.3	Measurement procedure . . . . .	5-25
65	5.3.4	Longevity studies results . . . . .	5-25
66	<b>6</b>	<b>Investigation on high rate RPCs</b>	<b>6-1</b>
67	6.1	Rate limitations and ageing of RPCs . . . . .	6-1
68	6.1.1	Low resistivity electrodes . . . . .	6-1
69	6.1.2	Low noise front-end electronics . . . . .	6-1
70	6.2	Construction of prototypes . . . . .	6-1
71	6.3	Results and discussions . . . . .	6-1
72	<b>7</b>	<b>Conclusions and outlooks</b>	<b>7-1</b>
73	7.1	Conclusions . . . . .	7-1
74	7.2	Outlooks . . . . .	7-1
75	<b>A</b>	<b>A data acquisition software for CAEN VME TDCs</b>	<b>A-1</b>
76	A.1	GIF++ DAQ file tree . . . . .	A-1
77	A.2	Usage of the DAQ . . . . .	A-2
78	A.3	Description of the readout setup . . . . .	A-3
79	A.4	Data read-out . . . . .	A-3
80	A.4.1	V1190A TDCs . . . . .	A-4
81	A.4.2	DataReader . . . . .	A-6
82	A.4.3	Data quality flag . . . . .	A-10
83	A.5	Communications . . . . .	A-12
84	A.5.1	V1718 USB Bridge . . . . .	A-13
85	A.5.2	Configuration file . . . . .	A-13
86	A.5.3	WebDCS/DAQ intercommunication . . . . .	A-17
87	A.5.4	Example of inter-process communication cycle . . . . .	A-18
88	A.6	Software export . . . . .	A-18
89	<b>B</b>	<b>Details on the offline analysis package</b>	<b>B-1</b>
90	B.1	GIF++ Offline Analysis file tree . . . . .	B-1
91	B.2	Usage of the Offline Analysis . . . . .	B-2
92	B.2.1	Output of the offline tool . . . . .	B-3
93	B.2.1.1	ROOT file . . . . .	B-3
94	B.2.1.2	CSV files . . . . .	B-5
95	B.3	Analysis inputs and information handling . . . . .	B-6
96	B.3.1	Dimensions file and IniFile parser . . . . .	B-6
97	B.3.2	TDC to RPC link file and Mapping . . . . .	B-7
98	B.4	Description of GIF++ setup within the Offline Analysis tool . . . . .	B-8
99	B.4.1	RPC objects . . . . .	B-9
100	B.4.2	Trolley objects . . . . .	B-9
101	B.4.3	Infrastructure object . . . . .	B-10
102	B.5	Handeling of data . . . . .	B-12
103	B.5.1	RPC hits . . . . .	B-12

104	B.5.2 Clusters of hits . . . . .	B-13
105	B.6 Analysis . . . . .	B-15
106	B.6.1 Determination of the run type . . . . .	B-15
107	B.6.2 Beam time window calculation for efficiency runs . . . . .	B-16
108	B.6.3 Data loop and histogram filling . . . . .	B-17
109	<b>C Structure of the hybrid simulation software</b>	<b>C-1</b>
110	C.1 Introduction . . . . .	C-1



# List of Figures

111

112	2.1	Absorbed dose in the CMS cavern after an integrated luminosity of 3000 fb. R is the transverse distance from the beamline and Z is the distance along the beamline from the Interaction Point at Z=0. . . . .	2-2
113	2.2	A quadrant of the muon system, showing DTs (yellow), RPCs (light blue), and CSCs (green). The locations of new forward muon detectors for Phase-II are contained within the dashed box and indicated in red for GEM stations (ME0, GE1/1, and GE2/1) and dark blue for improved RPC (iRPC) stations (RE3/1 and RE4/1). . . . .	2-2
114	2.3	RMS of the multiple scattering displacement as a function of muon $p_T$ for the proposed forward muon stations. All of the electromagnetic processes such as bremsstrahlung and magnetic field effect are included in the simulation. . . . .	2-3
115	4.1	Signals from the RPC strips are shaped by the FEE described on Figure 4.1a. Output LVDS signals are then read-out by a TDC module connected to a computer or converted into NIM and sent to scalers. Figure 4.1b describes how these converted signals are put in coincidence with the trigger. . . . .	4-3
116	4.2	Description of the principle of a CFD. A comparison of threshold triggering (left) and constant fraction triggering (right) is shown in Figure 4.2a. Constant fraction triggering is obtained thanks to zero-crossing technique as explained in Figure 4.2b. The signal arriving at the input of the CFD is split into three components. A first one is delayed and connected to the inverting input of a first comparator. A second component is connected to the noninverting input of this first comparator. A third component is connected to the noninverting input of another comparator along with a threshold value connected to the inverting input. Finally, the output of both comparators is fed through an AND gate. . . . .	4-4
117	5.1	(5.1a) Extrapolation from 2016 data of single hit rate per unit area in the barrel region. (5.1b) Extrapolation from 2016 data of single hit rate per unit area in the endcap region. . . . .	5-2
118	5.2	Background Fluka simulation compared to 2016 Data at $L = 10^{34} \text{ cm}^{-2} \cdot \text{s}^{-1}$ in the fourth endcap disk region. A mismatch in between simulation and data can be observed. [To be understood.] . . . . .	5-3
119	5.3	Layout of the test beam zone called X5c GIF at CERN. Photons from the radioactive source produce a sustained high rate of random hits over the whole area. The zone is surrounded by 8 m high and 80 cm thick concrete walls. Access is possible through three entry points. Two access doors for personnel and one large gate for material. A crane allows installation of heavy equipment in the area. . . . .	5-4
120	5.4	$^{137}\text{Cs}$ decays by $\beta^-$ emission to the ground state of $^{137}\text{Ba}$ (BR = 5.64%) and via the 662 keV isomeric level of $^{137}\text{Ba}$ (BR = 94.36%) whose half-life is 2.55 min. . . . .	5-5

148	5.5	Floor plan of the GIF++ facility. When the facility downstream of the GIF++ takes electron beam, a beam pipe is installed along the beam line (z-axis). The irradiator can be displaced laterally (its center moves from $x = 0.65$ m to 2.15 m), to increase the distance to the beam pipe. . . . .	5-5
149	5.6	Simulated unattenuated current of photons in the xz plane (Figure 5.6a) and yz plane (Figure 5.6b) through the source at $x = 0.65$ m and $y = 0$ m. With angular correction filters, the current of 662 keV photons is made uniform in xy planes. . . . .	5-6
150	5.7	Description of the RPC setup. Dimensions are given in mm. A tent containing RPCs is placed at 1720 mm from the source container. The source is situated in the center of the container. RE-4-2-BARC-161 chamber is 160 mm inside the tent. This way, the distance between the source and the chambers plan is 2060 mm. Figure 5.7a provides a side view of the setup in the xz plane while Figure 5.7b shows a top view in the yz plane. . . . .	5-7
151	5.8	RE-4-2-BARC-161 chamber is inside the tent as described in Figure 5.7. In the top right, the two scintillators used as trigger can be seen. This trigger system has an inclination of 10° relative to horizontal and is placed above half-partition B2 of the RPCs. PMT electronics are shielded thanks to lead blocks placed in order to protect them without stopping photons from going through the scintillators and the chamber. . . . .	5-8
152	5.9	Hit distributions over all 3 partitions of RE-4-2-BARC-161 chamber is showed on these plots. Top, middle and bottom figures respectively correspond to partitions A, B, and C. These plots show that some events still occur in other half-partitions than B2, which corresponds to strips 49 to 64, in front of which the trigger is placed, contributing to the inefficiency of detection of cosmic muons. In the case of partitions A and C, the very low amount of data can be interpreted as noise. On the other hand, it is clear that a little portion of muons reach the half-partition B1, corresponding to strips 33 to 48. . . . .	5-9
153	5.10	Results are derived from data taken on half-partition B2 only. On the 18 <sup>th</sup> of June 2014, data has been taken on chamber RE-2-BARC-161 at building 904 (Prevessin Site) with cosmic muons providing us a reference efficiency plateau of $(97.54 \pm 0.15)\%$ represented by a black curve. A similar measurement has been done at GIF on the 21 <sup>st</sup> of July with the same chamber giving a plateau of $(78.52 \pm 0.94)\%$ represented by a red curve. . . . .	5-10
154	5.11	Representation of the layout used for the simulations of the test setup. The RPC is represented as a yellow trapezoid while the two scintillators as blue cuboids looking at the sky. A green plane corresponds to the muon generation plane within the simulation. Figure 5.7a shows a global view of the simulated setup. Figure 5.7b shows a zommed view that allows to see the 2 scintillators as well as the full RPC plane. . . . .	5-11
155	5.12	$\gamma$ flux $F(D)$ is plot using values from table 5.1. As expected, the plot shows similar attenuation behaviours with increasing distance for each absorption factors. . . . .	5-14
156	5.13	Figure 5.13a shows the linear approximation fit done via formulae 5.7 on data from table 5.2. Figure 5.13b shows a comparison of this model with the simulated flux using a and b given in figure 5.13a in formulae 5.4 and the reference value $D_0 = 50\text{cm}$ and the associated flux for each absorption factor $F_0^{ABS}$ from table 5.1 . . . . .	5-16
157	5.14	Dose measurements has been done in a plane corresponding to the tents front side. This plan is 1900 mm away from the source. As explained in the first chapter, a lens-shaped lead filter provides a uniform photon flux in the vertical plan orthogonal to the beam direction. If the second line of measured fluxes is not taken into account because of lower values due to experimental equipments in the way between the source and the tent, the uniformity of the flux is well showed by the results. . . . .	5-18
158			
159			
160			
161			
162			
163			
164			
165			
166			
167			
168			
169			
170			
171			
172			
173			
174			
175			
176			
177			
178			
179			
180			
181			
182			
183			
184			
185			
186			
187			
188			
189			
190			
191			
192			
193			
194			
195			
196			

---

197	5.15 . . . . .	5-19
198	5.16 Evolution of the maximum efficiency for RE2 (5.16a) and RE4 (5.16b) chambers 199 with increasing extrapolated $\gamma$ rate per unit area at working point. Both irradiated 200 (blue) and non irradiated (red) chambers are shown. . . . .	5-21
201	5.17 Evolution of the working point for RE2 (5.17a) and RE4 (5.17b) with increasing 202 extrapolated $\gamma$ rate per unit area at working point. Both irradiated (blue) and non 203 irradiated (red) chambers are shown. . . . .	5-21
204	5.18 Evolution of the maximum efficiency at HL-LHC conditions, i.e. a background hit 205 rate per unit area of 300 Hz/cm <sup>2</sup> , with increasing integrated charge for RE2 (5.18a) 206 and RE4 (5.18b) detectors. Both irradiated (blue) and non irradiated (red) chambers 207 are shown. The integrated charge for non irradiated detectors is recorded during test 208 beam periods and stays small with respect to the charge accumulated in irradiated 209 chambers. . . . .	5-22
210	5.19 Comparison of the efficiency sigmoid before (triangles) and after (circles) irradiation 211 for RE2 (5.19a) and RE4 (5.19b) detectors. Both irradiated (blue) and non irradiated 212 (red) chambers are shown. . . . .	5-22
213	5.20 Evolution of the Bakelite resistivity for RE2 (5.20a) and RE4 (5.20b) detectors. Both 214 irradiated (blue) and non irradiated (red) chambers are shown. . . . .	5-23
215	5.21 Evolution of the noise rate per unit area for the irradiated chamber RE2-2-BARC-9 216 only. . . . .	5-23
217	A.1 (A.1a) View of the front panel of a V1190A TDC module [10]. (A.1b) View of the 218 front panel of a V1718 Bridge module [11]. (A.1c) View of the front panel of a 6U 219 6021 VME crate [12]. . . . .	A-3
220	A.2 Module V1190A <i>Trigger Matching Mode</i> timing diagram [10]. . . . .	A-4
221	A.3 Structure of the ROOT output file generated by the DAQ. The 5 branches ( <code>EventNumber</code> , 222 <code>number_of_hits</code> , <code>Quality_flag</code> , <code>TDC_channel</code> and <code>TDC_TimeStamp</code> ) are visible on 223 the left panel of the ROOT browser. On the right panel is visible the histogram cor- 224 responding to the variable <code>nHits</code> . In this specific example, there were approximately 225 50k events recorded to measure the gamma irradiation rate on the detectors. Each 226 event is stored as a single entry in the <code>TTree</code> . . . . .	A-10
227	A.4 The effect of the quality flag is explained by presenting the content of <code>TBranch</code> 228 <code>number_of_hits</code> of a data file without <code>Quality_flag</code> in Figure A.4a and the con- 229 tent of the same <code>TBranch</code> for data corresponding to a <code>Quality_flag</code> where all TDCs 230 were labelled as <code>GOOD</code> in Figure A.4b taken with similar conditions. It can be noted 231 that the number of entries in Figure A.4b is slightly lower then in Figure A.4a due 232 to the excluded events. . . . .	A-12
233	A.5 Using the same data as previously showed in Figure A.4, the effect of the quality 234 flag is explained by presenting the reconstructed hit multiplicity of a data file with- 235 out <code>Quality_flag</code> in Figure A.5a and the reconstructed content of the same RPC 236 partition for data corresponding to a <code>Quality_flag</code> where all TDCs were labelled as 237 <code>GOOD</code> in Figure A.5b taken with similar conditions. The artificial high content of bin 238 0 is completely suppressed. . . . .	A-12
239	A.6 WebDCS DAQ scan page. On this page, shifters need to choose the type of scan 240 (Rate, Efficiency or Noise Reference scan), the gamma source configuration at the 241 moment of data taking, the beam configuration, and the trigger mode. These in- 242 formation will be stored in the DAQ ROOT output. Are also given the minimal 243 measurement time and waiting time after ramping up of the detectors is over before 244 starting the data acquisition. Then, the list of HV points to scan and the number of 245 triggers for each run of the scan are given in the table underneath. . . . .	A-14



## List of Tables

254

255	5.1	Total photon flux ( $E\gamma \leq 662$ keV) with statistical error predicted considering a	
256		$^{137}\text{Cs}$ activity of 740 GBq at different values of the distance $D$ to the source along	
257		the x-axis of irradiation field [6]. . . . .	5-13
258	5.2	Correction factor $c$ is computed thanks to formulae 5.5 taking as reference $D_0 =$	
259		50 cm and the associated flux $F_0^{ABS}$ for each absorption factor available in table 5.1. . . . .	5-15
260	5.3	The data at $D_0$ in 1997 is taken from [6]. In a second step, using Equations 5.8	
261		and 5.9, the flux at $D$ can be estimated in 1997. Then, taking into account the	
262		attenuation of the source activity, the flux at $D$ can be estimated at the time of the	
263		tests in GIF in 2014. Finally, assuming a sensitivity of the RPC to $\gamma$ $s = 2 \cdot 10^{-3}$ ,	
264		an estimation of the hit rate per unit area is obtained. . . . .	5-17
265	A.1	Inter-process communication cycles in between the webDCS and the DAQ through	
266		file string signals. . . . .	A-19



# List of Acronyms

267

268

## List of Acronyms

269

270

### A

271

272

273 AFL

Almost Full Level

274

275

### B

276

277

278 BARC

Bhabha Atomic Research Centre

279 BLT

Block Transfer

280 BR

Branching Ratio

281

282

### C

283

285 CAEN

Costruzioni Apparecchiature Elettroniche Nucleari S.p.A.

286 CERN

European Organization for Nuclear Research

287 CFD

Constant Fraction Discriminator

288 CMS

Compact Muon Solenoid

289 CSC

Cathode Strip Chamber

290

291

### D

292

293

294 DAQ

Data Acquisition

295 DCS

Detector Control Software

296 DQM

Data Quality Monitoring

297 DT

Drift Tube

298

299

### F

300

301

302	<b>FEE</b>	Front-End Electronics
303	<b>FEB</b>	Front-End Board
304		
305	<b>G</b>	
306		
307		
308	<b>GE-/-</b>	Find a good description
309	<b>GE1/1</b>	Find a good description
310	<b>GE2/1</b>	Find a good description
311	<b>GEANT</b>	GEometry ANd Tracking - a series of software toolkit platforms developed by CERN
312		
313	<b>GEM</b>	Gas Electron Multiplier
314	<b>GIF</b>	Gamma Irradiation Facility
315	<b>GIF++</b>	new Gamma Irradiation Facility
316		
317	<b>H</b>	
318		
319		
320	<b>HL-LHC</b>	High Luminosity LHC
321	<b>HV</b>	High Voltage
322		
323	<b>I</b>	
324		
325		
326	<b>iRPC</b>	improved RPC
327	<b>IRQ</b>	Interrupt Request
328		
329	<b>L</b>	
330		
331		
332	<b>LHC</b>	Large Hadron Collider
333	<b>LS1</b>	First Long Shutdown
334	<b>LS3</b>	Third Long Shutdown
335	<b>LV</b>	Low Voltage
336	<b>LVDS</b>	Low-Voltage Differential Signaling
337		
338	<b>M</b>	
339		
340		
341	<b>MC</b>	Monte Carlo
342	<b>MCNP</b>	Monte Carlo N-Particle
343	<b>ME-/-</b>	Find good description
344	<b>ME0</b>	Find good description

---

345		
346	<b>N</b>	
347		
348		
349	<b>NIM</b>	Nuclear Instrumentation Module logic signals
350		
351	<b>P</b>	
352		
353		
354	<b>PMT</b>	PhotoMultiplier Tube
355		
356	<b>R</b>	
357		
358		
359	<b>RE-/-</b>	Find a good description
360	<b>RE2/2</b>	Find a good description
361	<b>RE3/1</b>	Find a good description
362	<b>RE3/2</b>	Find a good description
363	<b>RE4/1</b>	Find a good description
364	<b>RE4/2</b>	Find a good description
365	<b>RE4/3</b>	Find a good description
366	<b>RMS</b>	Root Mean Square
367	<b>ROOT</b>	a framework for data processing born at CERN
368	<b>RPC</b>	Resistive Plate Chamber
369		
370	<b>S</b>	
371		
372		
373	<b>SPS</b>	Super Proton Synchrotron
374		
375	<b>T</b>	
376		
377		
378	<b>TDC</b>	Time-to-Digital Converter
379		
380	<b>W</b>	
381		
382		
383	<b>webDCS</b>	Web Detector Control System



385

Nederlandse samenvatting  
–Summary in Dutch–

386

387 Le resume en Neerlandais (j'aurais peut-être de apprendre la langue juste pour ca...).



## English summary

<sup>389</sup> Le meme résume mais en Anglais (on commencera par la hein!).



# 1

## Introduction

390

391

<sup>392</sup> **1.1 A story of High Energy Physics**

<sup>393</sup> **1.2 Organisation of this study**



# 2

394

395

## Investigating the TeV scale

### 396 2.1 The Standard Model of Particle Physics

### 397 2.2 The Large Hadron Collider and the Compact Muon Solenoid

### 398 2.3 Muon Phase-II Upgrade

399 After the more than two years lasting First Long Shutdown (LS1), the Large Hadron Collider (LHC)  
400 delivered its very first Run-II proton-proton collisions early 2015. LS1 gave the opportunity to the  
401 LHC and to the its experiments to undergo upgrades. The accelerator is now providing collisions  
402 at center-of-mass energy of 13 TeV and bunch crossing rate of 40 MHz, with a peak luminosity  
403 exceeding its design value. During the first and upcoming second LHC Long Shutdown, the Compact  
404 Muon Solenoid (CMS) detector is also undergoing a number of upgrades to maintain a high system  
405 performance [1].

406 From the LHC Phase-2 or High Luminosity LHC (HL-LHC) period onwards, i.e. past the Third  
407 Long Shutdown (LS3), the performance degradation due to integrated radiation as well as the average  
408 number of inelastic collisions per bunch crossing, or pileup, will rise substantially and become a  
409 major challenge for the LHC experiments, like CMS that are forced to address an upgrade program  
410 for Phase-II [2]. Simulations of the expected distribution of absorbed dose in the CMS detector  
411 under HL-LHC conditions, show in figure 5.14 that detectors placed close to the beamline will have  
412 to withstand high irradiation, the radiation dose being of the order of a few tens of Gy.

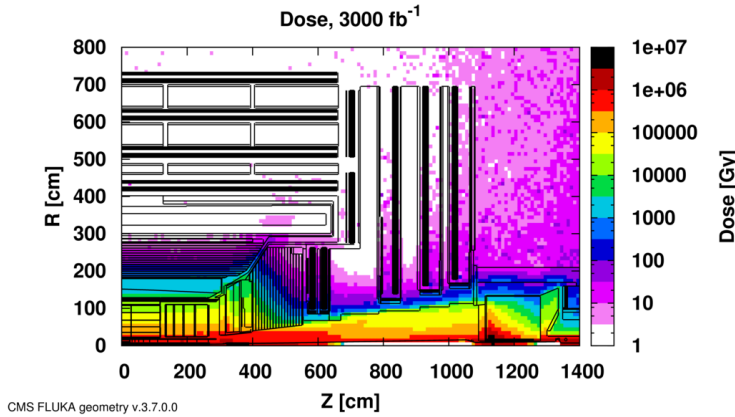


*Figure 2.1: Absorbed dose in the CMS cavern after an integrated luminosity of 3000 fb<sup>-1</sup>. R is the transverse distance from the beamline and Z is the distance along the beamline from the Interaction Point at Z=0.*

413     The measurement of small production cross-section and/or decay branching ratio processes, such  
 414     as the Higgs boson coupling to charge leptons or the  $B_s \rightarrow \mu^+\mu^-$  decay, is of major interest and  
 415     specific upgrades in the forward regions of the detector will be required to maximize the physics  
 416     acceptance on the largest possible solid angle. To ensure proper trigger performance within the  
 417     present coverage, the muon system will be completed with new chambers. In figure 2.2 one can  
 418     see that the existing Cathode Strip Chambers (CSCs) will be completed by Gas Electron Multipliers  
 419     (GEMs) and Resistive Plate Chambers (RPCs) in the pseudo-rapidity region  $1.6 < |\eta| < 2.4$  to  
 420     complete its redundancy as originally scheduled in the CMS Technical Proposal [3].

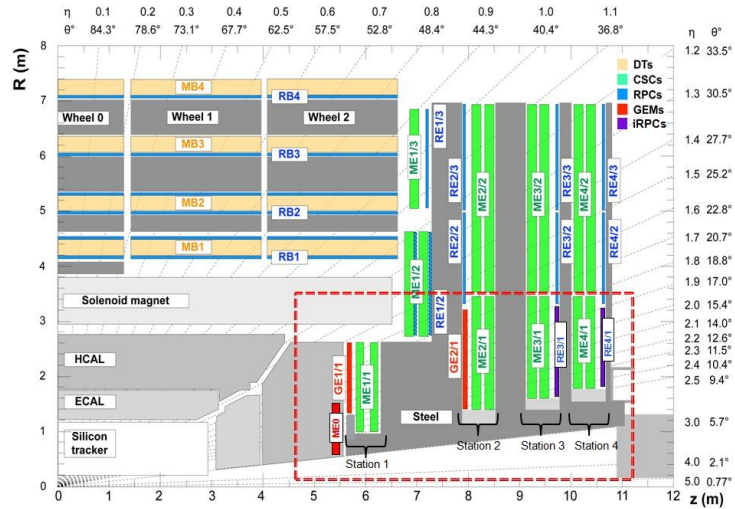


*Figure 2.2: A quadrant of the muon system, showing DTs (yellow), RPCs (light blue), and CSCs (green). The locations of new forward muon detectors for Phase-II are contained within the dashed box and indicated in red for GEM stations (ME0, GE1/1, and GE2/1) and dark blue for improved RPC (iRPC) stations (RE3/1 and RE4/1).*

421     RPCs are used by the CMS first level trigger for their good timing performances. Indeed, a very

good bunch crossing identification can be obtained with the present CMS RPC system, given their fast response of the order of 1 ns. In order to contribute to the precision of muon momentum measurements, muon chambers should have a spatial resolution less or comparable to the contribution of multiple scattering [1]. Most of the plausible physics is covered only considering muons with  $p_T < 100$  GeV thus, in order to match CMS requirements, a spatial resolution of  $\mathcal{O}(\text{few mm})$  the proposed new RPC stations, as shown by the simulation in figure 2.3. According to preliminary designs, RE3/1 and RE4/1 readout pitch will be comprised between 3 and 6 mm and 5  $\eta$ -partitions could be considered.

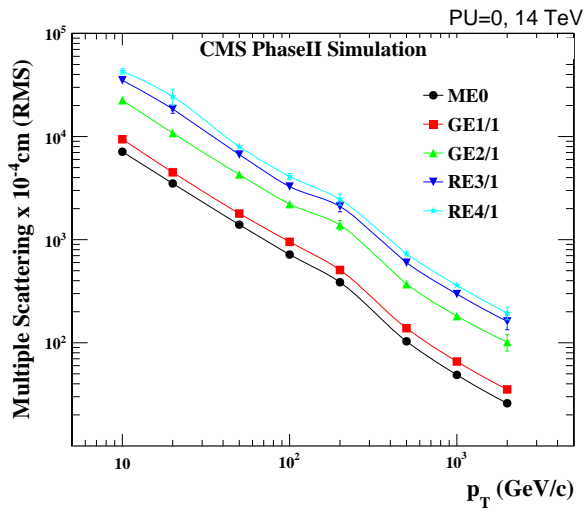


Figure 2.3: RMS of the multiple scattering displacement as a function of muon  $p_T$  for the proposed forward muon stations. All of the electromagnetic processes such as bremsstrahlung and magnetic field effect are included in the simulation.



# 3

430

431

## Amplification processes in gaseous detectors

432

### **3.1 Signal formation**

433

### **3.2 Gas transport parameters**



# 4

434

435

## Resistive Plate Chambers

436 **4.1 Principle**

437 **4.2 Rate capability of Resistive Plate Chambers**

438 **4.3 High time resolution**

439 **4.4 Resistive Plate Chambers at CMS**

440 **4.4.1 Overview**

441 The Resistive Plate Chambers (RPC) system, located in both barrel and endcap regions, provides a  
442 fast, independent muon trigger with a looser  $p_T$  threshold over a large portion of the pseudorapidity  
443 range ( $|\eta| < 1.6$ ) [add reconstruction].

444

445 During High-Luminosity LHC (HL-LHC) operations the expected conditions in terms of back-  
446 ground and pile-up will make the identification and correct  $P_T$  assignment a challenge for the Muon  
447 system. The goal of RPC upgrade is to provide additional hits to the Muon system with precise tim-  
448 ing. All these informations will be elaborated by the trigger system in a global way enhancing the  
449 performance of the trigger in terms of efficiency and rate control. The RPC Upgrade is based on two  
450 projects: an improved Link Board System and the extension of the RPC coverage up to  $|\eta| = 2.4$ .  
451 [FIXME 2.4 or 2.5?]

452 The Link Board system, that will be described in section xxx, is responsible to process, syn-  
453 chronize and zero-suppress the signals coming from the RPC front end boards. The Link Board  
454 components have been produced between 2006 and 2007 and will be subjected to aging and failure  
455 in the long term. The upgraded Link Board system will overcome the aging problems described in  
456 section xxx and will allow for a more precise timing information to the RPC hits from 25 to 1 ns [ref  
457 section xxx].

458 The extension of the RPC system up to  $|\eta| = 2.1$  was already planned in the CMS TDR [ref  
 459 cmstdr] and staged because of budget limitations and expected background rates higher than the rate  
 460 capability of the present CMS RPCs in that region. An extensive R&D program has been done in  
 461 order to develop an improved RPC that fulfills the CMS requirements. Two new RPC layers in the  
 462 innermost ring of stations 3 and 4 will be added with benefits to the neutron-induced background  
 463 reduction and efficiency improvement for both trigger and offline reconstruction.

#### 464 4.4.2 The present RPC system

465 The RPC system is organized in 4 stations called RB1 to RB4 in the barrel region, and RE1 to RE4  
 466 in the endcap region. The innermost barrel stations, RB1 and RB2, are instrumented with 2 layers  
 467 of RPCs facing the innermost (RB1in and RB2in) and outermost (RB1out and RB2out) sides of the  
 468 DT chambers. Every chamber is then divided from the read-out point of view into 2 or 3  $\eta$  partitions  
 469 called “rolls”. The RPC system consist of 480 barrel chambers and 576 endcap chambers. Details  
 470 on the geometry are discussed in the paper [ref to geo paper].

471 The CMS RPC chamber is a double-gap, operated in avalanche mode to ensure reliable operation  
 472 at high rates. Each RPC gap consists of two 2-mm-thick resistive High-Pressure Laminate (HPL)  
 473 plates separated by a 2-mm-thick gas gap. The outer surface of the HPL plates is coated with a thin  
 474 conductive graphite layer, and a voltage is applied. The RPCs are operated with a 3-component,  
 475 non-flammable gas mixture consisting of 95.2% freon ( $C_2H_2F_4$ , known as R134a), 4.5% isobutane  
 476 ( $i-C_4H_{10}$ ), and 0.3% sulphur hexafluoride ( $SF_6$ ) with a relative humidity of 40% - 50%. Readout  
 477 strips are aligned in  $\eta$  between the 2 gas gaps. [\[Add a sentence on FEBs.\]](#)

478 The discriminated signals coming from the Front End boards feed via twisted cables (10 to 20 m  
 479 long) the Link Board System located in UXC on the balconies around the detector. The Link System  
 480 consist of the 1376 Link Boards (LBs) and the 216 Control Boards (CBs), placed in 108 Link Boxes.  
 481 The Link Box is a custom crate (6U high) with 20 slots (for two CBs and eighteen LBs). The Link  
 482 Box contains custom backplane to which the cables from the chambers are connected, as well as the  
 483 cables providing the LBs and CBs power supply and the cables for the RPC FEBs control with use  
 484 of the I2C protocol (trough the CB). The backplane itself contains only connectors (and no any other  
 485 electronic devices).

486 The Link Board has 96 input channels (one channel corresponds to one RPC strip). The input  
 487 signals are the  $\sim 100$  ns binary pulses which are synchronous to the RPC hits, but not to the LHC  
 488 clock (which drives the entire CMS electronics). Thus the first step of the FEB signals processing  
 489 is synchronization, i.e. assignment of the signals to the BXes (25 ns periods). Then the data are  
 490 compressed with a simple zero-suppressing algorithm (the input channels are grouped into 8 bit  
 491 partitions, only the partitions with at least one nonzero bit are selected for each BX). Next, the non-  
 492 empty partitions are time-multiplexed i.e. if there are more than one such partition in a given BX,  
 493 they are sent one-by-one in consecutive BXes. The data from 3 neighbouring LBs are concentrated  
 494 by the middle LB which contains the optical transmitter for sending them to the USC over a fiber at  
 495 1.6 Gbps.

496 The Control Boards provide the communication of the control software with the LBs via the  
 497 FEC/CCU system. The CBs are connected into token rings, each ring consists of 12 CBs of one  
 498 detector tower and a FEC mezzanine board placed on the CCS board located in the VME crate in  
 499 the USC. In total, there are 18 rings in the entire Link System. The CBs also perform automatic  
 500 reloading of the LB’s firmware which is needed in order to avoid accumulation of the radiation  
 501 induced SEUs in the LBs firmware.

502 Both LBs and CB are based on the Xilinx Spartan III FPGAs, the CB additionally contains  
 503 radiation-tolerant (FLASH based) FPGA Actel ProAsicPlus.

504 The High Voltage power system is located in USC, not exposed to radiation and easily accessible  
 505 for any reparation. A single HV channel powers 2 RPC chambers both in the barrel and endcap  
 506 regions. The Low Voltage boards are located in UXC on the balconies and provide the voltage to the  
 507 front end electronics.

#### 508 4.4.3 Pulse processing of CMS RPCs

509 Signals induced by cosmic particle in the RPC strips are shaped by standard CMS RPC Front-End  
 510 Electronics (FEE) following the scheme of Figure 4.1. On a first stage, analogic signals are amplified  
 511 and then sent to the Constant Fraction Discriminator (CFD) described in Figure 4.2. At the end of  
 512 the chain, 100 ns long pulses are sent in the LVDS output. These output signal are sent on one side to  
 513 a V1190A Time-to-Digital Converter (TDC) module from CAEN and on the other to an OR module  
 514 to count the number of detected signals. Trigger and hit coïncidences are monitored using scalers.  
 515 The TDC is used to store the data into ROOT files. These files are thus analysed to understand the  
 516 detectors performance.

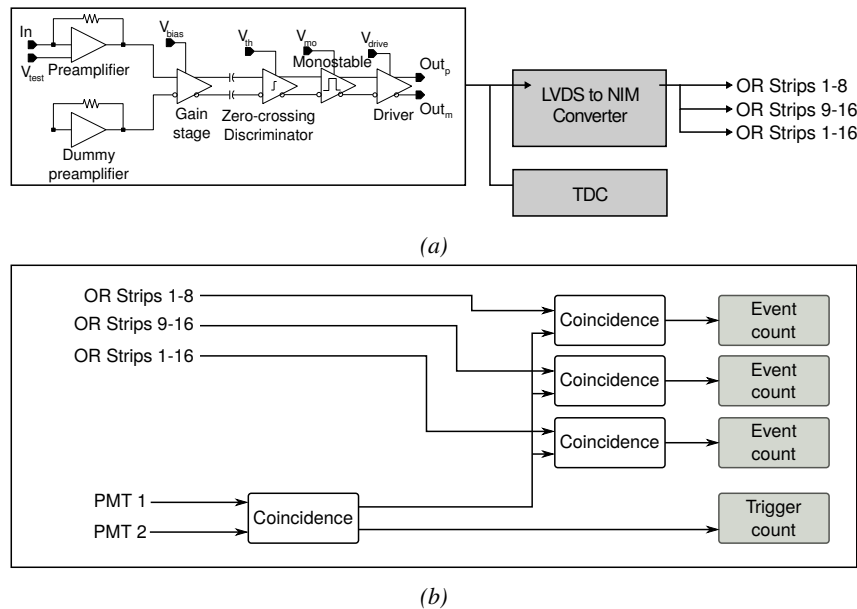
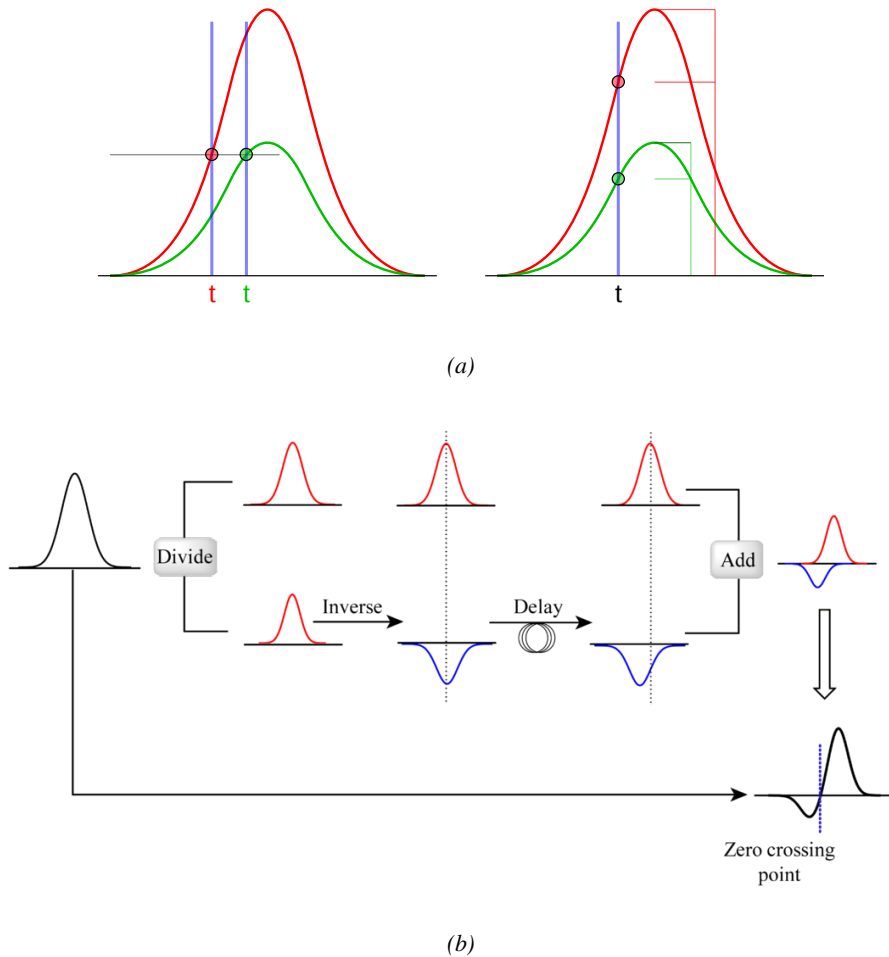


Figure 4.1: Signals from the RPC strips are shaped by the FEE described on Figure 4.1a. Output LVDS signals are then read-out by a TDC module connected to a computer or converted into NIM and sent to scalers. Figure 4.1b describes how these converted signals are put in coincidence with the trigger.



*Figure 4.2: Description of the principle of a CFD. A comparison of threshold triggering (left) and constant fraction triggering (right) is shown in Figure 4.2a. Constant fraction triggering is obtained thanks to zero-crossing technique as explained in Figure 4.2b. The signal arriving at the input of the CFD is split into three components. A first one is delayed and connected to the inverting input of a first comparator. A second component is connected to the noninverting input of another comparator along with a threshold value connected to the inverting input. Finally, the output of both comparators is fed through an AND gate.*

# 5

517

518  
519

## Longevity studies and Consolidation of the present CMS RPC subsystem

520

### 5.1 Testing detectors under extreme conditions

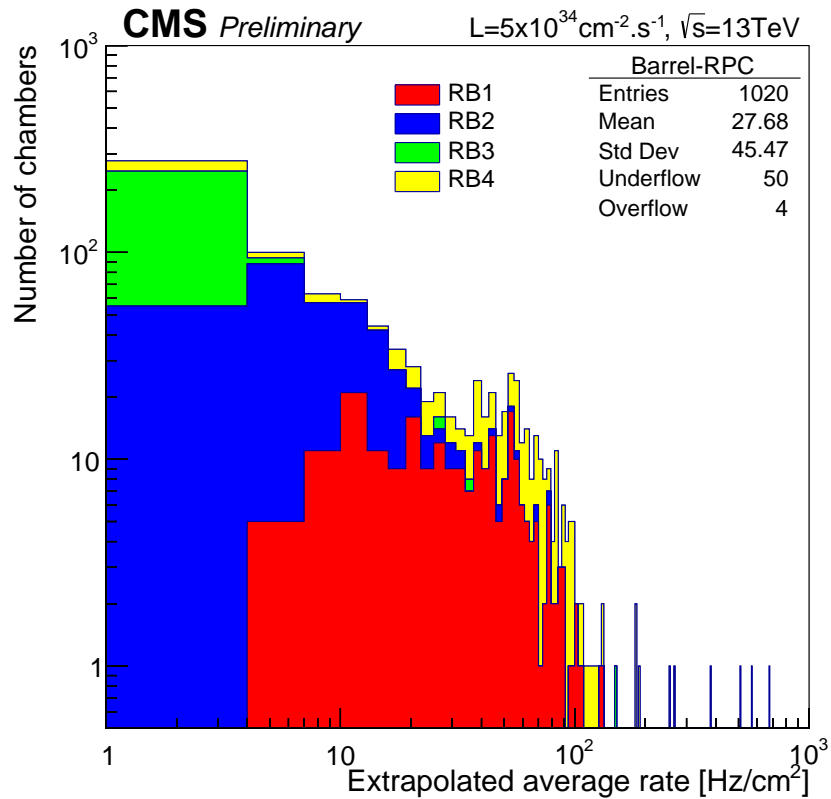
521  
522  
523  
524  
525  
526  
527  
528

The upgrade from LHC to HL-LHC will increase the peak luminosity from  $10^{34} \text{ cm}^{-2} \text{ s}^{-1}$  to reach  $5 \times 10^{34} \text{ cm}^{-2} \text{ s}^{-1}$ , increasing in the same way the total expected background to which the RPC system will be subjected to. Composed of low energy gammas and neutrons from  $p\text{-}p$  collisions, low momentum primary and secondary muons, puch-through hadrons from calorimeters, and particles produced in the interaction of the beams with collimators, the background will mostly affect the regions of CMS that are the closest to the beam line, i.e. the RPC detectors located in the endcaps.

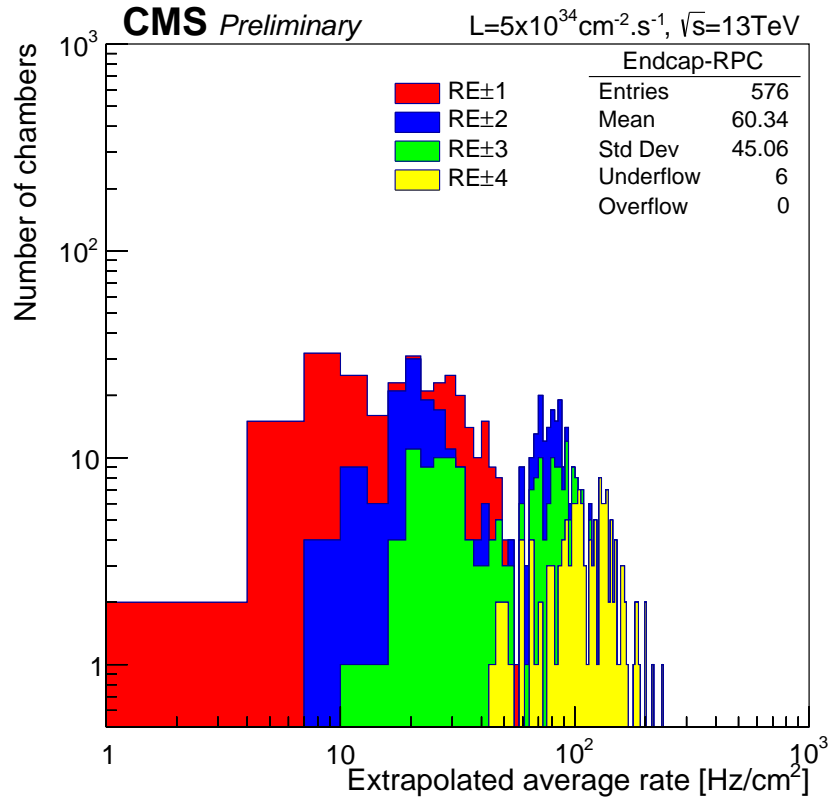
[To update.]

529  
530  
531  
532  
533  
534  
535  
536  
537

The 2016 data allowed to study the values of the background rate in all RPC system. In Figure 5.1, the distribution of the chamber background hit rate per unit area is shown at a luminosity of  $5 \times 10^{34} \text{ cm}^{-2} \cdot \text{s}^{-1}$  linearly extrapolating from data collected in 2016 [ref mentioning the linear dependency of rate vs lumi]. The maximum rate per unit area at HL-LHC conditions is expected to be of the order of  $600 \text{ Hz/cm}^2$  (including a safety factor 3). Nevertheless, Fluka simulations have conducted in order to understand the background at HL-LHC conditions. The comparison to the data has shown, in Figure 5.2, a discrepancy of a factor 2 even though the order of magnitude is consistent. [Understand mismatch.]



(a)



(b)

Figure 5.1: (5.1a) Extrapolation from 2016 data of single hit rate per unit area in the barrel region. (5.1b) Extrapolation from 2016 data of single hit rate per unit area in the endcap region.

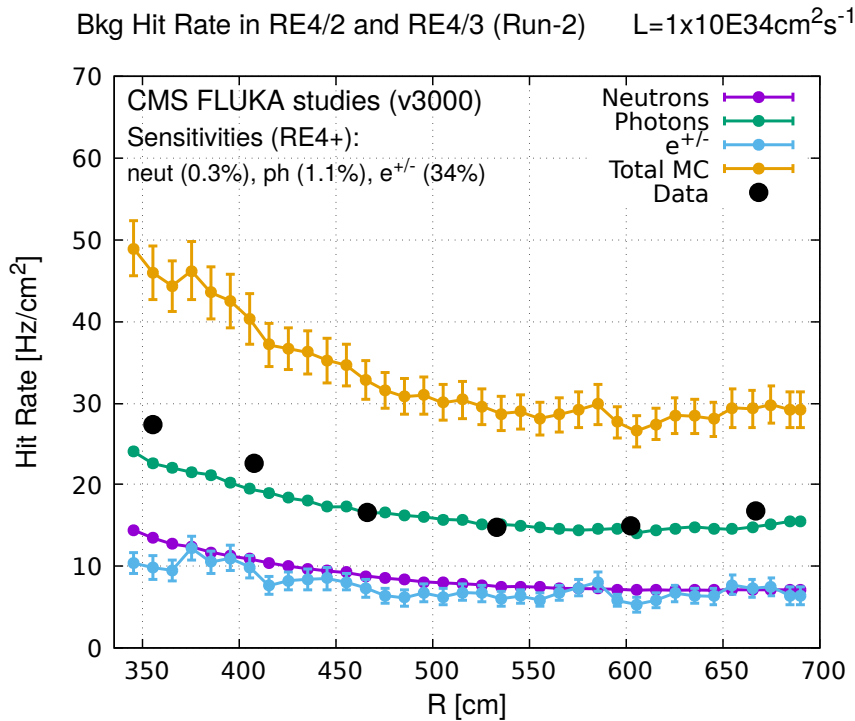


Figure 5.2: Background Fluka simulation compared to 2016 Data at  $L = 10^{34}\text{cm}^{-2}\text{s}^{-1}$  in the fourth endcap disk region. A mismatch in between simulation and data can be observed. [\[To be understood.\]](#)

538 In the past, extensive long-term tests were carried out at several gamma and neutron facilities  
 539 certifying the detector performance. Both full size and small prototype RPCs have been irradiated  
 540 with photons up to an integrated charge of  $\sim 0.05\text{C}/\text{cm}^2$  and  $\sim 0.4\text{C}/\text{cm}^2$ , respectively [4, 5].  
 541 During Run-I, the RPC system provided stable operation and excellent performance and did not  
 542 show any aging effects for integrated charge of the order of  $0.01\text{C}/\text{cm}^2$ . Projections on currents  
 543 from 2016 Data, has allowed to determine that the total integrated charge, by the end of HL-LHC,  
 544 would be of the order of  $1\text{C}/\text{cm}^2$  (including a safety factor 3). [\[Corresponding figure needed.\]](#)

545

### 546 5.1.1 The Gamma Irradiation Facilities

#### 547 5.1.1.1 GIF

548 Located in the SPS West Area at the downstream end of the X5 test beam, the Gamma Irradiation  
 549 Facility (GIF) was a test area in which particle detectors were exposed to a particle beam in presence  
 550 of an adjustable gamma background [6]. Its goal was to reproduce background conditions these  
 551 detectors would suffer in their operating environment at LHC. GIF layout is shown in Figure 5.3.  
 552 Gamma photons are produced by a strong  $^{137}\text{Cs}$  source installed in the upstream part of the zone  
 553 inside a lead container. The source container includes a collimator, designed to irradiate a  $6 \times 6\text{ m}^2$   
 554 area at 5 m maximum to the source. A thin lens-shaped lead filter helps providing with a uniform  
 555 outcoming flux in a vertical plane, orthogonal to the beam direction. The principal collimator hole  
 556 provides a pyramidal aperture of  $74^\circ \times 74^\circ$  solid angle and provides a photon flux in a pyramidal vol-

ume along the beam axis. The photon rate is controled by further lead filters allowing the maximum rate to be limited and to vary within a range of four orders of magnitude. Particle detectors under test are then placed within the pyramidal volume in front of the source, perpendicularly to the beam line in order to profit from the homogeneous photon flux. Adjusting the background flux of photons can then be done by using the filters and choosing the position of the detectors with respect to the source.

562

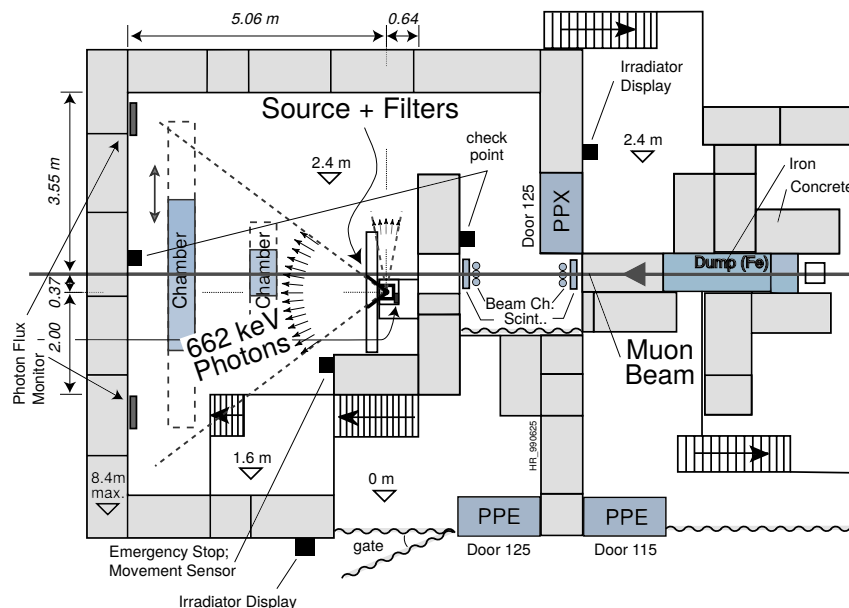


*Figure 5.3: Layout of the test beam zone called X5c GIF at CERN. Photons from the radioactive source produce a sustained high rate of random hits over the whole area. The zone is surrounded by 8 m high and 80 cm thick concrete walls. Access is possible through three entry points. Two access doors for personnel and one large gate for material. A crane allows installation of heavy equipment in the area.*

As described on Figure 5.4, the  $^{137}\text{Cs}$  source emits a 662 keV photon in 85% of the decays. An activity of 740 GBq was measured on the 5<sup>th</sup> March 1997. To estimate the strength of the flux in 2014, it is necessary to consider the nuclear decay through time assiciated to the Cesium source whose half-life is well known ( $t_{1/2} = (30.05 \pm 0.08)$  y). The GIF tests where done in between the 20<sup>th</sup> and the 31<sup>st</sup> of August 2014, i.e. at a time  $t = (17.47 \pm 0.02)$  y resulting in an attenuation of the activity from 740 GBq in 1997 to 494 GBq in 2014.

569

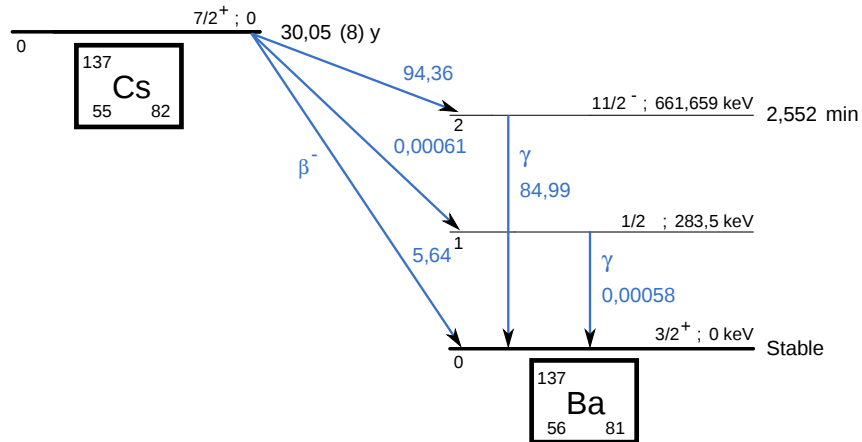


Figure 5.4:  $^{137}\text{Cs}$  decays by  $\beta^-$  emission to the ground state of  $^{137}\text{Ba}$  ( $BR = 5.64\%$ ) and via the 662 keV isomeric level of  $^{137}\text{Ba}$  ( $BR = 94.36\%$ ) whose half-life is 2.55 min.

### 5.1.1.2 GIF++

The new Gamma Irradiation Facility (GIF++), located in the SPS North Area at the downstream end of the H4 test beam, has replaced its predecessor during LS1 and has been operational since spring 2015 [7]. Like GIF, GIF++ features a  $^{137}\text{Cs}$  source of 662 keV gamma photons, their fluence being controlled with a set of filters of various attenuation factors. The source provides two separated large irradiation areas for testing several full-size muon detectors with continuous homogeneous irradiation, as presented in Figure 5.5.

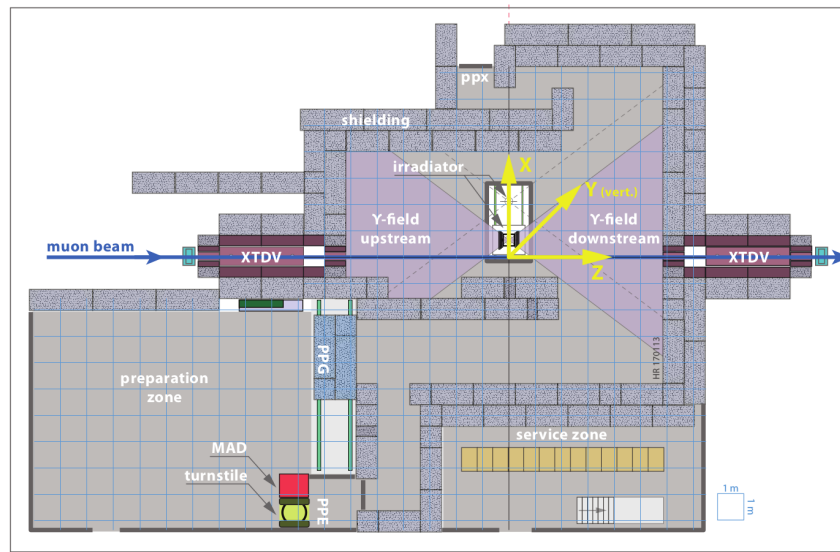


Figure 5.5: Floor plan of the GIF++ facility. When the facility downstream of the GIF++ takes electron beam, a beam pipe is installed along the beam line ( $z$ -axis). The irradiator can be displaced laterally (its center moves from  $x = 0.65 \text{ m}$  to  $2.15 \text{ m}$ ), to increase the distance to the beam pipe.

578      The source activity was measured to be about 13.5 TBq in March 2016. The photon flux being  
 579      far greater than HL-LHC expectations, GIF++ provides an excellent facility for accelerated aging  
 580      tests of muon detectors.

581

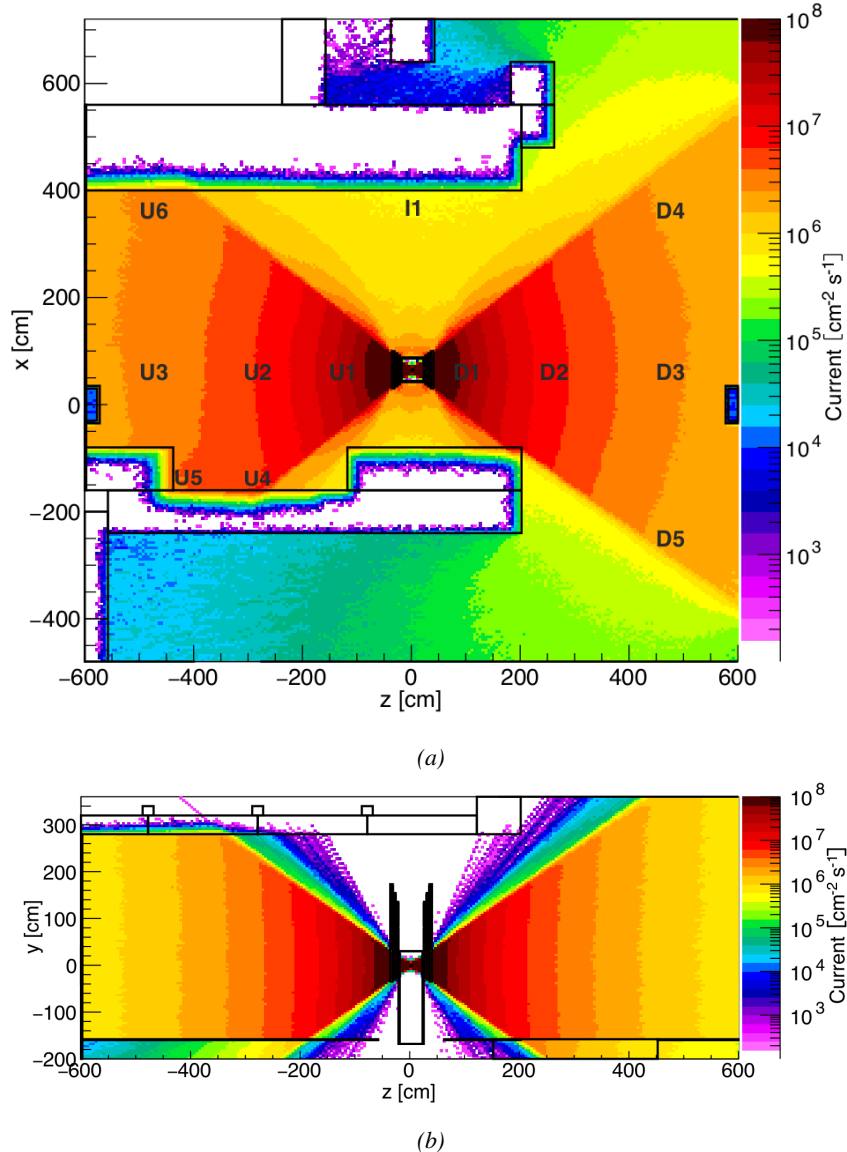


Figure 5.6: Simulated unattenuated current of photons in the xz plane (Figure 5.6a) and yz plane (Figure 5.6b) through the source at  $x = 0.65 \text{ m}$  and  $y = 0 \text{ m}$ . With angular correction filters, the current of 662 keV photons is made uniform in xy planes.

582      The source is situated in the muon beam line with the muon beam being available a few times a  
 583      year. The H4 beam, composed of muons with a momentum of about 150 GeV/c, passes through the  
 584      GIF++ zone and is used to study the performance of the detectors. Its flux is of 104 particles/ $\text{s cm}^2$

585 focused in an area similar to  $10 \times 10 \text{ cm}^2$ . Therefore, with properly adjusted filters, one can imitate  
 586 the HL-LHC background and study the performance of muon detectors with their trigger/readout  
 587 electronics in HL-LHC environment.

588

## 589 5.2 Preliminary tests at GIF

### 590 5.2.1 Resistive Plate Chamber test setup

591 During summer 2014, preliminary tests have been conducted in the GIF area on a newly produced  
 592 RE4/2 chamber labelled RE-4-2-BARC-161. This chamber has been placed into a trolley covered  
 593 with a tent. The position of the RPC inside the tent and of the tent related to the source is described  
 594 in Figure 5.7. To test this CMS RPC, three different absorber settings were used. First of all,  
 595 measurements were done with fully opened source. Then, to complete this preliminary study, the  
 596 gamma flux has been attenuated from a factor 2 and a factor 5. The expected gamma flux at the level  
 597 of our detector will be discussed in subsection ??.

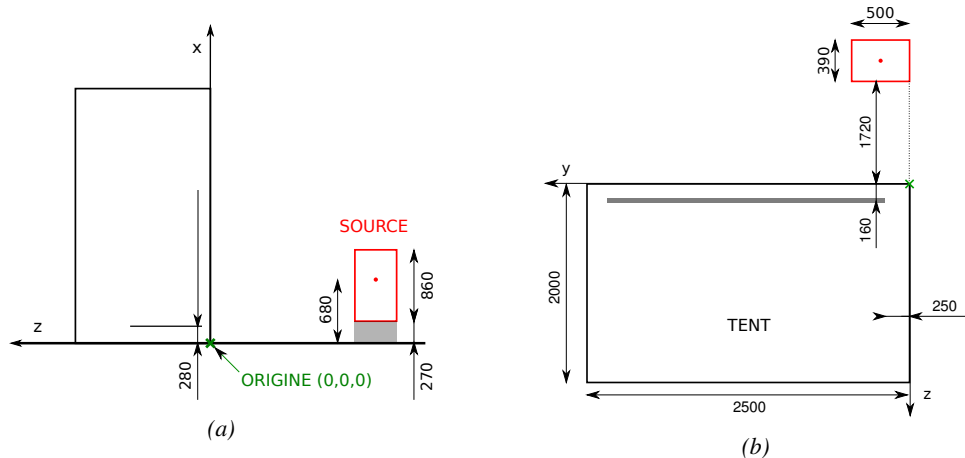
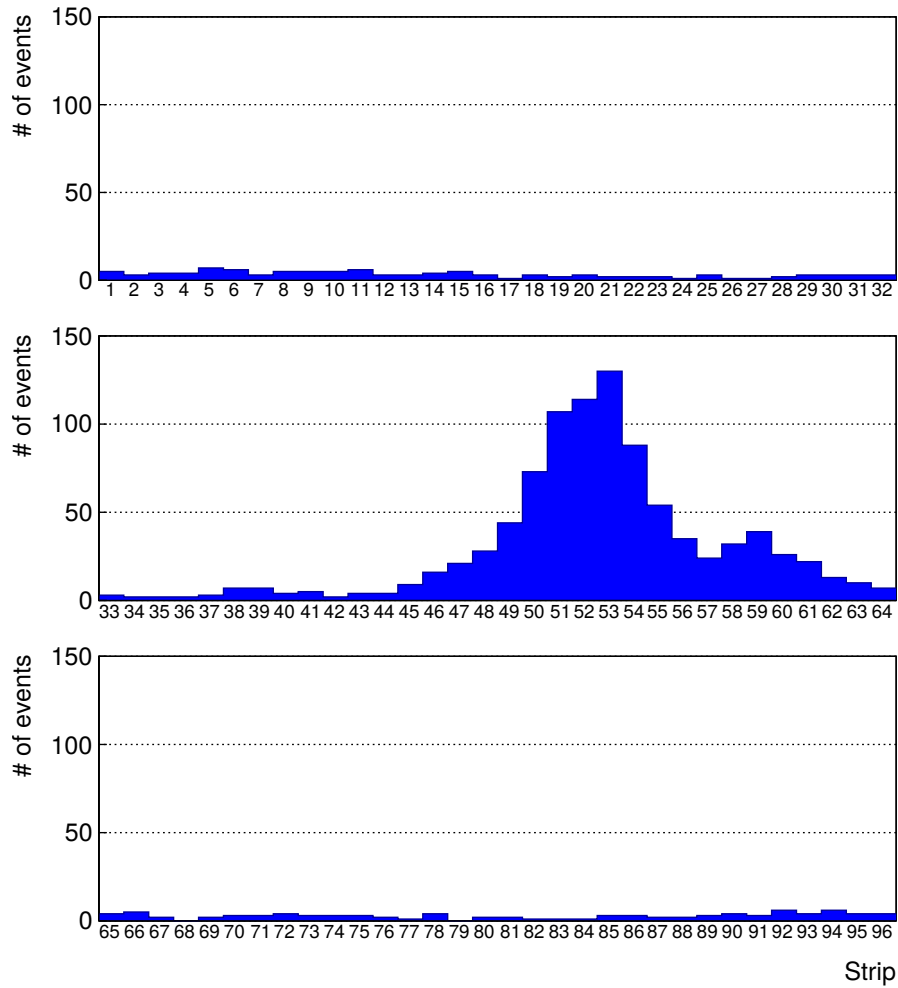


Figure 5.7: Description of the RPC setup. Dimensions are given in mm. A tent containing RPCs is placed at 1720 mm from the source container. The source is situated in the center of the container. RE-4-2-BARC-161 chamber is 160 mm inside the tent. This way, the distance between the source and the chambers plan is 2060 mm. Figure 5.7a provides a side view of the setup in the xz plane while Figure 5.7b shows a top view in the yz plane.



*Figure 5.8: RE-4-2-BARC-161 chamber is inside the tent as described in Figure 5.7. In the top right, the two scintillators used as trigger can be seen. This trigger system has an inclination of 10° relative to horizontal and is placed above half-partition B2 of the RPCs. PMT electronics are shielded thanks to lead blocks placed in order to protect them without stopping photons from going through the scintillators and the chamber.*

598 At the time of the tests, the beam not being operational anymore, a trigger composed of 2  
599 plastic scintillators has been placed in front of the setup with an inclination of 10 deg with respect to  
600 the detector plane in order to look at cosmic muons. Using this particular trigger layout, shown on  
601 Figure 5.8, leads to a cosmic muon hit distribution into the chamber similar to the one in Figure 5.9.  
602 Measured without gamma irradiation, two peaks can be seen on the profil of partition B, centered  
603 on strips 52 and 59. Section ?? will help us understand that these two peaks are due respectively to  
604 forward and backward coming cosmic particles where forward coming particles are first detected by  
605 the scintillators and then the RPC while the backward coming muons are first detected in the RPC.



*Figure 5.9: Hit distributions over all 3 partitions of RE-4-2-BARC-161 chamber is showed on these plots. Top, middle and bottom figures respectively correspond to partitions A, B, and C. These plots show that some events still occur in other half-partitions than B2, which corresponds to strips 49 to 64, in front of which the trigger is placed, contributing to the inefficiency of detection of cosmic muons. In the case of partitions A and C, the very low amount of data can be interpreted as noise. On the other hand, it is clear that a little portion of muons reach the half-partition B1, corresponding to strips 33 to 48.*

### 5.2.2 Data Acquisition

### 5.2.3 Geometrical acceptance of the setup layout to cosmic muons

In order to profit from a constant gamma irradiation, the detectors inside of the GIF bunker need to be placed in a plane orthogonal to the beam line. The muon beam that used to be available was meant to test the performance of detectors under test. This beam not being active anymore, another solution to test detector performance had to be used. Thus, it has been decided to use cosmic muons detected through a telescope composed of two scintillators. Lead blocks were used as shielding to

613 protect the photomultipliers from gammas as can be seen from Figure 5.8.

614 An inclination has been given to the cosmic telescope to maximize the muon flux. A good com-  
 615 promise had to be found between good enough muon flux and narrow enough hit distribution to  
 616 be sure to contain all the events into only one half partitions as required from the limited available  
 617 readout hardware. Nevertheless, a consequence of the misplaced trigger, that can be seen as a loss  
 618 of events in half-partition B1 in Figure 5.9, is an inefficiency. Nevertheless, the inefficiency of ap-  
 619 proximately 20 % highlighted in Figure 5.10 by comparing the performance of chamber BARC-161  
 620 in 904 and at GIF without irradiation seems too important to be explained only by the geometri-  
 621 cal acceptance of the setup itself. Simulations have been conducted to show how the setup brings  
 622 inefficiency.

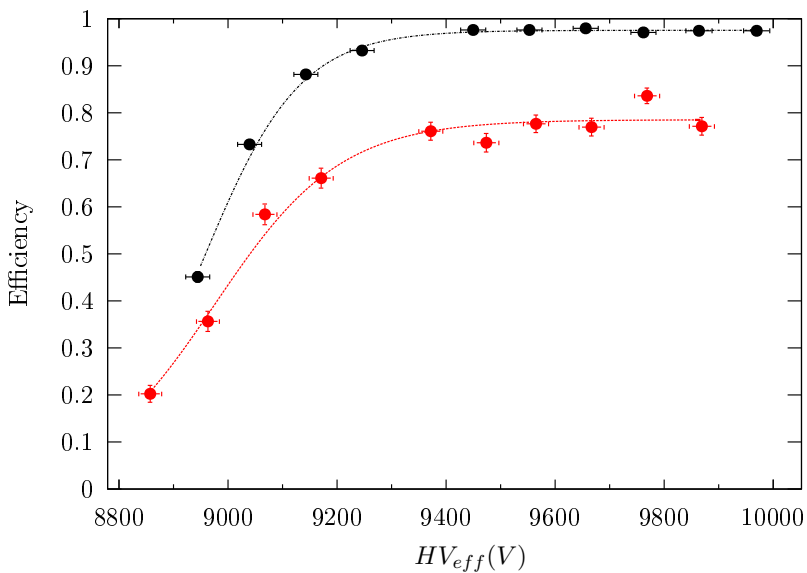
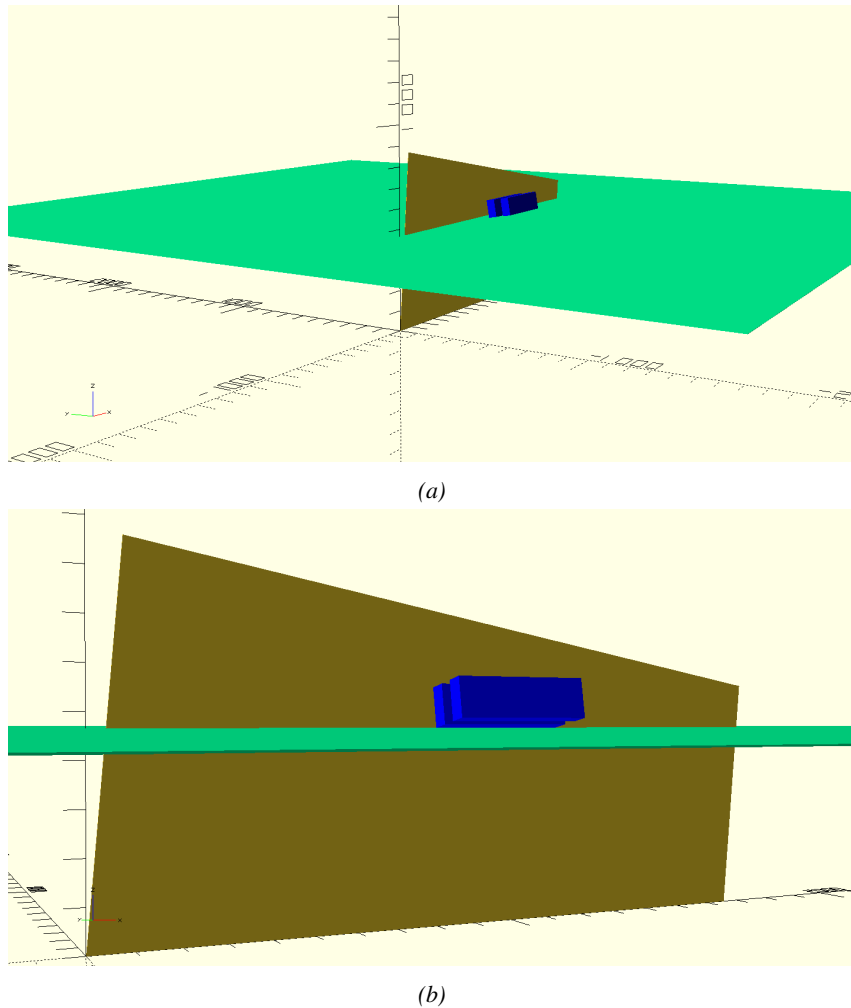


Figure 5.10: Results are derived from data taken on half-partition B2 only. On the 18<sup>th</sup> of June 2014, data has been taken on chamber RE-2-BARC-161 at building 904 (Prevessin Site) with cosmic muons providing us a reference efficiency plateau of  $(97.54 \pm 0.15)\%$  represented by a black curve. A similar measurement has been done at GIF on the 21<sup>st</sup> of July with the same chamber giving a plateau of  $(78.52 \pm 0.94)\%$  represented by a red curve.

### 623 5.2.3.1 Description of the simulation layout

624 The layout of GIF setup has been reproduced and incorporated into a Monte Carlo (MC) simulation  
 625 to study the influence of the disposition of the telescope on the final distribution measured by the  
 626 RPC. A 3D view of the simulated layout is given into Figure 5.11. Muons are generated randomly  
 627 in a horizontal plane located at a height corresponding to the lowest point of the PMTs. This way,  
 628 the needed size of the plane in order to simulate events happening at very big azimuthal angles (i.e.  
 629  $\theta \approx \pi$ ) can be kept relatively small. The muon flux is designed to follow the usual  $\cos^2\theta$  distribution  
 630 for cosmic particle. The goal of the simulation is to look at muons that pass through the muon  
 631 telescope composed of the two scintillators and define their distribution onto the RPC plane. During  
 632 the reconstruction, the RPC plane is then divided into its strips and each muon track is assigned to a  
 633 strip.



*Figure 5.11: Representation of the layout used for the simulations of the test setup. The RPC is represented as a yellow trapezoid while the two scintillators as blue cuboids looking at the sky. A green plane corresponds to the muon generation plane within the simulation. Figure 5.7a shows a global view of the simulated setup. Figure 5.7b shows a zoomed view that allows to see the 2 scintillators as well as the full RPC plane.*

634 In order to further refine the quality of the simulation and understand deeper the results the  
 635 dependance of the distribution has been studied for a range of telescope inclinations. Moreover,  
 636 the threshold applied on the PMT signals has been included into the simulation in the form of a  
 637 cut. In the approximation of uniform scintillators, it has been considered that the threshold can be  
 638 understood as the minimum distance particles need to travel through the scintillating material to give  
 639 a strong enough signal. Particles that travel a distance smaller than the set "threshold" are thus not  
 640 detected by the telescope and cannot trigger the data taking. Finally, the FEE threshold also has  
 641 been considered in a similar way. The mean momentum of horizontal cosmic rays is higher than  
 642 those of vertical ones but the stopping power of matter for momenta ranging from 1 GeV to 1 TeV  
 643 stays comparable. It is then possible to assume that the mean number of primary  $e^-/ion$  pairs per  
 644 unit length will stay similar and thus, depending on the applied discriminator threshold, muons with

645 the shortest path through the gas volume will deposit less charge and induce a smaller signal on the  
 646 pick-up strips that could eventually not be detected. These two thresholds also restrain the overall  
 647 geometrical acceptance of the system.

648 **5.2.3.2 Simulation procedure**

649 The simulation software has been designed using C++ and the output data is saved into ROOT  
 650 histograms. Simulations start for a threshold  $T_{scint}$  varying in a range from 0 to 45 mm in steps  
 651 of 5 mm, where  $T_{scint} = 0$  mm corresponds to the case where there isn't any threshold apply on  
 652 the input signal while  $T_{scint} = 45$  mm, which is the scintillator thickness, is the case where muons  
 653 cannot arrive orthogonally onto the scintillator surface. For a given  $T_{scint}$ , a set of RPC thresholds  
 654 are considered. The RPC threshold,  $T_{RPC}$  varies from 2 mm, the thickness of the gas volume, to  
 655 3 mm in steps of 0.25 mm. For each  $(T_{scint}; T_{RPC})$  pair,  $N_\mu = 10^8$  muons are randomly generated  
 656 inside the muon plane described in the previous paragraph with an azimuthal angle  $\theta$  chosen to follow  
 657 a  $\cos^2\theta$  distribution.

658 Planes are associated to each surface of the scintillators. Knowing muon position into the muon  
 659 plane and its direction allows us, by assuming that muons travel in a straight line, to compute the  
 660 intersection of the muon track with these planes. Applying conditions to the limits of the surfaces  
 661 of the scintillator faces then gives us an answer to whether or not the muon passed through the  
 662 scintillators. In the case the muon has indeed passed through the telescope, the path through each  
 663 scintillator is computed and muons whose path was shorter than  $T_{scint}$  are rejected and are thus  
 664 considered as having not interacted with the setup.

665 On the contrary, if the muon is labeled as good, its position within the RPC plane is computed  
 666 and the corresponding strip, determined by geometrical tests in the case the distance through the  
 667 gas volume was enough not to be rejected because of  $T_{RPC}$ , gets a hit and several histograms  
 668 are filled in order to keep track of the generation point on the muon plane, the intersection points  
 669 of the reconstructed muons within the telescope, or on the RPC plane, the path traveled through  
 670 each individual scintillator or the gas volume, as well as other histograms. Moreover, muons fill  
 671 different histograms whether they are forward or backward coming muons. They are discriminated  
 672 according to their direction components. When a muon is generated, an  $(x, y, z)$  position is assigned  
 673 into the muon plane as well as a  $(\theta; \phi)$  pair that gives us the direction it's coming from. This way,  
 674 muons satisfying the condition  $0 \leq \phi < \pi$  are designated as backward coming muons while muons  
 675 satisfying  $\pi \leq \phi < 2\pi$  as forward coming muons.

676 This simulation is then repeated for different telescope inclinations ranging in between 4 and  $20^\circ$   
 677 and varying in steps of  $2^\circ$ . Due to this inclination and to the vertical position of the detector under  
 678 test, the muon distribution reconstructed in the detector plane is asymmetrical. The choice as been  
 679 made to chose a skew distribution formula to fit the data built as the multiplication of gaussian and  
 680 sigmoidal curves together. A typical gaussian formula is given as 5.1 and has three free parameters  
 681 as  $A_g$ , its amplitude,  $\bar{x}$ , its mean value and  $\sigma$ , its root mean square. Sigmoidal curves as given by  
 682 formula 5.2 are functions converging to 0 and  $A_s$  as  $x$  diverges. The inflection point is given as  $x_i$   
 683 and  $\lambda$  is proportional to the slope at  $x = x_i$ . In the limit where  $\lambda \rightarrow \infty$ , the sigmoid becomes a  
 684 step function.

$$g(x) = A_g e^{-\frac{(x-\bar{x})^2}{2\sigma^2}} \quad (5.1)$$

$$s(x) = \frac{A_s}{1 + e^{-\lambda(x-x_i)}} \quad (5.2)$$

685 Finally, a possible representation of a skew distribution is given by formula 5.3 and is the product  
 686 of 5.1 and 5.2. Naturally, here  $A_{sk} = A_g \times A_s$  and represents the theoretical maximum in the limit  
 687 where the skew tends to a gaussian function.

$$sk(x) = g(x) \times s(x) = A_{sk} \frac{e^{\frac{-(x-\bar{x})^2}{2\sigma^2}}}{1 + e^{-\lambda(x-x_i)}} \quad (5.3)$$

688 **5.2.3.3 Results**

689 **Influence of  $T_{scint}$  on the muon distribution**

690 **Influence of  $T_{RPC}$  on the muon distribution**

691 **Influence of the telescope inclination on the muon distribution**

692 **Comparison to data taken at GIF without irradiation**

693 **5.2.4 Photon flux at GIF**

694 **5.2.4.1 Expectations from simulations**

695 In order to understand and evaluate the  $\gamma$  flux in the GIF area, simulations had been conducted in  
 696 1999 and published by S. Agosteo et al [6]. Table 5.1 presented in this article gives us the  $\gamma$  flux  
 697 for different distances  $D$  to the source. This simulation was done using GEANT and a Monte Carlo  
 698 N-Particle (MCNP) transport code, and the flux  $F$  is given in number of  $\gamma$  per unit area and unit time  
 699 along with the estimated error from these packages expressed in %.

Nominal ABS	Photon flux $F$ [ $s^{-1}cm^{-2}$ ]			
	at $D = 50$ cm	at $D = 155$ cm	at $D = 300$ cm	at $D = 400$ cm
1	$0.12 \cdot 10^8 \pm 0.2\%$	$0.14 \cdot 10^7 \pm 0.5\%$	$0.45 \cdot 10^6 \pm 0.5\%$	$0.28 \cdot 10^6 \pm 0.5\%$
2	$0.68 \cdot 10^7 \pm 0.3\%$	$0.80 \cdot 10^6 \pm 0.8\%$	$0.25 \cdot 10^6 \pm 0.8\%$	$0.16 \cdot 10^6 \pm 0.6\%$
5	$0.31 \cdot 10^7 \pm 0.4\%$	$0.36 \cdot 10^6 \pm 1.2\%$	$0.11 \cdot 10^6 \pm 1.2\%$	$0.70 \cdot 10^5 \pm 0.9\%$

Table 5.1: Total photon flux ( $E\gamma \leq 662$  keV) with statistical error predicted considering a  $^{137}Cs$  activity of 740 GBq at different values of the distance  $D$  to the source along the  $x$ -axis of irradiation field [6].

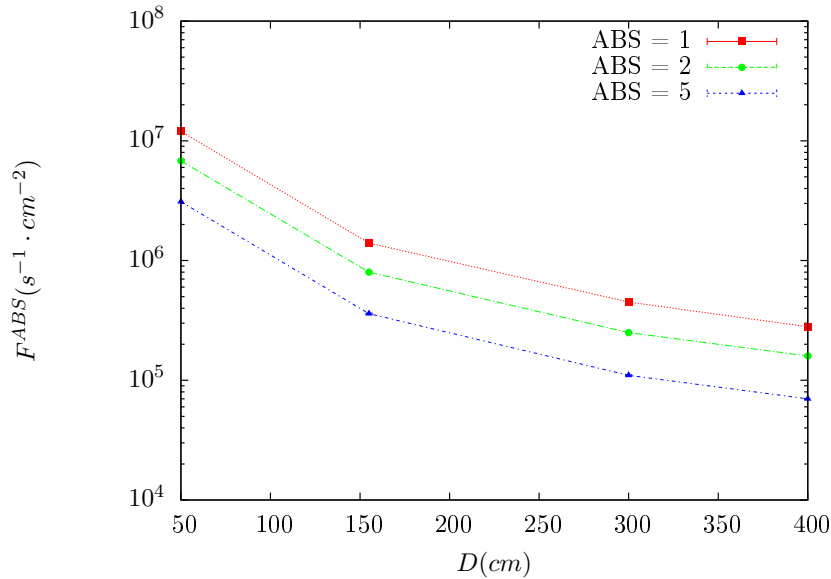


Figure 5.12:  $\gamma$  flux  $F(D)$  is plot using values from table 5.1. As expected, the plot shows similar attenuation behaviours with increasing distance for each absorption factors.

The simulation doesn't directly provide us with an estimated flux at the level of our RPC. First of all, it is needed to extract the value of the flux from the available data contained in the original paper and then to estimate the flux in 2014 at the time the experimentation took place. Figure 5.12 that contains the data from Table 5.1. In the case of a pointlike source emitting isotropic and homogeneous gamma radiations, the gamma flux  $F$  at a distance  $D$  to the source with respect to a reference point situated at  $D_0$  where a known flux  $F_0$  is measured will be expressed like in Equation 5.4, assuming that the flux decreases as  $1/D^2$ , where  $c$  is a fitting factor.

$$F^{ABS} = F_0^{ABS} \times \left( \frac{cD_0}{D} \right)^2 \quad (5.4)$$

By rewriting Equation 5.4, it comes that :

$$c = \frac{D}{D_0} \sqrt{\frac{F^{ABS}}{F_0^{ABS}}} \quad (5.5)$$

$$\Delta c = \frac{c}{2} \left( \frac{\Delta F^{ABS}}{F^{ABS}} + \frac{\Delta F_0^{ABS}}{F_0^{ABS}} \right) \quad (5.6)$$

Finally, using Equation 5.5 and the data in Table 5.1 with  $D_0 = 50$  cm as reference point, we can build Table 5.2. It is interesting to note that  $c$  for each value of  $D$  doesn't depend on the absorption factor.

Nominal ABS	Correction factor $c$		
	at $D = 155$ cm	at $D = 300$ cm	at $D = 400$ cm
1	$1.059 \pm 0.70\%$	$1.162 \pm 0.70\%$	$1.222 \pm 0.70\%$
2	$1.063 \pm 1.10\%$	$1.150 \pm 1.10\%$	$1.227 \pm 0.90\%$
5	$1.056 \pm 1.60\%$	$1.130 \pm 1.60\%$	$1.202 \pm 1.30\%$

Table 5.2: Correction factor  $c$  is computed thanks to formulae 5.5 taking as reference  $D_0 = 50$  cm and the associated flux  $F_0^{ABS}$  for each absorption factor available in table 5.1.

711 For the range of  $D/D_0$  values available, it is possible to use a simple linear fit to get the evolution  
 712 of  $c$ . The linear fit will then use only 2 free parameters,  $a$  and  $b$ , as written in Equation 5.7. This gives  
 713 us the results showed in Figure 5.13. Figure 5.13b confirms that using only a linear fit to extract  $c$  is  
 714 enough as the evolution of the rate that can be obtained superimposes well on the simulation points.

$$c \left( \frac{D}{D_0} \right) = a \frac{D}{D_0} + b \quad (5.7)$$

$$F^{ABS} = F_0^{ABS} \left( a + \frac{bD_0}{D} \right)^2 \quad (5.8)$$

$$\Delta F^{ABS} = F^{ABS} \left[ \frac{\Delta F_0^{ABS}}{F_0^{ABS}} + 2 \frac{\Delta a + \Delta b \frac{D_0}{D}}{a + \frac{bD_0}{D}} \right] \quad (5.9)$$

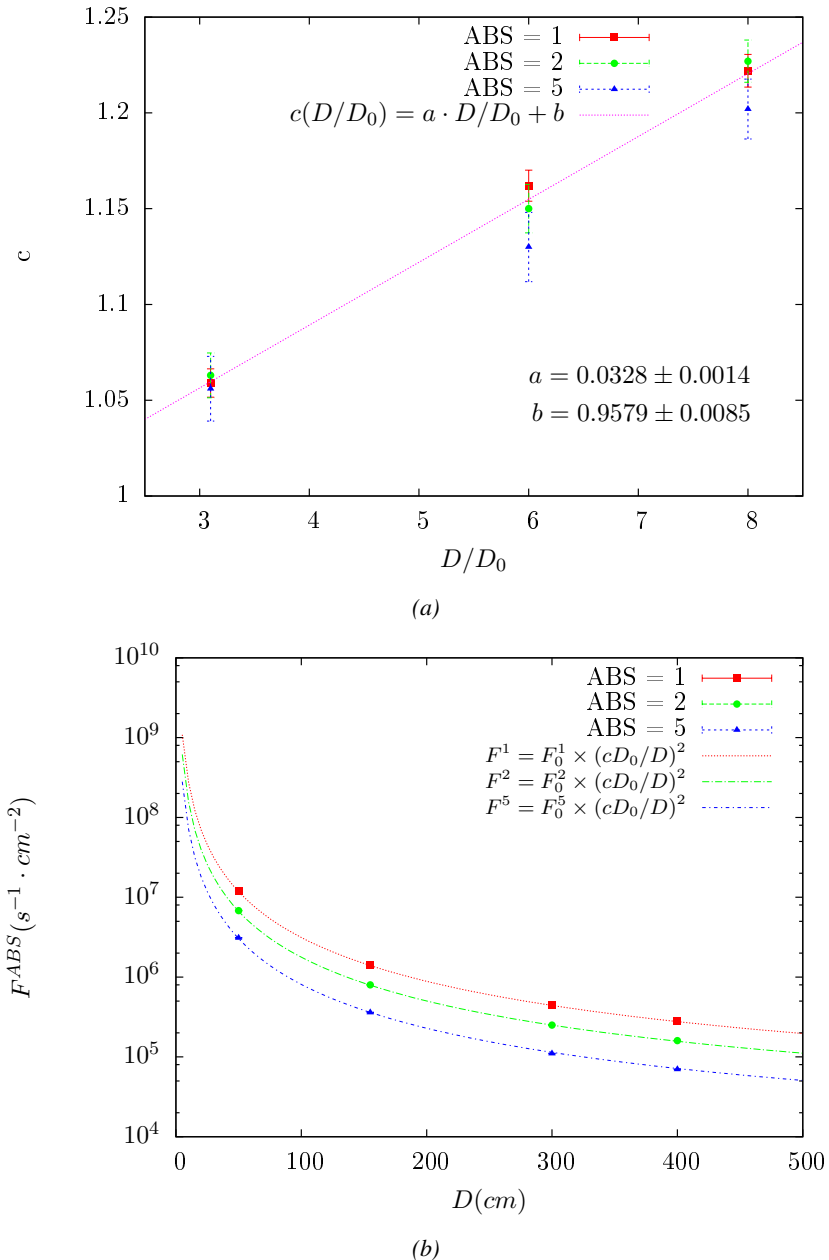


Figure 5.13: Figure 5.13a shows the linear approximation fit done via formulae 5.7 on data from table 5.2. Figure 5.13b shows a comparison of this model with the simulated flux using  $a$  and  $b$  given in figure 5.13a in formulae 5.4 and the reference value  $D_0 = 50\text{cm}$  and the associated flux for each absorption factor  $F_0^{ABS}$  from table 5.1

In the case of the 2014 GIF tests, the RPC plane is located at a distance  $D = 206\text{ cm}$  to the source. Moreover, to estimate the strength of the flux in 2014, it is necessary to consider the nuclear decay through time associated to the Cesium source whose half-life is well known ( $t_{1/2} = (30.05 \pm 0.08)\text{ y}$ ). The very first source activity measurement has been done on the 5<sup>th</sup> of March 1997 while the GIF

719 tests where done in between the 20<sup>th</sup> and the 31<sup>st</sup> of August 2014, i.e. at a time  $t = (17.47 \pm 0.02)$  y  
 720 resulting in an attenuation of the activity from 740 GBq in 1997 to 494 GBq in 2014. All the needed  
 721 information to extrapolate the flux through our detector in 2014 has now been assembled, leading  
 722 to the Table 5.3. It is interesting to note that for a common RPC sensitivity to  $\gamma$  of  $2 \cdot 10^{-3}$ , the  
 723 order of magnitude of the estimated hit rate per unit area is of the order of the kHz for the fully  
 724 opened source. Moreover, taking profit of the two working absorbers, it will be possible to scan  
 725 background rates at 0 Hz,  $\sim 300$  Hz as well as  $\sim 600$  Hz. Without source, a good estimate of the  
 726 intrinsic performance will be available. Then at 300 Hz, the goal will be to show that the detectors  
 727 fulfill the performance certification of CMS RPCs. Then a first idea of the performance of the  
 728 detectors at higher background will be provided with absorption factors 2 ( $\sim 600$  Hz) and 1 (no  
 729 absorption). *[Here I will also put a reference to the plot showing the estimated background rate at  
 730 the level of RE3/1 in the case of HL-LHC but this one being in another chapter, I will do it later.]*

Nominal ABS	Photon flux $F$ [ $s^{-1}cm^{-2}$ ]			Hit rate/unit area [ $Hz cm^{-2}$ ] at $D^{2014} = 206$ cm
	at $D_0^{1997} = 50$ cm	at $D_0^{1997} = 206$ cm	at $D^{2014} = 206$ cm	
1	$0.12 \cdot 10^8 \pm 0.2\%$	$0.84 \cdot 10^6 \pm 0.3\%$	$0.56 \cdot 10^6 \pm 0.3\%$	$1129 \pm 32$
2	$0.68 \cdot 10^7 \pm 0.3\%$	$0.48 \cdot 10^6 \pm 0.3\%$	$0.32 \cdot 10^6 \pm 0.3\%$	$640 \pm 19$
5	$0.31 \cdot 10^7 \pm 0.4\%$	$0.22 \cdot 10^6 \pm 0.3\%$	$0.15 \cdot 10^6 \pm 0.3\%$	$292 \pm 9$

Table 5.3: The data at  $D_0$  in 1997 is taken from [6]. In a second step, using Equations 5.8 and 5.9, the flux at  $D$  can be estimated in 1997. Then, taking into account the attenuation of the source activity, the flux at  $D$  can be estimated at the time of the tests in GIF in 2014. Finally, assuming a sensitivity of the RPC to  $\gamma$   $s = 2 \cdot 10^{-3}$ , an estimation of the hit rate per unit area is obtained.

<sup>731</sup> **5.2.4.2 Dose measurements**

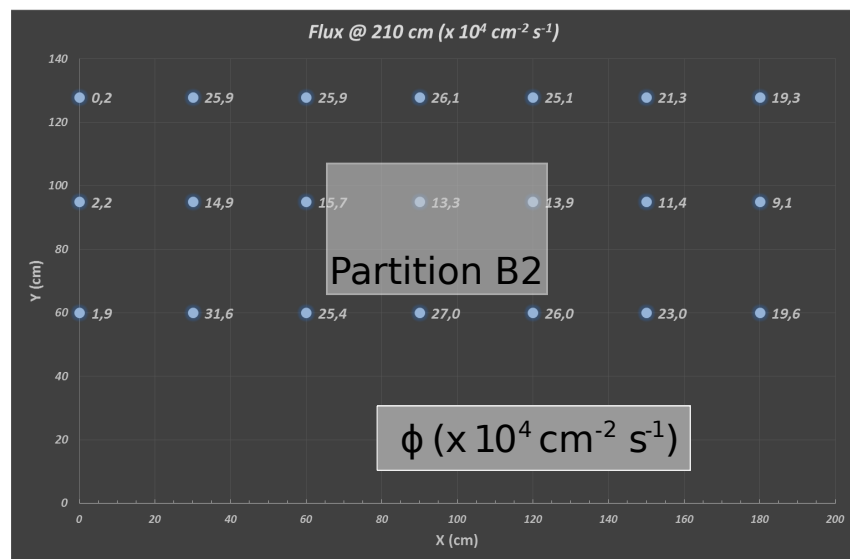


Figure 5.14: Dose measurements has been done in a plane corresponding to the tents front side. This plan is 1900 mm away from the source. As explained in the first chapter, a lens-shaped lead filter provides a uniform photon flux in the vertical plan orthogonal to the beam direction. If the second line of measured fluxes is not taken into account because of lower values due to experimental equipments in the way between the source and the tent, the uniformity of the flux is well showed by the results.

<sup>732</sup> **5.2.5 Results and discussions**

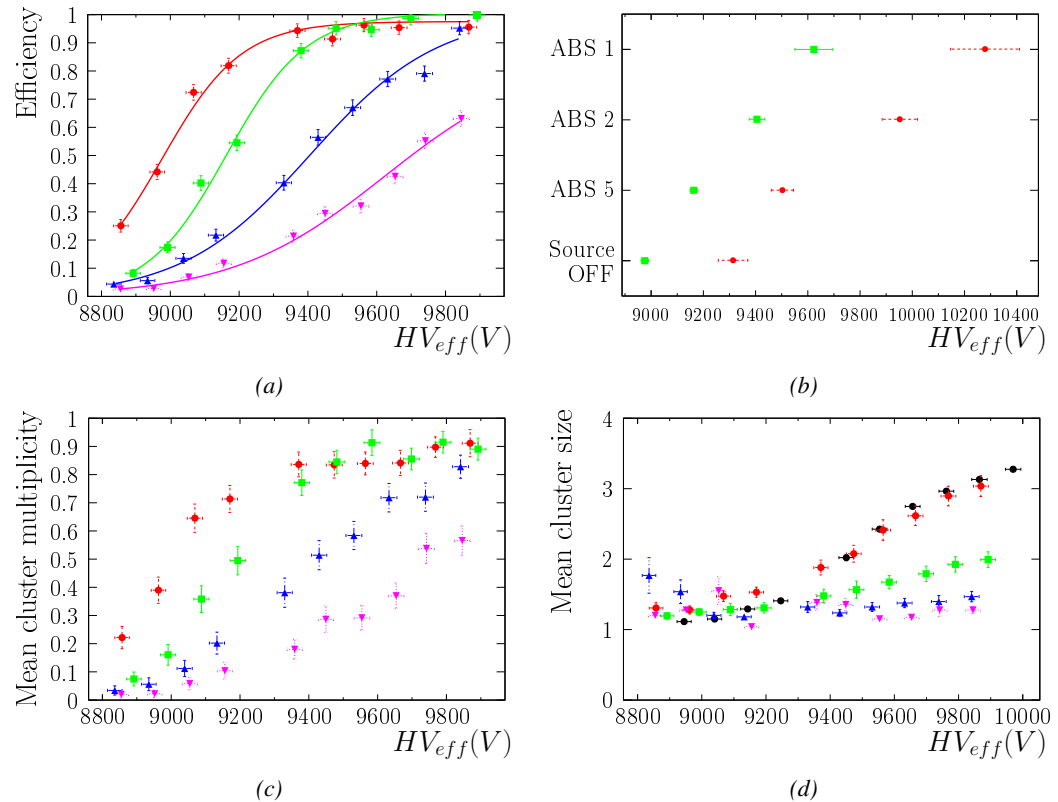


Figure 5.15

**733 5.3 Longevity tests at GIF++**

734 Longevity studies imply a monitoring of the performance of the detectors probed using a high inten-  
735 sity muon beam in a irradiated environment by periodically measuring their rate capability, the dark  
736 current running through them and the bulk resistivity of the Bakelite composing their electrodes.  
737 GIF++, with its very intense  $^{137}\text{Cs}$  source, provides the perfect environment to perform such kind  
738 of tests. Assuming a maximum acceleration factor of 3, it is expected to accumulate the equivalent  
739 charge in 1.7 years.

740 As the maximum background is found in the endcap, the choice naturally was made to focus the  
741 GIF++ longevity studies on endcap chambers. Most of the RPC system was installed in 2007. Nev-  
742 ertheless, the large chambers in the fourth endcap (RE4/2 and RE4/3) have been installed during  
743 LS1 in 2014. The Bakelite of these two different productions having different properties, four spare  
744 chambers of the present system were selected, two RE2,3/2 spares and two RE4/2 spares. Having  
745 two chambers of each type allows to always keep one of them non irradiated as reference, the per-  
746 formance evolution of the irradiated chamber being then compared through time to the performance  
747 of the non irradiated one.

748 The performance of the detectors under different level of irradiation is measured periodically dur-  
749 ing dedicated test beam periods using the H4 muon beam. In between these test beam periods, the  
750 two RE2,3/2 and RE4/2 chambers selected for this study are irradiated by the  $^{137}\text{Cs}$  source in order  
751 to accumulate charge and the gamma background is monitored, as well as the currents. The two  
752 remaining chambers are kept non-irradiated as reference detectors. Due to the limited gas flow in  
753 GIF++, the RE4 chamber remained non-irradiated until end of November 2016 where a new mass  
754 flow controller has been installed allowing for bigger volumes of gas to flow in the system.

755 Figures 5.16 and 5.17 give us for different test beam periods, and thus for increasing integrated  
756 charge through time, a comparison of the maximum efficiency, obtained using a sigmoid-like func-  
757 tion, and of the working point of both irradiated and non irradiated chambers [8]. No aging is yet to  
758 see from this data, the shifts in  $\gamma$  rate per unit area in between irradiated and non irradiated detec-  
759 tors and RE2 and RE4 types being easily explained by a difference of sensitivity due to the various  
760 Bakelite resistivities of the HPL electrodes used for the electrode production.

761 Collecting performance data at each test beam period allows us to extrapolate the maximum effi-  
762 ciency for a background hit rate of  $300\text{ Hz}/\text{cm}^2$  corresponding to the expected HL-LHC conditions.  
763 Aging effects could emerge from a loss of efficiency with increasing integrated charge over time,  
764 thus Figure 5.18 helps us understand such degradation of the performance of irradiated detectors in  
765 comparison with non irradiated ones. The final answer for an eventual loss of efficiency is given in  
766 Figure 5.19 by comparing for both irradiated and non irradiated detectors the efficiency sigmoids  
767 before and after the longevity study. Moreover, to complete the performance information, the Bake-  
768 lite resistivity is regularly measured thanks to  $Ag$  scans (Figure 5.20) and the noise rate is monitored  
769 weekly during irradiation periods (Figure 5.21). At the end of 2016, no signs of aging were observed  
770 and further investigation is needed to get closer to the final integrated charge requirements proposed  
771 for the longevity study of the present CMS RPC sub-system.

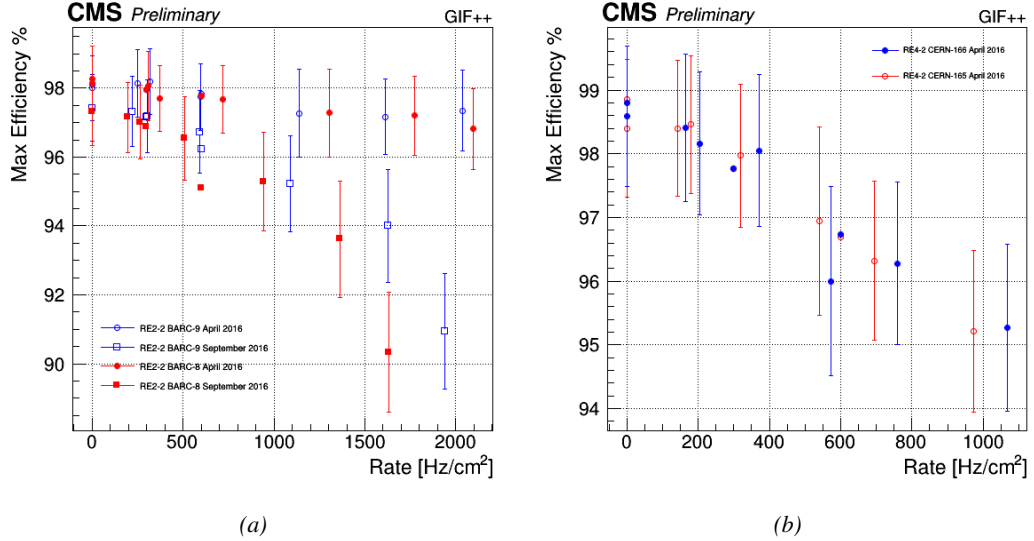


Figure 5.16: Evolution of the maximum efficiency for RE2 (5.16a) and RE4 (5.16b) chambers with increasing extrapolated  $\gamma$  rate per unit area at working point. Both irradiated (blue) and non irradiated (red) chambers are shown.

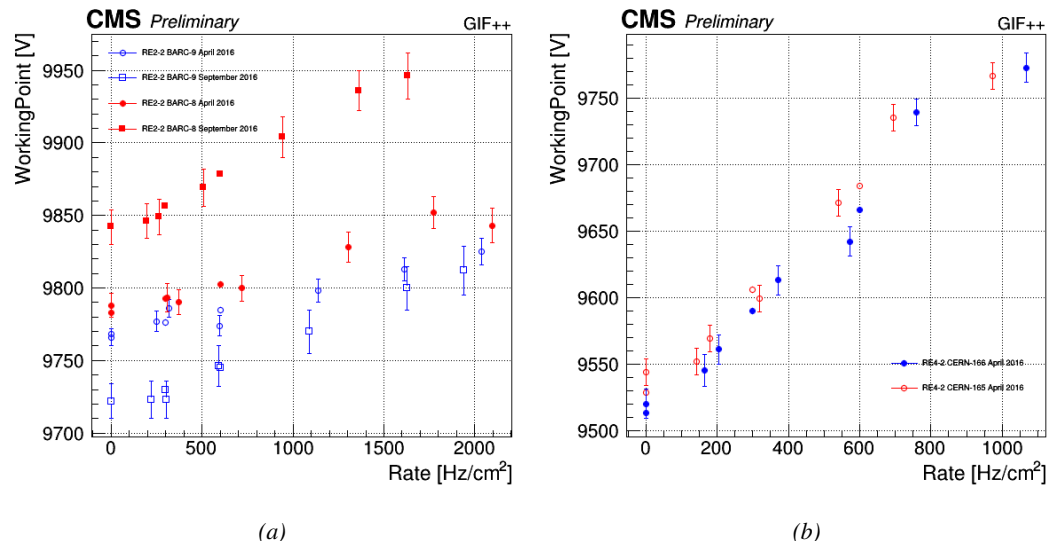
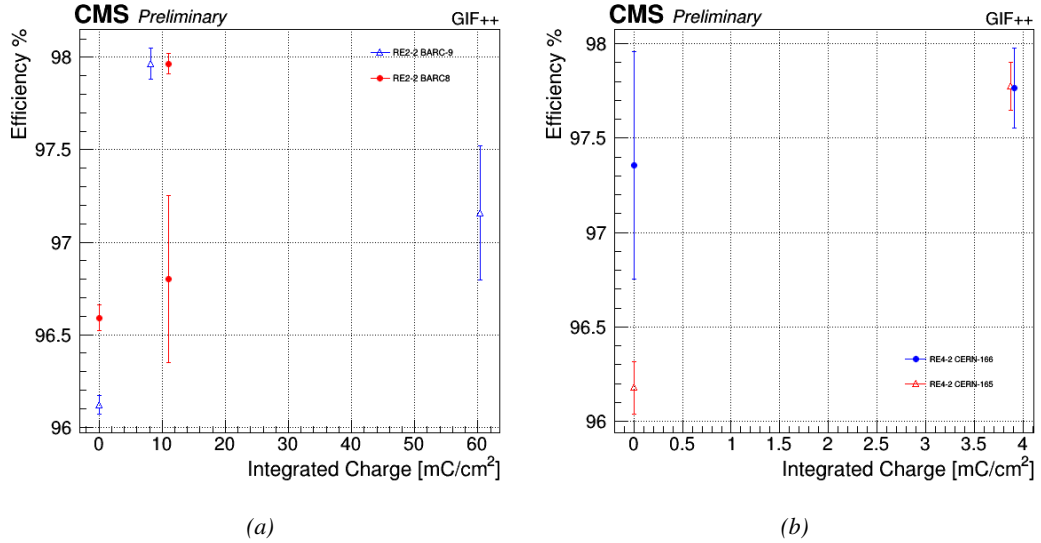
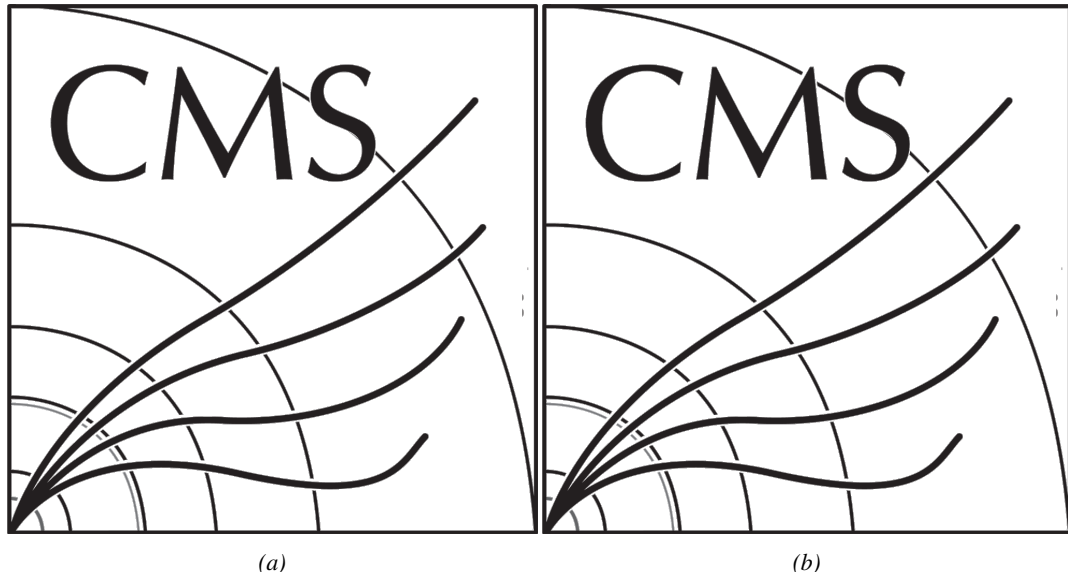


Figure 5.17: Evolution of the working point for RE2 (5.17a) and RE4 (5.17b) with increasing extrapolated  $\gamma$  rate per unit area at working point. Both irradiated (blue) and non irradiated (red) chambers are shown.



*Figure 5.18: Evolution of the maximum efficiency at HL-LHC conditions, i.e. a background hit rate per unit area of 300 Hz/cm<sup>2</sup>, with increasing integrated charge for RE2 (5.18a) and RE4 (5.18b) detectors. Both irradiated (blue) and non irradiated (red) chambers are shown. The integrated charge for non irradiated detectors is recorded during test beam periods and stays small with respect to the charge accumulated in irradiated chambers.*



*Figure 5.19: Comparison of the efficiency sigmoid before (triangles) and after (circles) irradiation for RE2 (5.19a) and RE4 (5.19b) detectors. Both irradiated (blue) and non irradiated (red) chambers are shown.*

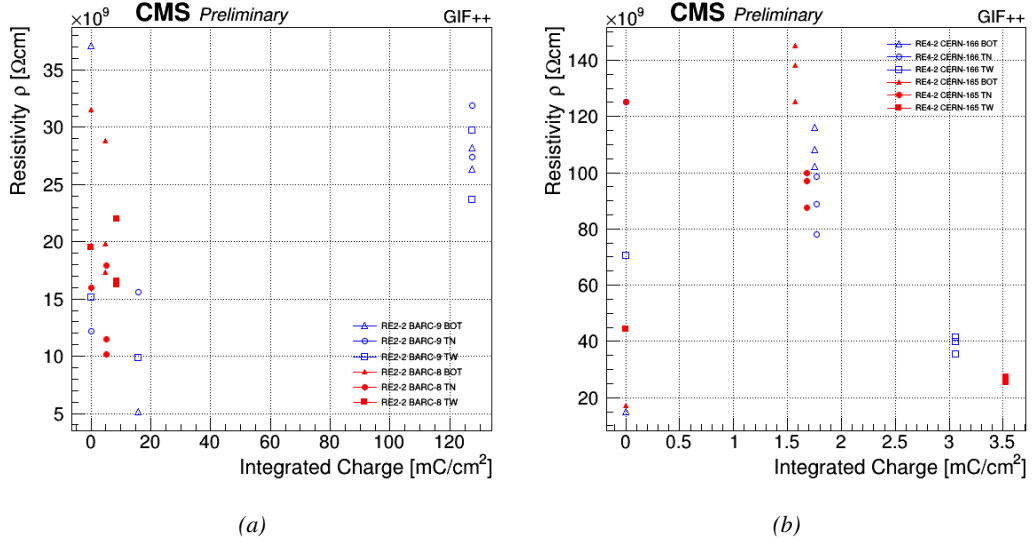


Figure 5.20: Evolution of the Bakelite resistivity for RE2 (5.20a) and RE4 (5.20b) detectors. Both irradiated (blue) and non-irradiated (red) chambers are shown.

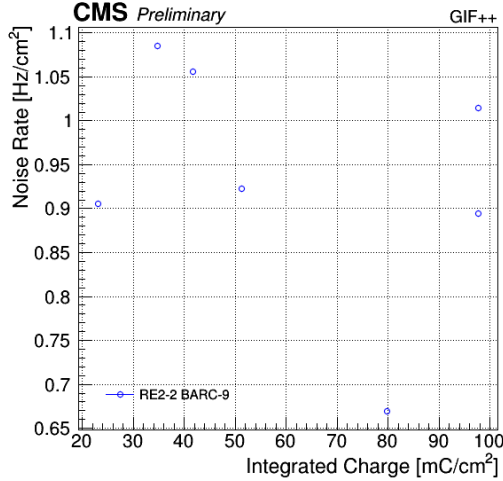


Figure 5.21: Evolution of the noise rate per unit area for the irradiated chamber RE2-2-BARC-9 only.

### 5.3.1 Description of the Data Acquisition

For the longevity studies, four spare chambers of the present system are used. Two spare RPCs of the RE2,3 stations as well as two spare RPCs from the new RE4 stations have been mounted in a Trolley. Six RE4 gaps are also placed in the trolley. The trolley is placed inside the GIF++ in the upstream region of the bunker, taking the cesium source as a reference. The trolley is oriented for the detection surface of the chambers to be orthogonal to the beam line. The system can be moved along the orthogonal plane in order to have the beam in all  $\eta$ -partitions. For the aging the trolley is

780 moved outside the beam line and is placed in a distance of 5.2 m to the source, which irradiates the  
 781 bunker using an attenuation filter of 2.2 which corresponds to a fluence of  $10^7 \text{ gamma/cm}^2$ .

782 During GIF++ operation, the data collected can be divided into different categories as several  
 783 parameters are monitored in addition to the usual RPC performance data. On one hand, to know  
 784 the performance of a chamber, it is need to measure its efficiency and to know the background  
 785 conditions in which it is operated. To do this, the hit signals from the chamber are recorded and  
 786 stored in a ROOT file via a Data Acquisition (DAQ) software. On the other hand, it is also very  
 787 important to monitor parameters such as environmental pressure and temperature, gas temperature  
 788 and humidity, RPC HV, LV, and currents, or even source and beam status. This is done through the  
 789 GIF++ web Detector Control Software (DCS) that stores this information in a database.

790 Two different types of tests are conducted on RPCs via the DAQ. Indeed, the performance of the  
 791 detectors is measured periodically during dedicated test beam periods using the H4 muon beam. In  
 792 between these test beam periods, when the beam is not available, the chambers are irradiated by the  
 793  $^{137}\text{Cs}$  in order to accumulate deposited charge and the gamma background is measured.

794 RPCs under test are connected through LVDS cables to V1190A Time-to-Digital Converter  
 795 (TDC) modules manufactured by CAEN. These modules, located in the rack area outside of the  
 796 bunker, get the logic signals sent by the chambers and save them into their buffers. Due to the  
 797 limited size of the buffers, the collected data is regularly erased and replaced. A trigger signal is  
 798 needed for the TDC modules to send the useful data to the DAQ computer via a V1718 CAEN USB  
 799 communication module.

800 In the case of performance test, the trigger signal used for data acquisition is generated by the  
 801 coincidence of three scintillators. A first one is placed upstream outside of the bunker, a second one  
 802 is placed downstream outside of the bunker, while a third one is placed in front of the trolley, close by  
 803 the chambers. Every time a trigger is sent to the TDCs, i.e. every time a muon is detected, knowing  
 804 the time delay in between the trigger and the RPC signals, signals located in the right time window  
 805 are extracted from the buffers and saved for later analysis. Signals are taken in a time window of  
 806 400 ns centered on the muon peak (here we could show a time spectrum). On the other hand, in the  
 807 case of background rate measurement, the trigger signal needs to be "random" not to measure muons  
 808 but to look at gamma background. A trigger pulse is continuously generated at a rate of 300 Hz using  
 809 a dual timer. To integrate an as great as possible time, all signals contained within a time window of  
 810 10us prior to the random trigger signal are extracted form the buffers and saved for further analysis  
 811 (here another time spectrum to illustrate could be useful, maybe even place both spectrum together  
 812 as a single Figure).

813 The signals sent to the TDCs correspond to hit collections in the RPCs. When a particle hits  
 814 a RPC, it induce a signal in the pickup strips of the RPC readout. If this signal is higher than the  
 815 detection threshold, a LVDS signal is sent to the TDCs. The data is then organised into 4 branches  
 816 keeping track of the event number, the hit multiplicity for the whole setup, and the time and channel  
 817 profile of the hits in the TDCs.

### 818 5.3.2 RPC current, environmental and operation parameter monitoring

819 In order to take into account the variation of pressure and temperature between different data taking  
 820 periods the applied voltage is corrected following the relationship :

$$821 \quad HV_{eff} = HV_{app} \times \left( 0.2 + 0.8 \cdot \frac{P_0}{P} \times \frac{T}{T_0} \right) \quad (5.10)$$

821 where  $T_0$  (=293 K) and  $P_0$  (=990 mbar) are the reference values.

822 **5.3.3 Measurement procedure**

823 Insert a short description of the online tools (DAQ, DCS, DQM).

824 Insert a short description of the offline tools : tracking and efficiency algorithm.

825 Identify long term aging effects we are monitoring the rates per strip.

826 **5.3.4 Longevity studies results**



# 6

827

828

## Investigation on high rate RPCs

829 **6.1 Rate limitations and ageing of RPCs**

830 **6.1.1 Low resistivity electrodes**

831 **6.1.2 Low noise front-end electronics**

832 **6.2 Construction of prototypes**

833 **6.3 Results and discussions**



# 7

834

835

## Conclusions and outlooks

<sup>836</sup> **7.1 Conclusions**

<sup>837</sup> **7.2 Outlooks**



## References

838

- 839 [1] CERN. Geneva. LHC Experiments Committee. *The CMS muon project : Technical Design*  
840 *Report*. Tech. rep. CERN-LHCC-97-032. CMS Collaboration, 1997.
- 841 [2] CERN. Geneva. LHC Experiments Committee. *Technical Proposal for the Phase-II Upgrade*  
842 *of the CMS Detector*. Tech. rep. CERN-LHCC-2015-010. CMS Collaboration, 2015.
- 843 [3] CERN. Geneva. LHC Experiments Committee. *CMS, the Compact Muon Solenoid : technical*  
844 *proposal*. Tech. rep. CERN-LHCC-94-38. CMS Collaboration, 1994.
- 845 [4] M. Abbrescia et al. “Study of long-term performance of CMS RPC under irradiation at the  
846 CERN GIF”. In: *NIMA* 533 (2004), pp. 102–106.
- 847 [5] H.C. Kim et al. “Quantitative aging study with intense irradiation tests for the CMS forward  
848 RPCs”. In: *NIMA* 602 (2009), pp. 771–774.
- 849 [6] S. Agosteo et al. “A facility for the test of large-area muon chambers at high rates”. In: *NIMA*  
850 452 (2000), pp. 94–104.
- 851 [7] PoS, ed. *CERN GIF ++ : A new irradiation facility to test large-area particle detectors for*  
852 *the high-luminosity LHC program*. Vol. TIPP2014. 2014, pp. 102–109.
- 853 [8] M. Abbrescia et al. “Cosmic ray tests of double-gap resistive plate chambers for the CMS  
854 experiment”. In: *NIMA* 550 (2005), pp. 116–126.
- 855 [9] A. Fagot. *GIF++ DAQ v4.0*. 2017. URL: [https://github.com/afagot/GIF\\_DAQ](https://github.com/afagot/GIF_DAQ).
- 856 [10] CAEN. *Mod. V1190-VX1190 A/B, 128/64 Ch Multihit TDC*. 14th ed. 2016.
- 857 [11] CAEN. *Mod. V1718 VME USB Bridge*. 9th ed. 2009.
- 858 [12] W-Ie-Ne-R. *VME 6021-23 VXI*. 5th ed. 2016.
- 859 [13] Wikipedia. *INI file*. 2017. URL: [https://en.wikipedia.org/wiki/INI\\_file](https://en.wikipedia.org/wiki/INI_file).
- 860 [14] S. Carrillo A. Fagot. *GIF++ Offline Analysis v6*. 2017. URL: [https://github.com/afagot/GIF\\_OfflineAnalysis](https://github.com/afagot/GIF_OfflineAnalysis).



# A

862

863

## A data acquisition software for CAEN VME TDCs

864

865 Certifying detectors in the perspective of HL-LHC required to develop tools for the GIF++ ex-  
866 periment. Among them was the C++ Data Acquisition (DAQ) software that allows to make the com-  
867 munications in between a computer and TDC modules in order to retrieve the RPC data [9]. In this  
868 appendix, details about this software, as of how the software was written, how it functions and how  
869 it can be exported to another similar setup, will be given.

### 870 A.1 GIF++ DAQ file tree

871 GIF++ DAQ source code is fully available on github at [https://github.com/afagot/GIF\\_](https://github.com/afagot/GIF_DAQ)  
872 DAQ. The software requires 3 non-optional dependencies:

- 873     • CAEN USB Driver, to mount the VME hardware,  
874     • CAEN VME Library, to communicate with the VME hardware, and  
875     • ROOT, to organize the collected data into a TTree.

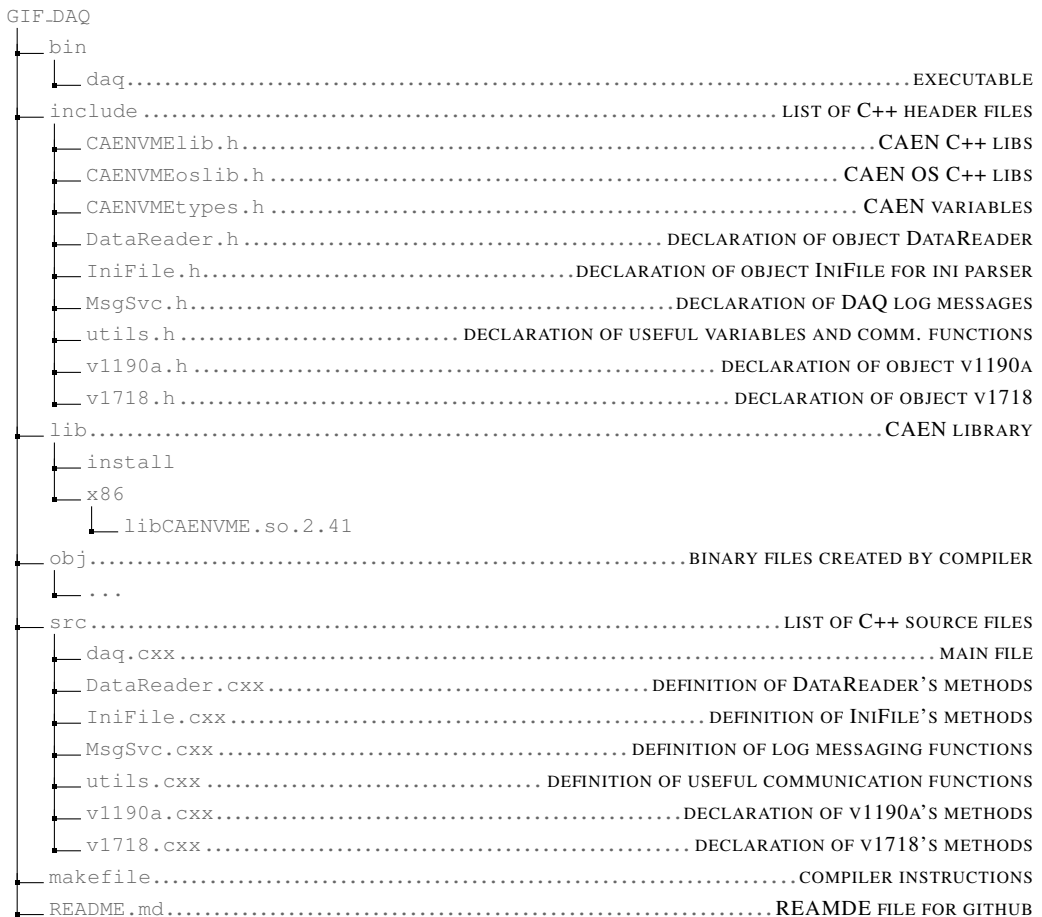
876     The CAEN VME library will not be packaged by distributions and will need to be installed man-  
877 ually. To compile the GIF++ DAQ project via a terminal, from the DAQ folder use the command:

878

879     make

880     The source code tree is provided below along with comments to give an overview of the files' con-  
881 tent. The different objects created for this project (`v1718`, `v1190a`, `IniFile` & `DataReader`) will be  
882 described in details in the following sections.

883



## 884 A.2 Usage of the DAQ

885 GIF++ DAQ, as used in GIF++, is not a standalone software. Indeed, the system being more complexe,  
 886 the DAQ only is a sub-layer of the software architecture developped to control and monitor  
 887 the RPCs that are placed into the bunker for performance study in an irradiated environment. The top  
 888 layer of GIF++ is a Web Detector Control System (webDCS) application. The DAQ is only called  
 889 by the webDCS when data needs to be acquired. The webDCS operates the DAQ through command  
 890 line. To start the DAQ, the webDCS calls:

891

892   bin/daq /path/to/the/log/file/in/the/output/data/folder

893 where /path/to/the/log/file/in/the/output/data/folder is the only argument required. This  
 894 log file is important for the webDCS as this file contains all the content of the communication of the  
 895 webDCS and the different systems monitored by the webDCS. Its content is constantly displayed  
 896 during data taking for the users to be able to follow the operations. The communication messages  
 897 are normally sent to the webDCS log file via the functions declared in file MsgSvc.h, typically  
 898 MSG\_INFO(string message).

899

### 900 A.3 Description of the readout setup

901 The CMS RPC setup at GIF++ counts 5 V1190A Time-to-Digital Converter (TDC) manufactured  
 902 by CAEN [10]. V1190A are VME units accepting 128 independent Multi-Hit/Multi-Event TDC  
 903 channels whose signals are treated by 4 100 ps high performance TDC chips developed by CERN  
 904 / ECP-MIC Division. The communication between the computer and the TDCs to transfer data is  
 905 done via a V1718 VME master module also manufactured by CAEN and operated from a USB  
 906 port [11]. These VME modules are all hosted into a 6U VME 6021 powered crate manufactured by  
 907 W-Ie-Ne-R than can accommodate up to 21 VME bus cards [12]. These 3 components of the DAQ  
 908 setup are shown in Figure A.1.

909

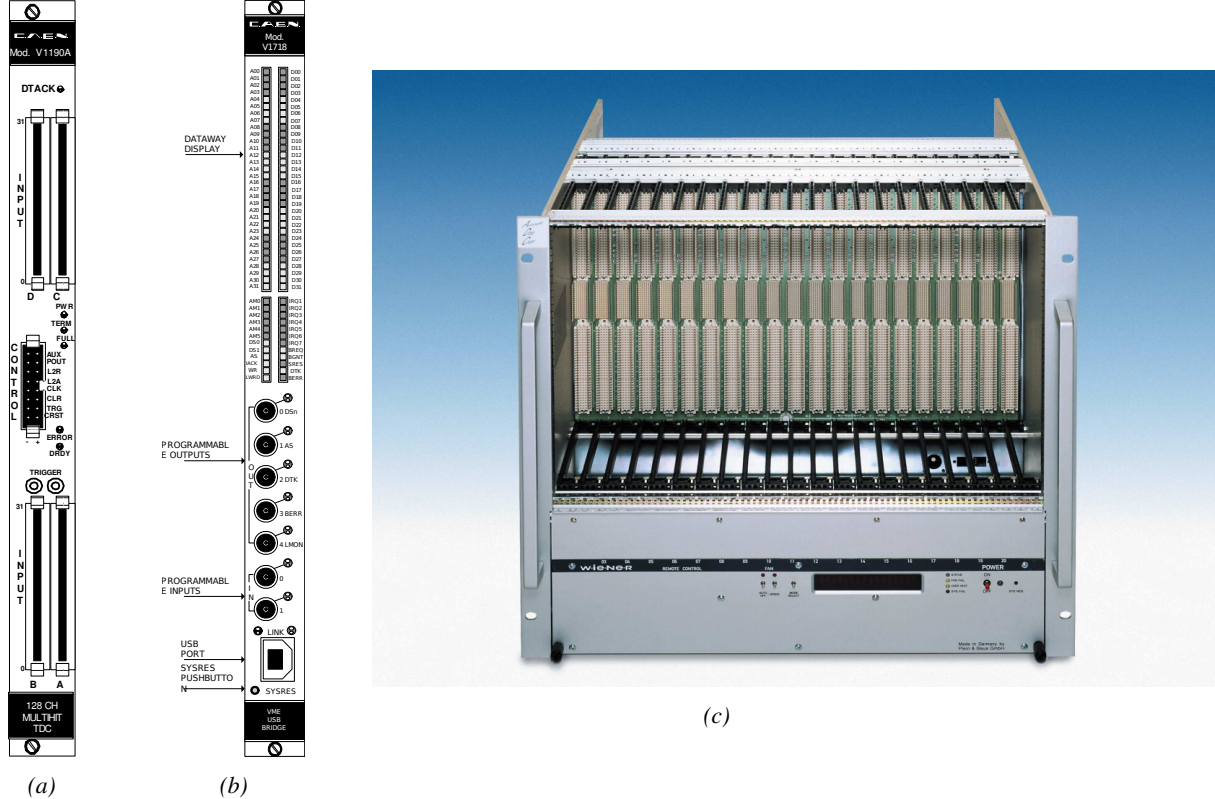


Figure A.1: (A.1a) View of the front panel of a V1190A TDC module [10]. (A.1b) View of the front panel of a V1718 Bridge module [11]. (A.1c) View of the front panel of a 6U 6021 VME crate [12].

910

### A.4 Data read-out

911 To efficiently perform a data readout algorithm, C++ objects to handle the VME modules (TDCs  
 912 and VME bridge) have been created along with objects to store data and read the configuration file

913 that comes as an input of the DAQ software.

914

### 915 A.4.1 V1190A TDCs

916 The DAQ used at GIF takes profit of the *Trigger Matching Mode* offered by V1190A modules.  
 917 This setting is enabled through the method `v1190a::SetTrigMatching (int ntdcs)` where `ntdcs`  
 918 is the total number of TDCs in the setup this setting needs to be enabled for (Source Code A.1). A  
 919 trigger matching is performed in between a trigger time tag, a trigger signal sent into the TRIGGER  
 920 input of the TDC visible on Figure A.1a, and the channel time measurements, signals recorded from  
 921 the detectors under test in our case. Control over this data acquisition mode, explained through  
 922 Figure A.2, is offered via 4 programmable parameters:

- 923 • **match window:** the matching between a trigger and a hit is done within a programmable time  
 924 window. This is set via the method

```
925     void v1190a::SetTrigWindowWidth(UINT windowWidth, int ntdcs)
```

- 926 • **window offset:** temporal distance between the trigger tag and the start of the trigger matching  
 927 window. This is set via the method

```
928     void v1190a::SetTrigWindowWidth(UINT windowWidth, int ntdcs)
```

- 929 • **extra search margin:** an extended time window is used to ensure that all matching hits are  
 930 found. This is set via the method

```
931     void v1190a::SetTrigSearchMargin(UINT searchMargin, int ntdcs)
```

- 932 • **reject margin:** older hits are automatically rejected to prevent buffer overflows and to speed  
 933 up the search time. This is set via the method

```
934     void v1190a::SetTrigRejectionMargin(UINT rejectMargin, int ntdcs)
```

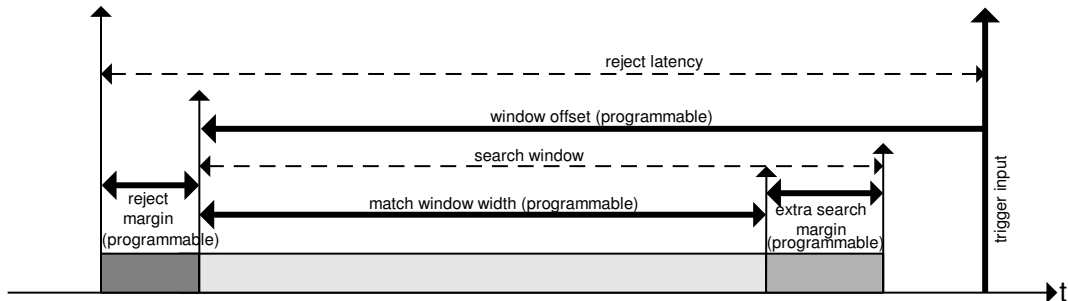


Figure A.2: Module V1190A Trigger Matching Mode timing diagram [10].

935 Each of these 4 parameters are given in number of clocks, 1 clock being 25 ns long. It is easy to  
 936 understand at this level that there are 3 possible functioning settings:

- 937 • **1:** the match window is entirely contained after the trigger signal,

- 938 • **2:** the match window overlaps the trigger signal, or

- 939 • **3:** the match window is entirely contained before the trigger signal as displayed on Figure A.2.

940 In both the first and second cases, the sum of the window width and of the offset can be set to  
941 a maximum of 40 clocks, which corresponds to 1  $\mu$ s. Evidently, the offset can be negative, allowing  
942 for a longer match window, with the constraint of having the window ending at most 1  $\mu$ s after the  
943 trigger signal. In the third case, the maximum negative offset allowed is of 2048 clocks (12 bit) cor-  
944 responding to 51.2  $\mu$ s, the match window being strictly smaller than the offset. In the case of GIF++,  
945 the choice has been made to use this last setting by delaying the trigger signal. During the studies  
946 performed in GIF++, both the efficiency of the RPCs, probed using a muon beam, and the noise or  
947 gamma background rate are monitored. The extra search and reject margins are left unused.  
948 To probe the efficiency of RPC detectors, the trigger time tag is provided by the coïncidence of  
949 scintillators when a bunch of muons passes through GIF++ area is used to trigger the data acquisi-  
950 tion. For this measurement, it is useful to reduce the match window width only to contain the muon  
951 information. Indeed, the delay in between a trigger signal and the detection of the corresponding  
952 muon in the RPC being very contant (typically a few tens of ns due to jitter and cable length), the  
953 muon signals are very localised in time. Thus, due to a delay of approximalety 325 ns in between  
954 the muons and the trigger, the settings where chosen to have a window width of 24 clocks (600 ns)  
955 centered on the muon peak thanks to a negative offset of 29 clocks (725 ns).  
956 On the otherhand, monitoring the rates don't require for the DAQ to look at a specific time window.  
957 It is important to integrate enough time to have a robust measurement of the rate as the number of  
958 hits per time unit. The triggerring signal is provided by a pulse generator at a frequency of 300 Hz  
959 to ensure that the data taking occurs in a random way, with respect to beam physics, to probe only  
960 the irradiation spectrum on the detectors. The match window is set to 400 clocks (10  $\mu$ s) and the  
961 negative offset to 401 clocks as it needs to exceed the value of the match window.

```

962
class v1190a
{
    private :
        long             Handle;
        vector<Data32>   Address;
        CVDataWidth      DataWidth;
        CVAddressModifier AddressModifier;

    public:

        v1190a(long handle, IniFile *inifile, int ntdcs);
        ~v1190a();
        Data16 write_op_reg(Data32 address, int code, string error);
        Data16 read_op_reg(Data32 address, string error);
        void Reset(int ntdcs);
        void Clear(int ntdcs);
        void TestWR(Data16 value,int ntdcs);
        void CheckTDCStatus(int ntdcs);
        void CheckCommunication(int ntdcs);
        void SetTDCTestMode(Data16 mode,int ntdcs);
        void SetTrigMatching(int ntdcs);
        void SetTrigTimeSubtraction(Data16 mode,int ntdcs);
        void SetTrigWindowWidth(Uint windowHeight,int ntdcs);
        void SetTrigWindowOffset(Uint windowOffset,int ntdcs);
        void SetTrigSearchMargin(Uint searchMargin,int ntdcs);
        void SetTrigRejectionMargin(Uint rejectMargin,int ntdcs);
        void GetTrigConfiguration(int ntdcs);
        void SetTrigConfiguration(IniFile *inifile,int ntdcs);
        void SetTDCDetectionMode(Data16 mode,int ntdcs);
        void SetTDCResolution(Data16 lsb,int ntdcs);
        void SetTDCDeadTime(Data16 time,int ntdcs);
        void SetTDCHeadTrailer(Data16 mode,int ntdcs);
        void SetTDCEventSize(Data16 size,int ntdcs);
        void SwitchChannels(IniFile *inifile,int ntdcs);
        void SetIRQ(Data32 level, Data32 count,int ntdcs);
        void SetBlockTransferMode(Data16 mode,int ntdcs);
        void Set(IniFile *inifile,int ntdcs);
        void CheckStatus(CVErrorCodes status) const;
        int ReadBlockD32(Uint tdc, const Data16 address,
                         Data32 *data, const Uint words, bool ignore_berr);
        Uint Read(RAWData *DataList,int ntdcs);
};

963

```

964       *Source Code A.1: Description of C++ object v1190a.*

965       The v1190a object, defined in the DAQ software as in Source Code A.1, offers the possibility to  
 966       concatenate all TDCs in the readout setup into a single object containing a list of hardware addresses  
 967       (addresses to access the TDCs' buffer through the VME crate) and each constructor and method acts  
 968       on the list of TDCs.  
 969

#### 970     **A.4.2 DataReader**

971       Enabled thanks to v1190a::SetBlockTransferMode(Data16 mode, int ntdcs), the data transfer  
 972       is done via Block Transfer (BLT). Using BLT allows to tranfer a fixed number of events called a  
 973       *block*. This is used together with an Almost Full Level (AFL) of the TDCs' output buffers, defined

974 through `v1190a::SetIRQ(Data32 level, Data32 count, int ntdcs)`. This AFL gives the maximum amount of 32735 words (16 bits, corresponding to the depth of a TDC output buffer) that can  
 975 be written in a buffer before an Interrupt Request (IRQ) is generated and seen by the VME Bridge,  
 976 stopping the data acquisition to transfer the content of each TDC buffers before resuming. For each  
 977 trigger, 6 words or more are written into the TDC buffer:

- 979     • a **global header** providing information of the event number since the beginning of the data  
     acquisition,
- 981     • a **TDC header**,
- 982     • the **TDC data** (*if any*), 1 for each hit recorded during the event, providing the channel and the  
     time stamp associated to the hit,
- 984     • a **TDC error** providing error flags,
- 985     • a **TDC trailer**,
- 986     • a **global trigger time tag** that provides the absolute trigger time relatively to the last reset,  
     and
- 988     • a **global trailer** providing the total word count in the event.

989     As previously described in Section 4.4.3, CMS RPC FEEs provide us with 100 ns long LVDS  
 990 output signals that are injected into the TDCs' input. Any avalanche signal that gives a signal above  
 991 the FEEs threshold is thus recorded by the TDCs as a hit within the match window. Each hit is  
 992 assigned to a specific TDC channel with a time stamp, with a precision of 100 ps. The reference  
 993 time,  $t_0 = 0$ , is provided by the beginning of the match window. Thus for each trigger, coming from  
 994 a scintillator coincidence or the pulse generator, a list of hits is stored into the TDCs' buffers and  
 995 will then be transferred into a ROOT Tree.

996     When the BLT is used, it is easy to understand that the maximum number of words that have  
 997 been set as ALF will not be a finite number of events or, at least, the number of events that would  
 998 be recorded into the TDC buffers will not be a multiple of the block size. In the last BLT cycle to  
 1000 transfer data, the number of events to transfer will most probably be lower than the block size. In that  
 1001 case, the TDC can add fillers at the end of the block but this option requires to send more data to the  
 1002 computer and is thus a little slower. Another solution is to finish the transfer after the last event by  
 1003 sending a bus error that states that the BLT reached the last event in the pile. This method has been  
 1004 chosen in GIF++.

1005     Due to irradiation, an event in GIF++ can count up to 300 words per TDC. A limit of 4096 words  
 1006 (12 bits) has been set to generate IRQ which represent from 14 to almost 700 events depending on  
 1007 the average of hits collected per event. Then the block size has been set to 100 events with enabled  
 1008 bus errors. When an AFL is reached for one of the TDCs, the VME bridge stops the acquisition by  
 1009 sending a BUSY signal.

1011

```
1012 The data is then transferred one TDC at a time into a structure called RAWData (Source Code A.2).  
1013  
struct RAWData{  
    vector<int> *EventList;  
    vector<int> *NHitsList;  
    vector<int> *QFlagList;  
    vector<vector<int> > *ChannelList;  
    vector<vector<float> > *TimeStampList;  
};
```

*Source Code A.2: Description of data holding C++ structure RAWData.*

In order to organize the data transfer and the data storage, an object called `DataReader` was created (Source Code A.3). On one hand, it has `v1718` and `v1190a` objects as private members for communication purposes, such as VME modules settings via the configuration file `*iniFile` or data read-out through `v1190a::Read()` and on the other hand, it contains the struture `RAWData` that allows to organise the data in vectors reproducing the tree structure of a ROOT file.

```
1021 class DataReader
{
    private:
        bool      StopFlag;
        IniFile  *iniFile;
        Data32   MaxTriggers;
        v1718    *VME;
        int       nTDCs;
        v1190a   *TDCs;
        RAWData  TDCData;

1022 public:
    DataReader();
    virtual ~DataReader();
    void     SetIniFile(string inifilename);
    void     SetMaxTriggers();
    Data32  GetMaxTriggers();
    void     SetVME();
    void     SetTDC();
    int      GetQFlag(Uint it);
    void     Init(string inifilename);
    void     FlushBuffer();
    void     Update();
    string  GetFileName();
    void     WriteRunRegistry(string filename);
    void     Run();
};

};
```

1023 *Source Code A.3: Description of C++ object DataReader.*

1024 Each event is transferred from `TDCData` and saved into branches of a ROOT `TTree` as 3 integers  
 1025 that represent the event ID (`EventCount`), the number of hits read from the TDCs (`nHits`), and the  
 1026 quality flag that provides information for any problem in the data transfer (`qflag`), and 2 lists of  
 1027 `nHits` elements containing the fired TDC channels (`TDCCN`) and their respective time stamps (`TDCTS`),  
 1028 as presented in Source Code A.4. The ROOT file file is named using information contained into  
 1029 the configuration file, presented in section A.5.2. The needed information is extracted using method  
 1030 `DataReader::GetFileName()` and allow to build the output filename format `ScanXXXXXX_HVX_DAQ.root`

1031 where ScanXXXXXX is a 6 digit number representing the scan number into GIFT++ database and HVX  
 1032 the HV step within the scan that can be more than a single digit. An example of ROOT data file is  
 1033 provided with Figure A.3.

```
1034
RAWData TDCData;
TFile *outputFile = new TFile(outputFileName.c_str(),"recreate");
TTree *RAWDataTree = new TTree("RAWData","RAWData");

int EventCount = -9;
int nHits = -8;
int qflag = -7;
vector<int> TDCCh;
vector<float> TDCTS;

RAWDataTree->Branch("EventNumber",&EventCount, "EventNumber/I");
RAWDataTree->Branch("number_of_hits",&nHits,"number_of_hits/I");
RAWDataTree->Branch("Quality_flag",&qflag,"Quality_flag/I");
RAWDataTree->Branch("TDC_channel",&TDCCh);
RAWDataTree->Branch("TDC_TimeStamp",&TDCTS);

1035
//...
//Here read the TDC data using v1190a::Read() and place it into
//TDCData for as long as you didn't collect the requested amount
//of data.
//...

for(Uint i=0; i<TDCData.EventList->size(); i++){
    EventCount = TDCData.EventList->at(i);
    nHits = TDCData.NHitsList->at(i);
    qflag = TDCData.QFlagList->at(i);
    TDCCh = TDCData.ChannelList->at(i);
    TDCTS = TDCData.TimeStampList->at(i);
    RAWDataTree->Fill();
}
```

1036 *Source Code A.4: Highlight of the data transfer and organisation within DataReader::Run() after the data has been collected into TDCData.*

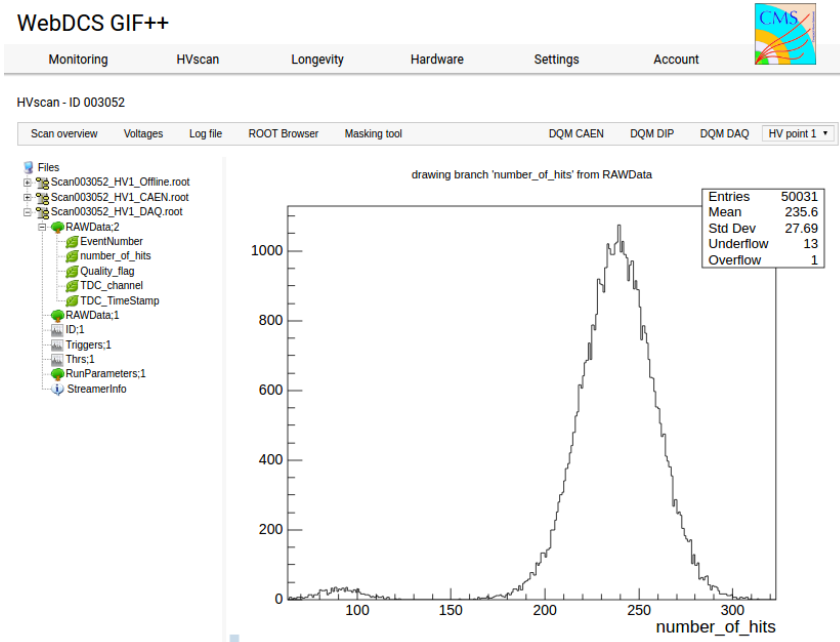


*Figure A.3: Structure of the ROOT output file generated by the DAQ. The 5 branches (EventNumber, number\_of\_hits, Quality\_flag, TDC\_channel and TDC\_TimeStamp) are visible on the left panel of the ROOT browser. On the right panel is visible the histogram corresponding to the variable nHits. In this specific example, there were approximately 50k events recorded to measure the gamma irradiation rate on the detectors. Each event is stored as a single entry in the TTree.*

#### 1037    A.4.3 Data quality flag

1038    Among the parameters that are recorded for each event, the quality flag, defined in Source Code A.5,  
 1039    is determined on the fly by checking the data recorded by every single TDC. From method `v1190a::Read()`,  
 1040    it can be understood that the content of each TDC buffer is readout one TDC at a time. Entries are  
 1041    created in the data list for the first TDC and then, when the second buffer is readout, events corre-  
 1042    sponding to entries that have already been created to store data for the previous TDC are added to  
 1043    the existing list element. On the contrary, when an event entry has not been yet created in the data  
 1044    list, a new entry is created.

```
1045
  typedef enum _QualityFlag {
    GOOD      = 1,
    CORRUPTED = 0
} QualityFlag;
```

1047    *Source Code A.5: Definition of the quality flag `enum`.*

1048    It is possible that each TDC buffer contains a different number of events. In cases where the first  
 1049    element in the buffer list is an event for corresponds to a new entry, the difference in between the  
 1050    entry from the buffer and the last entry in the data list is recorded and checked. If it is greater than 1,  
 1051    what should never be the case, the quality flag is set to CORRUPTED for this TDC and an empty entry  
 1052    is created in the place of the missing ones. Missing entries are believe to be the result of a bad hold

1053 on the TDC buffers at the moment of the readout. Indeed, the software hold is effective only on 1  
 1054 TDC at a time and no solution as been found yet to completely block the writting in the buffers when  
 1055 an IRQ is received.

1056 At the end of each BLT cycle, the ID of the last entry stored for each TDC buffer is not recorded.  
 1057 When starting the next cycle, if the first entry in the pile corresponds to an event already existing  
 1058 in the list, the readout will start from this list element and will not be able to check the difference  
 1059 in between this entry's ID and the one of the last entry that was recorded for this TDC buffer in  
 1060 the previous cycle. In the case events were missing, the flag stays at its initial value of 0, which is  
 1061 similar to CORRUPTED and it is assumed that then this TDC will not contribute to `number_of_hits`,  
 1062 `TDC_channel` or `TDC_TimeStamp`.

1063 Finally, since there will be 1 `RAWData` entry per TDC for each event (meaning `nTDCs` entries,  
 1064 referring to `DataReader` private attribute), the individual flags of each TDC will be added together.  
 1065 The final format is an integer composed `nTDCs` digits where each digit is the flag of a specific TDC.  
 1066 This is constructed using powers of 10 like follows:

```
1067 TDC 0: QFlag = 100 × _QualityFlag
1068 TDC 1: QFlag = 101 × _QualityFlag
1069 ...
1070 TDC N: QFlag = 10N × _QualityFlag
```

1071 and the final flag to be with N digits:

```
1072 QFlag = n....3210
```

1073 each digit being 1 or 0. Below is given an example with a 4 TDCs setup.

1074 If all TDCs were good : `QFlag = 1111`,

1075 but if TDC 2 was corrupted : `QFlag = 1011`.

1076 When data taking is over and the data contained in the dynamical `RAWData` structure is transferred  
 1077 to the ROOT file, all the 0s are changed into 2s by calling the method `DataReader::GetQFlag()`.  
 1078 This will help translating the flag without knowing the number of TDCs beforehand. Indeed, a flag  
 1079 111 could be due to a 3 TDC setup with 3 good individual TDC flags or to a more than 3 TDC setup  
 1080 with TDCs those ID is greater than 2 being CORRUPTED, thus giving a 0.

1081 The quality flag has been introduced quite late, in October 2017 only, to the list of GIFT++ DAQ  
 1082 parameters to be recorded into the output ROOT file. Before this addition, the missing data, corrupting  
 1083 the quality for the offline analysis, was contributing to artificially fill data with lower multiplicity.  
 1084 Looking at `TBranch number_of_hits` provides an information about the data of the full GIFT++  
 1085 setup. When a TDC is not able to transfer data for a specific event, the effect is a reduction of the  
 1086 total number of hits recorded in the full setup, this is what can be seen from Figure A.4. After offline  
 1087 reconstruction detector by detector, the effect of missing events can be seen in the artificially filled  
 1088 bin at multiplicity 0 shown in Figure A.5. Nonetheless, for data with high irradiation levels, as it is  
 1089 the case for Figure A.5a, discarding the fake multiplicity 0 data can be done easily during the offline  
 1090 analysis. At lower radiation, the missing events contribution becomes more problematic the multi-  
 1091 plicity distribution overlaps the multiplicity 0 and that in the same time the proportion of missing

1092 events decreases. Attempts to fit the distribution with a Poisson or skew distribution function were  
 1093 not conclusive.

1094

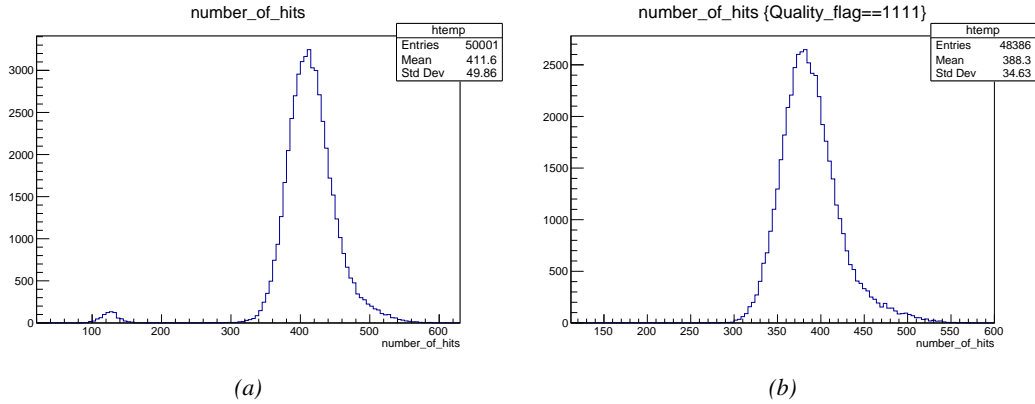


Figure A.4: The effect of the quality flag is explained by presenting the content of TBranch `number_of_hits` of a data file without `Quality_flag` in Figure A.4a and the content of the same TBranch for data corresponding to a `Quality_flag` where all TDCs were labelled as `GOOD` in Figure A.4b taken with similar conditions. It can be noted that the number of entries in Figure A.4b is slightly lower than in Figure A.4a due to the excluded events.

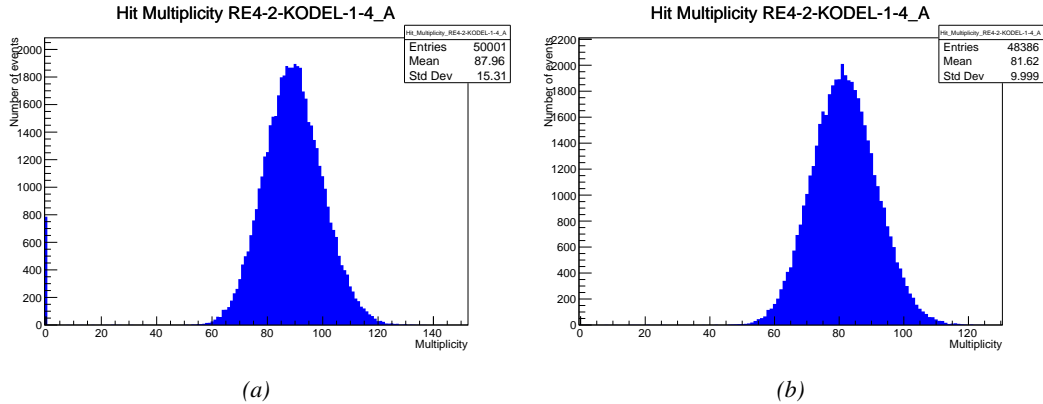


Figure A.5: Using the same data as previously showed in Figure A.4, the effect of the quality flag is explained by presenting the reconstructed hit multiplicity of a data file without `Quality_flag` in Figure A.5a and the reconstructed content of the same RPC partition for data corresponding to a `Quality_flag` where all TDCs were labelled as `GOOD` in Figure A.5b taken with similar conditions. The artificial high content of bin 0 is completely suppressed.

## 1095 A.5 Communications

1096 To ensure data readout and dialog in between the machine and the TDCs or in between the webDCS  
 1097 and the DAQ, different communication solutions were used. First of all, it is important to have a  
 1098 module to allow the communication in between the TDCs and the computer from which the DAQ

1099 operates. When this communication is effective, shifters using the webDCS to control data taking  
 1100 can thus send instructions to the DAQ.

1101

### 1102 A.5.1 V1718 USB Bridge

1103 In the previous section, the data transfer has been discussed. The importance of the `v1718` object  
 1104 (Source Code A.6), used as private member of `DataReader`, was not explicated. VME master  
 1105 modules are used for communication purposes as they host the USB port that connects the pow-  
 1106 ered crate buffer to the computer where the DAQ is installed. From the source code point of view,  
 1107 this object is used to control the communication status, by reading the returned error codes with  
 1108 `v1718::CheckStatus()`, or to check for IRQs coming from the TDCs through `v1718::CheckIRQ()`.  
 1109 Finally, to ensure that triggers are blocked at the hardware level, a NIM pulse is sent out of one of the  
 1110 5 programmable outputs (`v1718::SendBUSY()`) to the VETO of the coincidence module where the  
 1111 trigger signals originate from. As long as this signal is ON, no trigger can reach the TDCs anymore.

```
1112
1113 class v1718{
1114     private:
1115         int             Handle;
1116         Data32          Data;           // Data
1117         CVIRQLevels    Level;         // Interrupt level
1118         CVAddressModifier AM;          // Addressing Mode
1119         CVDataWidth     DataSize;       // Data Format
1120         Data32          BaseAddress;   // Base Address
1121
1122     public:
1123         v1718(IniFile *inifile);
1124         ~v1718();
1125         long            GetHandle(void) const;
1126         int             SetData(Data16 data);
1127         Data16          GetData(void);
1128         int             SetLevel(CVIRQLevels level);
1129         CVIRQLevels    GetLevel(void);
1130         int             SetAM(CVAddressModifier am);
1131         CVAddressModifier GetAM(void);
1132         int             SetDatasize(CVDataWidth datasize);
1133         CVDataWidth     GetDataSize(void);
1134         int             SetBaseAddress(Data16 baseaddress);
1135         Data16          GetBaseAddress(void);
1136         void            CheckStatus(CVErrorCodes status) const;
1137         void            CheckIRQ();
1138         void            SetPulsers();
1139         void            SendBUSY(BusyLevel level);
1140     };
1141
1142
1143
1144
1145
1146
1147
1148
1149
```

*Source Code A.6: Description of C++ object v1718.*

### 115 A.5.2 Configuration file

116 The DAQ software takes as input a configuration file written using INI standard [13]. This file is  
 117 partly filled with the information provided by the shifters when starting data acquisition using the  
 118 webDCS, as shown by Figure A.6. This information is written in section [`General`] and will later  
 119 be stored in the ROOT file that contains the DAQ data as can be seen from Figure A.3. Indeed,

1120 another `TTree` called `RunParameters` as well as the 2 histograms `ID`, containing the scan number,  
 1121 start and stop time stamps, and `Triggers`, containing the number of triggers requested by the shifter,  
 1122 are available in the data files. Moreover, `ScanID` and `HV` are then used to construct the file name  
 1123 thanks to the method `DataReader::GetFileName()`.

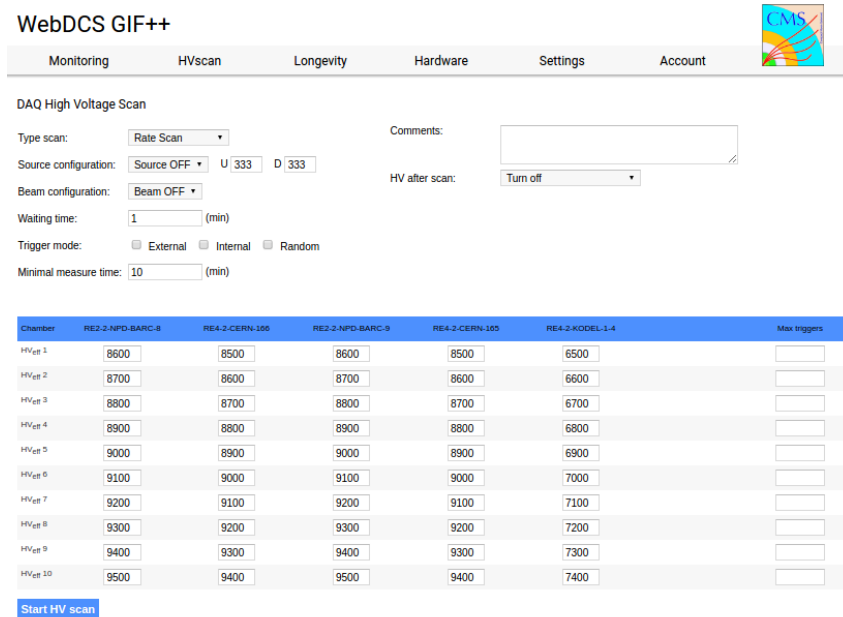


Figure A.6: WebDCS DAQ scan page. On this page, shifters need to choose the type of scan (Rate, Efficiency or Noise Reference scan), the gamma source configuration at the moment of data taking, the beam configuration, and the trigger mode. These information will be stored in the DAQ ROOT output. Are also given the minimal measurement time and waiting time after ramping up of the detectors is over before starting the data acquisition. Then, the list of HV points to scan and the number of triggers for each run of the scan are given in the table underneath.

1124 The rest of the information is written beforehand in the configuration file template, as explicated  
 1125 in Source Code A.7, and contains the hardware addresses to the different VME modules in the  
 1126 setup as well as settings for the TDCs. As the TDC settings available in the configuration file are not  
 1127 supposed to be modified, an improvement would be to remove them from the configuration file and  
 1128 to hardcode them inside of the DAQ code itself or to place them into a different INI file that would  
 1129 host only the TDC settings to lower the probability for a bad manipulation of the configuration file  
 1130 that can be modified from one of webDCS' menus.

```
1131
[General]
Tdcs=4
ScanID=$scanid
HV=$HV
RunType=$runtype
MaxTriggers=$maxtriggers
Beam=$beam
[VMEInterface]
Type=V1718
BaseAddress=0xFF0000
Name=VmeInterface
[TDC0]
Type=V1190A
BaseAddress=0x00000000
Name=Tdc0
StatusA00-15=1
StatusA16-31=1
StatusB00-15=1
StatusB16-31=1
StatusC00-15=1
StatusC16-31=1
StatusD00-15=1
StatusD16-31=1
[TDC1]
Type=V1190A
BaseAddress=0x11110000
Name=Tdc1
StatusA00-15=1
StatusA16-31=1
StatusB00-15=1
StatusB16-31=1
StatusC00-15=1
StatusC16-31=1
StatusD00-15=1
StatusD16-31=1
1132
[TDC2]
Type=V1190A
BaseAddress=0x22220000
Name=Tdc2
StatusA00-15=1
StatusA16-31=1
StatusB00-15=1
StatusB16-31=1
StatusC00-15=1
StatusC16-31=1
StatusD00-15=1
StatusD16-31=1
[TDC3]
Type=V1190A
BaseAddress=0x44440000
Name=Tdc3
StatusA00-15=1
StatusA16-31=1
StatusB00-15=1
StatusB16-31=1
StatusC00-15=1
StatusC16-31=1
StatusD00-15=1
StatusD16-31=1
[TDCSettings]
TriggerExtraSearchMargin=0
TriggerRejectMargin=0
TriggerTimeSubstraction=0b1
TdcDetectionMode=0b01
TdcResolution=0b10
TdcDeadTime=0b00
TdcHeadTrailer=0b1
TdcEventSize=0b1001
TdcTestMode=0b0
BLTMode=1
```

*Source Code A.7: INI configuration file template for 4 TDCs. In section [General], the number of TDCs is explicitated and information about the ongoing run is given. Then, there are sections for each and every VME modules. There buffer addresses are given and for the TDCs, the list of channels to enable is given. Finally, in section [TDCSettings], a part of the TDC settings are given.*

1134     In order to retrieve the information of the configuration file, the object `IniFile` has been developed  
 1135     to provide an INI parser, presented in Source Code A.8. It contains private methods returning a  
 1136     boolean to check the type of line written in the file, whether a comment, a group header or a key line  
 1137     (`IniFile::CheckIfComment()`, `IniFile::CheckIfGroup()` and `IniFile::CheckIfToken()`). The  
 1138     key may sometimes be referred to as *token* in the source code. Moreover, the private element  
 1139     `FileData` is a map of `const string` to `string` that allows to store the data contained inside the  
 1140     configuration file via the public method `IniFile::GetFileData()` following the formatting (see  
 1141     method `IniFile::Read()`):

```
1142
  1143     string group, token, value;
  // Get the field values for the 3 strings.
  // Then concatenate group and token together as a single string
  // with a dot separation.
  token = group + "." + token;
  FileData[token] = value;
```

1144     More methods have been written to translate the different keys into the right variable format  
 1145     when used by the DAQ. For example, to get a `float` value out of the configuration file data, knowing  
 1146     the group and the key needed, the method `IniFile::floatType()` can be used. It takes 3 arguments  
 1147     being the group name and key name (both `string`), and a default `float` value used as exception in  
 1148     the case the expected combination of group and key cannot be found in the configuration file. This  
 1149     default value is then used and the DAQ continues on working after sending an alert in the log file for  
 1150     further debugging.

```

1151     typedef map< const string, string > IniFileData;
1152
class IniFile{
    private:
        bool          CheckIfComment (string line);
        bool          CheckIfGroup(string line, string& group);
        bool          CheckIfToken(string line, string& key, string& value);
        string         FileName;
        IniFileData   FileData;
        int           Error;

    public:
        IniFile();
        IniFile(string filename);
        virtual      ~IniFile();

        // Basic file operations
        void          SetFileName(string filename);
        int           Read();
        int           Write();
        IniFileData   GetFileData();

        // Data readout methods
        Data32         addressType (string groupname, string keyname, Data32
→      defaultValue);
        long          intType     (string groupname, string keyname, long
→      defaultValue);
        long long    longType    (string groupname, string keyname, long long
→      defaultValue );
        string         stringType  (string groupname, string keyname, string
→      defaultValue );
        float         floatType   (string groupname, string keyname, float
→      defaultValue );

        // Error methods
        string         GetErrorMsg();
    };

```

1153       *Source Code A.8: Description of C++ object `IniFile` used as a parser for INI file format.*

### 1154     A.5.3 WebDCS/DAQ intercommunication

1155     When shifters send instructions to the DAQ via the configuration file, it is the webDCS itself that  
 1156     gives the start command to the DAQ and then the 2 softwares use inter-process communication  
 1157     through file to synchronise themselves. This communication file is represented by the variable **const**  
 1158     string \_\_runstatuspath.

1159     On one side, the webDCS sends commands or status that are readout by the DAQ:

- 1160       • INIT, status sent when launching a scan and read via function `CtrlRunStatus(...)`,
- 1161       • START, command to start data taking and read via function `CheckSTART()`,
- 1162       • STOP, command to stop data taking at the end of the scan and read via function `CheckSTOP()`,  
 1163        and
- 1164       • KILL, command to kill data taking sent by user and read via function `CheckKILL()`

1165 and on the other, the DAQ sends status that are controled by the webDCS:

- 1166     ● `DAQ_RDY`, sent with `SendDAQReady()` to signify that the DAQ is ready to receive commands  
1167       from the webDCS,
- 1168     ● `RUNNING`, sent with `SendDAQRunning()` to signify that the DAQ is taking data,
- 1169     ● `DAQ_ERR`, sent with `SendDAQError()` to signify that the DAQ didn't receive the expected com-  
1170       mand from the webDCS or that the launch command didn't have the right number of argu-  
1171       ments,
- 1172     ● `RD_ERR`, sent when the DAQ wasn't able to read the communication file, and
- 1173     ● `WR_ERR`, sent when the DAQ wasn't able to write into the communication file.

#### 1174     **A.5.4 Example of inter-process communication cycle**

1175 Under normal conditions, the webDCS and the DAQ processes exchange commands and status via  
1176 the file hosted at the address `__runstatuspath`, as explained in subsection A.5.3. An example of  
1177 cycle is given in Table A.1. In this example, the steps 3 to 5 are repeated as long as the webDCS tells  
1178 the DAQ to take data. A data taking cycle is the equivalent as what is called a *Scan* in GIFT++ jargon,  
1179 referring to a set a runs with several HV steps. Each repetition of steps 3 to 5 is then equivalent to a  
1180 single *Run*.

1181

1182 At any moment during the data taking, for any reason, the shifter can decide that the data taking  
1183 needs to be stopped before it reached the end of the scheduled cycle. Thus at any moment on the  
1184 cycle, the content of the inter-process communication file will be changed to `KILL` and the DAQ will  
1185 shut down right away. The DAQ checks for `KILL` signals every 5s after the TDCs configuration is  
1186 over. So far, the function `CheckKILL()` has been used only inside of the data taking loop of method  
1187 `DataReader::Run()` and thus, if the shifter decides to KILL the data taking during the TDC con-  
1188 figuration phase or the HV ramping in between 2 HV steps, the DAQ will not be stopped smoothly  
1189 and a *force kill* command will be sent to stop the DAQ process that is still awake on the computer.  
1190 Improvements can be brought on this part of the software to make sure that the DAQ can safely  
1191 shutdown at any moment.

1192

## 1193     **A.6 Software export**

1194 In section A.2 was discussed the fact that the DAQ as written in its last version is not a standalone  
1195 software. It is possible to make it a standalone program that could be adapted to any VME setup  
1196 using V1190A and V1718 modules by creating a GUI for the software or by printing the log mes-  
1197 sages that are normally printed in the webDCS through the log file, directly into the terminal. This  
1198 method was used by the DAQ up to version 3.0 moment where the webDCS was completed. Also, it  
1199 is possible to check branches of DAQ v2.X to have example of communication through a terminal.

1200

1201     DAQ v2.X is nonetheless limited in it's possibilities and requires a lot of offline manual interven-  
1202       tions from the users. Indeed, there is no communication of the software with the detectors' power  
1203       supply system that would allow for a user a predefine a list of voltages to operate the detectors at

step	actions of webDCS	status of DAQ	__runstatuspath
1	launch DAQ ramp voltages ramping over wait for currents stabilization	readout of IniFile configuration of TDCs	INIT
2		configuration done send DAQ ready wait for START signal	DAQ_RDY
3	waiting time over send START		START
4	wait for run to end monitor DAQ run status	data taking ongoing check for KILL signal	RUNNING
5		run over send DAQ_RDY wait for next DCS signal	DAQ_RDY
6	ramp voltages ramping over wait for currents stabilization		DAQ_RDY
3	waiting time over send START		START
4	wait for run to end monitor DAQ run status	update IniFile information data taking ongoing check for KILL signal	RUNNING
5		run over send DAQ_RDY wait for next DCS signal	DAQ_RDY
7	send command STOP	DAQ shuts down	STOP

Table A.1: Inter-process communication cycles in between the webDCS and the DAQ through file string signals.

1204 and loop over to take data without any further manual intervention. In v2.X, the data is taken for a  
1205 single detector setting and at the end of each run, the softwares asks the user if he intends on taking  
1206 more runs. If so, the software invites the user to set the operating voltages accordingly to what is  
1207 necessary and to manual update the configuration file in consequence. This working mode can be a  
1208 very first approach before an evolution and has been successfully used by colleagues from different  
1209 collaborations.

1210  
1211 For a more robust operation, it is recommended to develop a GUI or a web application to inter-  
1212 face the DAQ. Moreover, to limit the amount of manual interventions, and thus the probability to  
1213 make mistakes, it is also recommended to add an extra feature into the DAQ by installing the HV  
1214 Wrapper library provided by CAEN of which an example of use in a similar DAQ software devel-  
1215 opped by a master student of UGent, and called TinyDAQ, is provided on UGent's github. Then, this  
1216 HV Wrapper will help you communicating with and give instructions to a CAEN HV powered crate  
1217 and can be added into the DAQ at the same level where the communication with the user was made  
1218 in DAQ v2.X. In case you are using another kind of power system for your detectors, it is stringly  
1219 adviced to use HV modules or crates that can be remotely controled via a using C++ libraries.  
1220

# B

1221

1222

## Details on the offline analysis package

1223 The data collected in GIF++ thanks to the DAQ described in Appendix A is difficult to interpret by  
1224 a human user that doesn't have a clear idea of the raw data architecture of the ROOT data files. In  
1225 order to render the data human readable, a C++ offline analysis tool was designed to provide users  
1226 with detector by detector histograms that give a clear overview of the parameters monitored during  
1227 the data acquisition [14]. In this appendix, details about this software in the context of GIF++, as of  
1228 how the software was written and how it functions will be given.

### 1229 **B.1 GIF++ Offline Analysis file tree**

1230 GIF++ Offline Analysis source code is fully available on github at [https://github.com/afagot/GIF\\_OfflineAnalysis](https://github.com/afagot/GIF_OfflineAnalysis). The software requires ROOT as non-optionnal dependency  
1231 as it takes ROOT files in input and write an output ROOT file containing histograms. To compile the  
1232 GIF++ Offline Analysis project is compiled with cmake. To compile, first a build/ directory must  
1233 be created to compile from there:

```
1235 mkdir build
1236 cd build
1237 cmake ..
1238 make
1239 make install
```

1237 To clean the directory and create a new build directory, the bash script cleandir.sh can be used:

```
1238
1239 ./cleandir.sh
```

1240 The source code tree is provided below along with comments to give an overview of the files' con-  
1241 tent. The different objects created for this project (`Infrastructure`, `Trolley`, `RPC`, `Mapping`, `RPCHit`,  
1242 `RPCCluster` and `Inifile`) will be described in details in the following sections.

1243

```

GIF_OfflineAnalysis
├── bin
│   └── offlineanalysis ..... EXECUTABLE
├── build..... CMAKE COMPILATION DIRECTORY
└── ...
    ├── include..... LIST OF C++ HEADER FILES
    │   ├── Cluster.h..... DECLARATION OF OBJECT RPCCLUSTER
    │   ├── Current.h..... DECLARATION OF GETCURRENT ANALYSIS MACRO
    │   ├── GIFTrolley.h..... DECLARATION OF OBJECT TROLLEY
    │   ├── Infrastructure.h..... DECLARATION OF OBJECT INFRASTRUCTURE
    │   ├── IniFile.h..... DECLARATION OF OBJECT INI FILE FORINI PARSER
    │   ├── Mapping.h..... DECLARATION OF OBJECT MAPPING
    │   ├── MsgSvc.h..... DECLARATION OF OFFLINE LOG MESSAGES
    │   ├── OfflineAnalysis.h..... DECLARATION OF DATA ANALYSIS MACRO
    │   ├── RPCTracker.h..... DECLARATION OF OBJECT RPC
    │   ├── RPCHit.h..... DECLARATION OF OBJECT RPCHIT
    │   ├── types.h..... DEFINITION OF USEFUL VARIABLE TYPES
    │   └── utils.h..... DECLARATION OF USEFUL FUNCTIONS
    ├── obj..... BINARY FILES CREATED BY COMPILER
    └── ...
        ├── src..... LIST OF C++ SOURCE FILES
        │   ├── Cluster.cc..... DEFINITION OF OBJECT RPCCLUSTER
        │   ├── Current.cc..... DEFINITION OF GETCURRENT ANALYSIS MACRO
        │   ├── GIFTrolley.cc..... DEFINITION OF OBJECT TROLLEY
        │   ├── Infrastructure.cc..... DEFINITION OF OBJECT INFRASTRUCTURE
        │   ├── IniFile.cc..... DEFINITION OF OBJECT INI FILE FORINI PARSER
        │   ├── main.cc..... MAIN FILE
        │   ├── Mapping.cc..... DEFINITION OF OBJECT MAPPING
        │   ├── MsgSvc.cc..... DEFINITION OF OFFLINE LOG MESSAGES
        │   ├── OfflineAnalysis.cc..... DEFINITION OF DATA ANALYSIS MACRO
        │   ├── RPCTracker.cc..... DEFINITION OF OBJECT RPC
        │   ├── RPCHit.cc..... DEFINITION OF OBJECT RPCHIT
        │   └── utils.cc..... DEFINITION OF USEFUL FUNCTIONS
        ├── cleandir.sh..... BASH SCRIPT TO CLEAN BUILD DIRECTORY
        ├── CMakeLists.txt..... SET OF INSTRUCTIONS FOR CMAKE
        ├── config.h.in..... DEFINITION OF VERSION NUMBER
        └── README.md..... README FILE FOR GITHUB

```

1244

## B.2 Usage of the Offline Analysis

1245

In order to use the Offline Analysis tool, it is necessary to know the Scan number and the HV Step of the run that needs to be analysed. This information needs to be written in the following format:

1247

1248

```
Scan00XXXX_HVY
```

1249

where XXXX is the scan ID and Y is the high voltage step (in case of a high voltage scan, data will be taken for several HV steps). This format corresponds to the base name of data files in the database

1250

1251 of the GIF++ webDCS. Usually, the offline analysis tool is automatically called by the webDCS at  
 1252 the end of data taking or by a user from the webDCS panel if an update of the tool was brought.  
 1253 Nonetheless, an expert can locally launch the analysis for tests on the GIF++ computer, or a user can  
 1254 get the code on its local machine from github and download data from the webDCS for its own anal-  
 1255 ysis. To launch the code, the following command can be used from the `GIF_OfflineAnalysis` folder:

```
1256
1257 bin/offlineanalysis /path/to/Scan00XXXX_HVY
```

1258 where, `/path/to/Scan00XXXX_HVY` refers to the local data files. Then, the offline tool will by itself  
 1259 take care of finding all available ROOT data files present in the folder, as listed below:

- 1260     • `Scan00XXXX_HVY_DAQ.root` containing the TDC data as described in Appendix ?? (events, hit  
 1261         and timestamp lists), and
- 1262     • `Scan00XXXX_HVY_CAEN.root` containing the CAEN mainframe data recorded by the monitor-  
 1263         ing tool webDCS during data taking (HVs and currents of every HV channels). This file is  
 1264         created independently of the DAQ.

## 1265     **B.2.1 Output of the offline tool**

### 1266         **B.2.1.1 ROOT file**

1267 The analysis gives in output ROOT datafiles that are saved into the data folder and called using the  
 1268 naming convention `Scan00XXXX_HVY_Offline.root`. Inside those, a list of `TH1` histograms can be  
 1269 found. Its size will vary as a function of the number of detectors in the setup as each set of histograms  
 1270 is produced detector by detector. For each partition of each chamber, can be found:

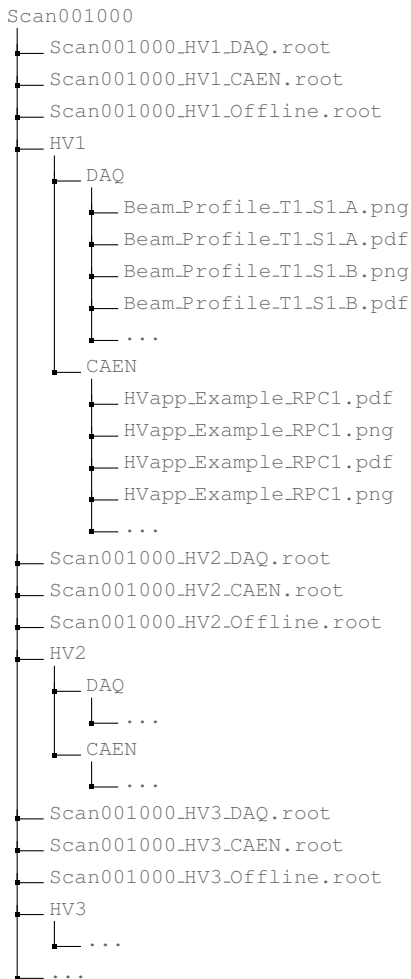
- 1271     • `Time_Profile_Tt_Sc_p` shows the time profile of all recorded events (number of events per  
 1272         time bin),
- 1273     • `Hit_Profile_Tt_Sc_p` shows the hit profile of all recorded events (number of events per chan-  
 1274         nel),
- 1275     • `Hit_Multiplicity_Tt_Sc_p` shows the hit multiplicity (number of hits per event) of all recorded  
 1276         events (number of occurrences per multiplicity bin),
- 1277     • `Strip_Mean_Noise_Tt_Sc_p` shows noise/gamma rate per unit area for each strip in a se-  
 1278         lected time range. After filters are applied on `Time_Profile_Tt_Sc_p`, the filtered version  
 1279         of `Hit_Profile_Tt_Sc_p` is normalised to the total integrated time and active detection area  
 1280         of a single channel,
- 1281     • `Strip_Activity_Tt_Sc_p` shows noise/gamma activity for each strip (normalised version of  
 1282         previous histogram - strip activity = strip rate / average partition rate),
- 1283     • `Strip_Homogeneity_Tt_Sc_p` shows the *homogeneity* of a given partition ( $\text{homogeneity} = \exp(-\text{strip rates standard deviation(strip rates in partition/average partition rate)})$ ),
- 1285     • `mask_Strip_Mean_Noise_Tt_Sc_p` shows noise/gamma rate per unit area for each masked  
 1286         strip in a selected time range. Offline, the user can control the noise/gamma rate and decide to  
 1287         mask the strips that are judged to be noisy or dead. This is done via the *Masking Tool* provided  
 1288         by the webDCS,

- 1289     ● `mask_Strip_Activity_Tt_Sc_p` shows noise/gamma activity per unit area for each masked  
1290       strip with respect to the average rate of active strips,
- 1291     ● `NoiseCSize_H_Tt_Sc_p` shows noise/gamma cluster size, a cluster being constructed out of  
1292       adjacent strips giving a signal at the *same time* (hits within a time window of 25 ns),
- 1293     ● `NoiseCMult_H_Tt_Sc_p` shows noise/gamma cluster multiplicity (number of reconstructed  
1294       clusters per event),
- 1295     ● `Chip_Mean_Noise_Tt_Sc_p` shows the same information than `Strip_Mean_Noise_Tt_Scp` us-  
1296       ing a different binning (1 chip corresponds to 8 strips),
- 1297     ● `Chip_Activity_Tt_Sc_p` shows the same information than `Strip_Activity_Tt_Scp` using  
1298       chip binning,
- 1299     ● `Chip_Homogeneity_Tt_Sc_p` shows the homogeneity of a given partition using chip binning,
- 1300     ● `Beam_Profile_Tt_Sc_p` shows the estimated beam profile when taking efficiency scan. This  
1301       is obtained by filtering `Time_Profile_Tt_Sc_p` to only consider the muon peak where the  
1302       noise/gamma background has been subtracted. The resulting hit profile corresponds to the  
1303       beam profile on the detector channels,
- 1304     ● `L0_Efficiency_Tt_Sc_p` shows the level 0 efficiency that was estimated **without** muon track-  
1305       ing,
- 1306     ● `MuonCSize_H_Tt_Sc_p` shows the level 0 muon cluster size that was estimated **without** muon  
1307       tracking, and
- 1308     ● `MuonCMult_H_Tt_Sc_p` shows the level 0 muon cluster multiplicity that was estimated **without**  
1309       muon tracking.

1310     In the histogram labels,  $t$  stands for the trolley number (1 or 3),  $c$  for the chamber slot label in  
1311       trolley  $t$  and  $p$  for the partition label (A, B, C or D depending on the chamber layout) as explained  
1312       in Chapter 5.3.

1313     In the context of GIF++, an extra script called by the webDCS is called to extract the histograms  
1314       from the ROOT files. The histograms are then stored in PNG and PDF formats into the correspond-  
1315       ing folder (a single folder per HV step, so per ROOT file). the goal is to then display the histograms  
1316       on the Data Quality Monitoring (DQM) page of the webDCS in order for the users to control the  
1317       quality of the data taking at the end of data taking. An example of histogram organisation is given  
1318       below:

1319  
1320



1321     *Here can put some screens from the webDCS to show the DQM and the plots available to users.*  
 1322

### 1323     B.2.1.2 CSV files

1324     Moreover, up to 3 CSV files can be created depending on which ones of the 3 input files were in the  
 1325     data folder:

- 1326       • Offline-Rate.csv : contains the summary of the noise/gamma hit and cluster rates for each  
 1327        chamber partitions,
- 1328       • Offline-Current.csv : contains the summary of the currents and voltages applied on each  
 1329        RPC HV channel, and
- 1330       • Offline-L0-EffCl.csv : contains the summary of the level 0 efficiency and muon cluster  
 1331        information **without** tracking.

1332     Note that these 3 CSV files are created along with their *headers* (Offline-[...]-Header.csv  
 1333     containing the names of each data columns) and are automatically merged together when the offline

1334 analysis tool is called from the webDCS, contrary to the case where the tool is runned locally from  
 1335 the terminal as the merging bash script is then not called. Thus, the resulting files, used to make  
 1336 official plots, are:

- 1337     ● Rate.csv ,
- 1338     ● Current.csv ,
- 1339     ● L0-EffCl.csv .

## 1340     **B.3 Analysis inputs and information handling**

1341 The usage of the Offline Analysis tool as well as its output have been presented in the previous sec-  
 1342 tion. It is now important to dig further and start looking at the source code and the inputs necessary  
 1343 for the tool to work. Indeed, other than the raw ROOT data files that are analysed, more information  
 1344 needs to be imported inside of the program to perform the analysis such as the description of the  
 1345 setup inside of GIF++ at the time of data taking (number of trolleys, of RPCs, dimensions of the  
 1346 detectors, etc...) or the mapping that links the TDC channels to the coresponding RPC channels in  
 1347 order to translate the TDC information into human readable data. 2 files are used to transmit all this  
 1348 information:

- 1349
- 1350     ● Dimensions.ini, that provides the necessary setup and RPC information, and
  - 1351     ● ChannelsMapping.csv, that gives the link between the TDC and RPC channels as well as the  
       *mask* for each channel (masked or not?).

### 1353     **B.3.1 Dimensions file and IniFile parser**

1354 This input file, present in every data folder, allows the analysis tool to know of the number of ac-  
 1355 tive trolleys, the number of active RPCs in those trolleys, and the details about each RPCs such as  
 1356 the number of RPC gaps, the number of pseudo-rapidity partitions (for CMS-like prototypes), the  
 1357 number of strips per partion or the dimensions. To do so, there are 3 types of groups in the INI file  
 1358 architecture. A first general group, appearing only once at the head of the document, gives informa-  
 1359 tion about the number of active trolleys as well as their IDs, as presented in Source Code B.1. For  
 1360 each active trolley, a group similar to Source Code B.2 can be found containing information about  
 1361 the number of active detectors in the trolley and their IDs. Each trolley group as a `Tt` name format,  
 1362 where `t` is the trolley ID. Finally, for each detector stored in slots of an active trolley, there is a group  
 1363 providing information about their names and dimensions, as showed in Source Code B.3. Each slot  
 1364 group as a `TtSs` name format, where `s` is the slot ID of trolley `t` where the active RPC is hosted.

1365     [General]  
 1366       nTrolleys=2  
 1367       TrolleysID=13

1367 *Source Code B.1: Example of [General] group as might be found in Dimensions.ini. In GIF++, only 2 trolleys are available to hold RPCs and place them inside of the bunker for irradiation. The IDs of the trolleys are written in a signle string as "13" and then read character by character by the program.*

```
1368 [T1]
nSlots=4
SlotsID=1234
```

Source Code B.2: Example of trolley group as might be found in `Dimensions.ini`. In this example, the file tells that there are 4 detectors placed in the holding slots of the trolley T1 and that their IDs, written as a single string variable, are 1, 2, 3 and 4.

```
1370 [T1S1]
Name=RE2-2-NPD-BARC-8
Partitions=3
Gaps=3
Gap1=BOT
Gap2=TN
Gap3=TW
AreaGap1=11694.25
AreaGap2=6432
AreaGap3=4582.82
Strips=32
ActiveArea-A=157.8
ActiveArea-B=121.69
ActiveArea-C=93.03
```

Source Code B.3: Example of slot group as might be found in `Dimensions.ini`. In this example, the file provides information about a detector named `RE2-2-NPD-BARC-8`, having 3 pseudo-rapidity readout partitions and stored in slot S1 of trolley T1. This is a CMS RE2-2 type of detector. This information will then be used for example to compute the rate per unit area calculation.

This information is readout and stored in a C++ object called `IniFile`, that parses the information in the INI input file and stores it into a local buffer for later use. This INI parser is the exact same one that was previously developed for the GIFT++ DAQ and described in Appendix A.5.2.

### B.3.2 TDC to RPC link file and Mapping

The same way the INI dimension file information is stored using `map`, the channel mapping and mask information is stored and accessed through `map`. First of all, the mapping CSV file is organised into 3 columns separated by tabulations (and not by commas, as expected for CSV files as it is easier using streams to read tab or space separated data using C++):

```
1380
1381     RPC_channel      TDC_channel      mask
```

using as formatting for each field:

```
1382
1383     TSCCC      TCCC      M
```

`TSCCC` is a 5-digit integer where `T` is the trolley ID, `s` the slot ID in which the RPC is held insite the trolley `T` and `ccc` is the RPC channel number, or `strip` number, that can take values up to 3-digits depending on the detector,

`TCCC` is a 4 digit integer where `T` is the TDC ID, `ccc` is the TDC channel number that can take values in between 0 and 127, and

1390     `M` is a 1-digit integer indicating if the channel should be considered (`M = 1`) or discarded (`M = 0`)  
 1391     during analysis.

1392     This mapping and masking information is readout and stored thanks to the object `Mapping`, pre-  
 1393     sented in Source Code B.4. Similarly to `IniFile` objects, this class has private methods. The first  
 1394     one, `Mapping::CheckIfNewLine()` is used to find the newline character '`\n`' or return character  
 1395     '`\r`' (depending on which kind of operating system interacted with the file). This is used for the  
 1396     simple reason that the masking information has been introduced only during the year 2017 but the  
 1397     channel mapping files exist since 2015 and the very beginning of data taking at GIFT++. This means  
 1398     that in the older data folders, before the upgrade, the channel mapping file only had 2 columns, the  
 1399     RPC channel and the TDC channel. For compatibility reasons, this method helps controlling the  
 1400     character following the readout of the 2 first fields of a line. In case any end of line character is  
 1401     found, no mask information is present in the file and the default `M = 1` is used. On the contrary, if  
 1402     the next character was a tabulation or a space, the mask information is present.

1403     Once the 3 fields have been readout, the second private method `Mapping::CheckIfTDCCh()` is  
 1404     used to control that the TDC channel is an existing TDC channel. Finally, the information is stored  
 1405     into 3 different maps (`Link`, `ReverseLink` and `Mask`) thanks to the public method `Mapping::Read()`.  
 1406     `Link` allows to get the RPC channel by knowing the TDC channel while `ReverseLink` does the op-  
 1407     posite by returning the TDC channel by knowing the RPC channel. Finally, `Mask` returns the mask  
 1408     associated to a given RPC channel.

```
1409
1410 typedef map<UInt, UInt> MappingData;
1411
1412 class Mapping {
1413   private:
1414     bool          CheckIfNewLine(char next);
1415     bool          CheckIfTDCCh(UInt channel);
1416     string        FileName;
1417     MappingData  Link;
1418     MappingData  ReverseLink;
1419     MappingData  Mask;
1420     int           Error;
1421
1422   public:
1423     Mapping();
1424     Mapping(string baseName);
1425     ~Mapping();
1426
1427     void SetFileName(const string filename);
1428     int  Read();
1429     UInt GetLink(UInt tdcchannel);
1430     UInt GetReverse(UInt rpcchannel);
1431     UInt GetMask(UInt rpcchannel);
1432 };
1433
```

1411 *Source Code B.4: Description of C++ object `Mapping` used as a parser for the channel mapping and mask file.*

## 1412 **B.4 Description of GIFT++ setup within the Offline Analysis tool**

1413 In the previous section, the tool input files have been discussed. The dimension file information is  
 1414 stored in a map hosted by the `IniFile` object. But this information is then used to create a series of

1415 new objects that helps defining the Gif++ infrastructure directly into the Offline Analysis. Indeed,  
 1416 from the `RPC`, to the more general `Infrastructure`, every element of the Gif++ infrastrucutre is  
 1417 recreated for each data analysis based on the information provided in input. All this information  
 1418 about the infrastructure will be used to assign each hit signal to a specific strip channel of a specific  
 1419 detector, and having a specific active area. This way, rate per unit area calculation is possible.

1420

### 1421 B.4.1 RPC objects

1422 `RPC` objects have been developped to represent physical active detectors in Gif++ at the moment  
 1423 of data taking. Thus, there are as many `RPC` objects created during the analysis than there were  
 1424 active RPCs tested during a run. Each `RPC` hosts the information present in the corresponding INI  
 1425 slot group, as shown in B.3, and organises it using a similar architecture. This can be seen from  
 1426 Source Code B.5.

1427 To make the object more compact, the lists of gap labels, of gap active areas and strip active  
 1428 areas are stored into `vector` dynamical containers. `RPC` objects are always contructed thanks to the  
 1429 dimension file information stored into the `IniFILE` and their ID, using the format `TtSs`. Using the  
 1430 `RPC` ID, the constructor calls the methods of `IniFile` to initialise the `RPC`. The other constructors  
 1431 are not used but exist in case of need. Finally, some getters have been written to access the different  
 1432 private parameters storing the detector information.

1433

```
1434 class RPC{
1435     private:
1436         string           name;          //RPC name as in webDCS database
1437         Uint             nGaps;        //Number of gaps in the RPC
1438         Uint             nPartitions; //Number of partitions in the RPC
1439         Uint             nStrips;      //Number of strips per partition
1440         vector<string> gaps;        //List of gap labels (BOT, TOP, etc...)
1441         vector<float>   gapGeo;       //List of gap active areas
1442         vector<float>   stripGeo;    //List of strip active areas
1443
1444     public:
1445         RPC();
1446         RPC(string ID, IniFile* geofile);
1447         RPC(const RPC& other);
1448         ~RPC();
1449         RPC& operator=(const RPC& other);
1450
1451         string GetName();
1452         Uint  GetNGaps();
1453         Uint  GetNPartitions();
1454         Uint  GetNStrips();
1455         string GetGap(Uint g);
1456         float GetGapGeo(Uint g);
1457         float GetStripGeo(Uint p);
1458     };

```

1435 *Source Code B.5: Description of C++ objects `RPC` that describe each active detectors used during data taking.*

### 1436 B.4.2 Trolley objects

1437 `Trolley` objects have been developped to represent physical active trolleys in Gif++ at the moment

1438 of data taking. Thus, there are as many trolley objects created during the analysis than there were  
 1439 active trolleys hosting tested RPCs during a run. Each `Trolley` hosts the information present in the  
 1440 corresponding INI trolley group, as shown in B.2, and organises it using a similar architecture. In  
 1441 addition to the information hosted in the INI file, these object have a dynamical container of `RPC`  
 1442 objects, representing the active detectors the active trolley was hosting at the time of data taking.  
 1443 This can been seen from Source Code B.6.

1444 `Trolley` objects are always contructed thanks to the dimension file information stored into the  
 1445 `IniFILE` and their ID, using the format `Tt`. Using the Trolley ID, the constructor calls the methods  
 1446 of `IniFile` to initialise the `Trolley`. Retrieving the information of the RPC IDs via `SlotsID`, a new  
 1447 `RPC` is constructed and added to the container `RPCs` for each character in the ID string. The other  
 1448 constructors are not used but exist in case of need. Finally, some getters have been written to access  
 1449 the different private parameters storing the trolley and detectors information.

1450

```
class Trolley{
    private:
        Uint      nSlots; //Number of active RPCs in the considered trolley
        string    SlotsID; //Active RPC IDs written into a string
        vector<RPC*> RPCs; //List of active RPCs

    public:
        //Constructors, destructor and operator =
        Trolley();
        Trolley(string ID, IniFile* geofile);
        Trolley(const Trolley& other);
        ~Trolley();
        Trolley& operator=(const Trolley& other);

        //Get GIFTrolley members
        Uint    GetNSlots();
        string  GetSlotsID();
        Uint    GetSlotID(Uint s);

        //Manage RPC list
        RPC*   GetRPC(Uint r);
        void   DeleteRPC(Uint r);

        //Methods to get members of RPC objects stored in RPCs
        string GetName(Uint r);
        Uint    GetNGaps(Uint r);
        Uint    GetNPartitions(Uint r);
        Uint    GetNStrips(Uint r);
        string  GetGap(Uint r, UInt g);
        float   GetGapGeo(Uint r, UInt g);
        float   GetStripGeo(Uint r, UInt p);
};
```

1452 *Source Code B.6: Description of C++ objects `Trolley` that describe each active trolley used during data  
 taking.*

### 1453 B.4.3 Infrastructure object

1454 The `Infrastructure` object has been developped to represent the GIFT++ bunker area dedicated to  
 1455 CMS RPC experiments. With this very specific object, all the information about the CMS RPC  
 1456 setup within GIFT++ at the moment of data taking is stored. It hosts the information present in the

1457 corresponding INI general group, as shown in B.1, and organises it using a similar architecture. In  
 1458 addition to the information hosted in the INI file, this object have a dynamical container of `Trolley`  
 1459 objects, representing the active tolleys in GIFT++ area. This can been seen from Source Code B.7.

1460 The `Infrastructure` object is always contructed thanks to the dimension file information stored  
 1461 into the `IniFILE`. Retrieving the information of the trolley IDs via `TrolleysID`, a new `Trolley` is  
 1462 constructed and added to the container `Trolleys` for each character in the ID string. By extension,  
 1463 it is easy to understand that the process described in Section B.4.2 for the construction of RPCs  
 1464 takes place when a trolley is constructed. The other constructors are not used but exist in case of  
 1465 need. Finally, some getters have been written to access the different private parameters storing the  
 1466 infrastructure, tolleys and detectors information.

1467

```

class Infrastructure {
private:
    Uint             nTrolleys; //Number of active Trolleys in the run
    string          TrolleysID; //Active trolley IDs written into a string
    vector<Trolley*> Trolleys; //List of active Trolleys (struct)

public:
    //Constructors and destructor
    Infrastructure();
    Infrastructure(IniFile* geofile);
    Infrastructure(const Infrastructure& other);
    ~Infrastructure();
    Infrastructure& operator=(const Infrastructure& other);

    //Get Infrastructure members
    Uint   GetNTrolleys();
    string GetTrolleysID();
    Uint   GetTrolleyID(Uint t);

    //Manage Trolleys
    Trolley* GetTrolley(Uint t);
    void    DeleteTrolley(Uint t);

    //Methods to get members of GIFTrolley objects stored in Trolleys
    Uint   GetNSlots(Uint t);
    string GetSlotsID(Uint t);
    Uint   GetSlotID(Uint t, Uint s);
    RPC*  GetRPC(Uint t, Uint r);

    //Methods to get members of RPC objects stored in RPCs
    string GetName(Uint t, Uint r);
    Uint   GetNGaps(Uint t, Uint r);
    Uint   GetNPartitions(Uint t, Uint r);
    Uint   GetNStrips(Uint t, Uint r);
    string GetGap(Uint t, Uint r, Uint g);
    float  GetGapGeo(Uint t, Uint r, Uint g);
    float  GetStripGeo(Uint t, Uint r, Uint p);
};


```

1469

*Source Code B.7: Description of C++ object `Infrastructure` that contains the full information about CMS  
 RPC experiment in GIFT++.*

## 1470 B.5 Handeling of data

1471 As discussed in Appendix A.4.2, the raw data as a `TTree` architecture where every entry is related to  
 1472 a trigger signal provided by a muon or a random pulse, whether the goal of the data taking was to  
 1473 measure the performance of the detector or the noise/gamma background respectively. Each of these  
 1474 entries, referred also as events, contain a more or less full list of hits in the TDC channels to which  
 1475 the detectors are connected. To this list of hits corresponds a list of time stamps, marking the arrival  
 1476 of the hits within the TDC channel.

1477 The infrastructure of the CMS RPC experiment within `GIF++` being defined, combining the  
 1478 information about the raw data with the information provided by both the mapping/mask file and the  
 1479 dimension file allows to build new physical objects that will help in computing efficiency or rates.

### 1480 B.5.1 RPC hits

1481 The raw data stored in the ROOT file as output of the `GIF++` DAQ, is readout by the analysis tool  
 1482 using the structure `RAWData` presented in Source Code B.9 that differs from the structure presented  
 1483 in Appendix A.4.2 as it is not meant to hold all of the data contained in the ROOT file. In this sense,  
 1484 this structure is in the case of the offline analysis tool not a dynamical object and will only be storing  
 1485 a single event contained in a single entry of the `TTree`.

```
1486
1487 class RPCHit {
1488     private:
1489         Uint Channel;      //RPC channel according to mapping (5 digits)
1490         Uint Trolley;      //0, 1 or 3 (1st digit of the RPC channel)
1491         Uint Station;      //Slot where is held the RPC in Trolley (2nd digit)
1492         Uint Strip;        //Physical RPC strip where the hit occured (last 3
1493         → digits)
1494         Uint Partition;    //Readout partition along eta segmentation
1495         float TimeStamp;   //Time stamp of the arrival in TDC
1496
1497     public:
1498         //Constructors, destructor & operator =
1499         RPCHit();
1500         RPCHit(Uint channel, float time, Infrastructure* Infra);
1501         RPCHit(const RPCHit& other);
1502         ~RPCHit();
1503         RPCHit& operator=(const RPCHit& other);
1504
1505         //Get RPCHit members
1506         Uint GetChannel();
1507         Uint GetTrolley();
1508         Uint GetStation();
1509         Uint GetStrip();
1510         Uint GetPartition();
1511         float GetTime();
1512     };
1513
1514     typedef vector<RPCHit> HitList;
1515     typedef struct GIFHitList { HitList rpc[NTROLLEYS][NSLOTS][NPARTITIONS]; } →
1516     → GIFHitList;
1517
1518     bool SortHitbyStrip(RPCHit h1, RPCHit h2);
1519     bool SortHitbyTime(RPCHit h1, RPCHit h2);
```

```

1489 struct RAWData{
1490     int iEvent;      //Event i
1491     int TDCNHits;   //Number of hits in event i
1492     int QFlag;      //Quality flag list (1 flag digit per TDC)
1493     vector<UInt> *TDCCh;    //List of channels giving hits per event
1494     vector<float> *TDCTS;    //List of the corresponding time stamps
1495 };

```

1490       *Source Code B.9: Description of C++ structure RAWData.*

1491       Each member of the structure is then linked to the corresponding branch of the ROOT data tree,  
1492       as shown in the example of Source Code B.10, and using the method `GetEntry(int i)` of the ROOT  
1493       class `TTree` will update the state of the members of `RAWData`.

```

1494 TTree* dataTree = (TTree*)dataFile.Get("RAWData");
1495 RAWData data;
1496
1497 dataTree->SetBranchAddress("EventNumber", &data.iEvent);
1498 dataTree->SetBranchAddress("number_of_hits", &data.TDCNHits);
1499 dataTree->SetBranchAddress("Quality_flag", &data.QFlag);
1500 dataTree->SetBranchAddress("TDC_channel", &data.TDCCh);
1501 dataTree->SetBranchAddress("TDC_TimeStamp", &data.TDCTS);

```

1496       *Source Code B.10: Example of link in between RAWData and TTree.*

1497       The data is then analysed entry by entry and to each element of the TDC channel list, a `RPCHit` is  
1498       constructed by linking each TDC channel to the corresponding RPC channel thanks to the `Mapping`  
1499       object. The information carried by the RPC channel format allows to easily retrieve the trolley and  
1500       slot from which the hit was recorded (see section B.3.2). Using these 2 values, the readout partition  
1501       can be found by knowing the strip channel and comparing it with the number of partitions and strips  
1502       per partition stored into the `Infrastructure` object.

1503       Thus `RPCHit` objects are then stored into 3D dynamical list called `GIFHitList` (Source Code B.9)  
1504       where the 3 dimensions refer to the 3 layers of the readout in `GIF++` : in the bunker there are *trolleys*  
1505       ( $\tau$ ) holding detectors in *slots* ( $s$ ) and each detector readout is divided into 1 or more pseudo-rapidity  
1506       *partitions* ( $p$ ). Using these 3 information allows to assign an address to each readout partition and  
1507       this address will point to a specific hit list.

1508

## 1509     **B.5.2 Clusters of hits**

1510       All the hits contained in the ROOT file have been sorted into the different hit lists through the  
1511       `GIFHitList`. At this point, it is possible to start looking for clusters. A cluster is a group of adjacent  
1512       strips getting hits within a time window of 25 ns. These strips are then assumed to be part of the same  
1513       physical avalanche signal generated by a muon passing through the chamber or by the interaction of  
1514       a gamma stopping into the electrodes of the RPCs.

1515       To keep the cluster information, `RPCCluster` objects have been defined as shown in Source  
1516       Code B.11. Using the information of each individual `RPCHit` taken out of the hit list, it stores  
1517       the cluster size (number of adjacent strips composing the cluster), the first and last hit, the center for  
1518       spatial reconstruction and finally the start and stop time stamps as well as te time spread in between

```

1519 the first and last hit.

1520
1521
1522
1523
1524
1525
1526
1527
1528
1529
1530
1531
1532
1533
1534

class RPCCluster{
    private:
        Uint ClusterSize; //Size of cluster #ID
        Uint FirstStrip; //First strip of cluster #ID
        Uint LastStrip; //Last strip of cluster #ID
        float Center; //Center of cluster #ID ((first+last)/2)
        float StartStamp; //Time stamp of the earliest hit of cluster #ID
        float StopStamp; //Time stamp of the latest hit of cluster #ID
        float TimeSpread; //Time difference between earliest and latest hits
                           //of cluster #ID
    public:
        //Constructors, destructor & operator =
        RPCCluster();
        RPCCluster(HitList List, Uint cID, Uint cSize, Uint first, Uint firstID);
        RPCCluster(const RPCCluster& other);
        ~RPCCluster();
        RPCCluster& operator=(const RPCCluster& other);

        //Get Cluster members
        Uint GetID();
        Uint GetSize();
        Uint GetFirstStrip();
        Uint GetLastStrip();
        float GetCenter();
        float GetStart();
        float GetStop();
        float GetSpread();
    };

    typedef vector<RPCCluster> ClusterList;

    //Other functions to build cluster lists out of hit lists
    void BuildClusters(HitList &cluster, ClusterList &clusterList);
    void Clusterization(HitList &hits, TH1 *hcSize, TH1 *hcMult);
}

```

1522       *Source Code B.11: Description of C++ object Cluster.*

1523       To investigate the hit list of a given detector partition, the function `Clusterization()` defined  
 1524       in `include/Cluster.h` needs the hits in the list to be time sorted. This is achieved by calling func-  
 1525       tion `sort()` of library `<algorithm>` using the comparator `SortHitbyTime(RPCHit h1, RPCHit h2)`  
 1526       defined in `include/RPCHit.h` that returns `true` if the time stamp of hit `h1` is lower than that of `h2`.  
 1527       A first isolation of strips is made only based on time information. All the hits within the 25 ns win-  
 1528       dow are taken separately from the rest. Then, this sub-list of hits is sorted this time by ascending  
 1529       strip number, using this time the comparator `SortHitbyStrip(RPCHit h1, RPCHit h2)`. Finally, the  
 1530       groups of adjacent strips are used to construct `RPCCluster` objects that are then stored in a temporary  
 1531       list of clusters that is at the end of the process used to know how many clusters were reconstructed  
 1532       and to fill their sizes into an histogram that will allows to know the mean size of muon or gamma  
 1533       clusters.

1534

## 1535 B.6 Analysis

1536 All the ingredients to analyse Gif++ data have been defined. This section will focus on the different  
 1537 part of the analysis performed on the data, from determining the type of data the tool is dealing with  
 1538 to calculating the rate in each detector or reconstructing muon or gamma clusters.

### 1539 B.6.1 Determination of the run type

1540 In Gif++, both the performance of the detectors in detecting muons in an irradiated environment and  
 1541 the gamma background can be independantly measured. These corresponds to different run types  
 1542 and thus, to different TDC settings giving different data to look at.  
 1543

1544 In the case of performance measurements, the trigger for data taking is provided by the coïncidence  
 1545 of several scintillators when muons from the beam passing through the area are detected. Data  
 1546 is collected in a 600 ns wide window around the arrival of muons in the RPCs. The expected time  
 1547 distribution of hits is shown in Figure B.1a. The muon peak is clearly visible in the center of the  
 1548 distribution and is to be extracted from the gamma background that composes the flat part of the  
 1549 distribution.

1550 On the other hand, gamma background or noise measurements are focussed on the non muon  
 1551 related physics and the trigger needs to be independant from the muons to give a good measurement  
 1552 of the gamma/noise distribution as seen by the detectors. The trigger is then provided by a pulse  
 1553 generator at a frequency of 300 Hz whose pulse is not likely to be on time with a muon. In order  
 1554 to increase the integrated time without increasing the acquisition time too much, the width of the  
 1555 acquisition windows are increased to 10  $\mu$ s. The time distribution of the hits is expected to be flat, as  
 1556 shown by Figure B.1b.

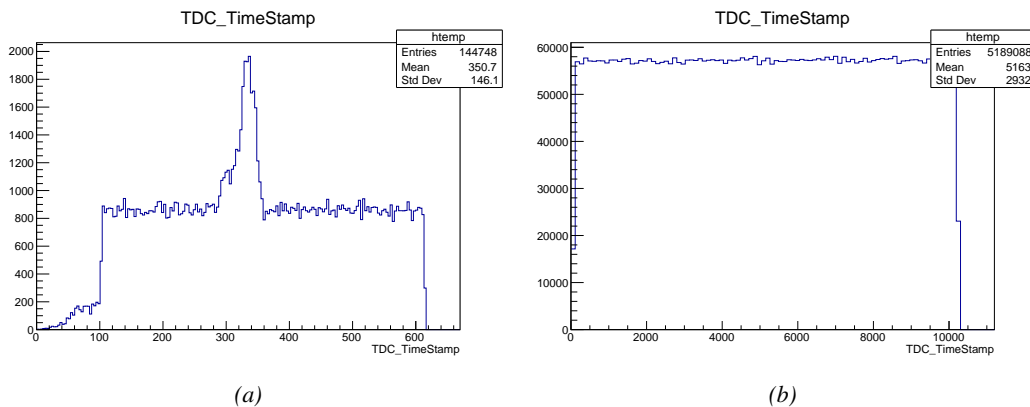


Figure B.1: Example of expected hit time distributions in the cases of efficiency (Figure B.1a) and noise/gamma rate per unit area (Figure B.1b) measurements as extracted from the raw ROOT files. The unit along the x-axis corresponds to ns. The fact that "the" muon peak is not well defined in Figure B.1a is due to the contribution of all the RPCs being tested at the same time that don't necessarily have the same signal arrival time. Each individual peak can have an offset with the ones of other detectors. The inconsistancy in the first 100 ns of both time distributions is an artefact of the TDCs and are systematically rejected during the analysis.

1557 The ROOT files include a TTree called RunParameters containing, among other things, the information  
 1558 related to the type of run. The run type can then be accessed as described by Sourcree

1559 Code B.12 and the function `IsEfficiencyRun()` is then used to determine if the run file is an efficiency run or, on the contrary, another type of run (noise or gamma measurement).

```
1561
1562     TTree* RunParameters = (TTree*)dataFile.Get("RunParameters");
1563     TString* RunType = new TString();
1564     RunParameters->SetBranchAddress("RunType", &RunType);
1565     RunParameters->GetEntry(0);
```

1563 *Source Code B.12: Access to the run type contained in `TTree* RunParameters`.*

1564 Finally, the data files will have a slightly different content whether it was collected before or after  
 1565 October 2017 and the upgrade of the DAQ software that brought a new information into the ROOT  
 1566 output. This is discussed in Appendix A.4.3 and implies that the analysis will differ a little depending  
 1567 on the data format. Indeed, as no information on the data quality is stored, in older data files, the cor-  
 1568 rections for missing events has to be done at the end of the analysis. The information about the type  
 1569 of data format is stored in the variable `bool isNewFormat` by checking the list of branches contained  
 1570 in the data tree via the methods `TTree::GetListOfBranches()` and `TCollection::Contains()`.

## 1571 B.6.2 Beam time window calculation for efficiency runs

1572 Knowing the run type is important first of all to know the width of the acquisition window to be used  
 1573 for the rate calculation and finally to be able to seek for muons. Indeed, the peak that appears in the  
 1574 time distribution for each detectors is then fitted to extract the most probable time window in which  
 1575 the tool should look for muon hits. The data outside of this time window is then used to evaluate the  
 1576 noise or gamma background the detector was subjected too during the data taking. Computing the  
 1577 position of the peak is done calling the function `SetBeamWindow()` defined in file `src/RPCHit.cc` that  
 1578 loops a first time on the data. The data is first sorted in a 3D array of 1D histograms (`GIFH1Array`, see  
 1579 `include/types.h`). Then the location of the highest bin is determined using `TH1::GetMaximumBin()`  
 1580 and is used to define a window in which a gaussian fit will be applied to compute the peak width.  
 1581 This window is a 80 ns defined by Formula B.1 around the central bin.

$$t_{center}(ns) = \text{bin} \times \text{width}_{bin}(ns) \quad (\text{B.1a})$$

$$[t_{low}; t_{high}] = [t_{center} - 40; t_{center} + 40] \quad (\text{B.1b})$$

1582 Before the fit is performed, the average number of noise/gamma hits per bin is evaluated using  
 1583 the data outside of the fit window. Excluding the first 100 ns, the average number of hits per bin  
 1584 due to the noise or gamma is defined by Formula B.2 after extracting the amount of hits in the time  
 1585 windows  $[100; t_{low}]$  and  $[t_{high}; 600]$  thanks to the method `TH1::Integral()`. This average number  
 1586 of hits is then subtracted to every bin of the 1D histogram, in order to *clean* it from the noise or  
 1587 gamma contribution as much as possible. Bins where  $\langle n_{hits} \rangle$  is greater than the actual bin content  
 1588 are set to 0.

$$\Delta t_{noise}(ns) = 600 \overbrace{-t_{high} + t_{low}}^{-80ns} - 100 = 420ns \quad (\text{B.2a})$$

$$\langle n_{hits} \rangle = \text{width}_{bin}(ns) \times \frac{\sum_{t=100}^{t_{low}} + \sum_{t=t_{high}}^{600}}{\Delta t_{noise}(ns)} \quad (\text{B.2b})$$

1589 Finally, the fit parameters are extracted and saved for each detector in 3D arrays of `float`  
 1590 (`muonPeak`, see `include/types.h`), a first one for the mean arrival time of the muons, `PeakTime`,  
 1591 and a second one for the width of the peak, `PeakWidth`. The width is defined as  $6\sigma$  of the gaussian  
 1592 fit.

### 1593 **B.6.3 Data loop and histogram filling**

1594 3D arrays of histogram are created to store the data and display it on the DQM of GIF++ webDCS  
 1595 for the use of shifters. These histograms, presented in section B.2.1.1, are filled while looping on  
 1596 the data. The data is accessed entry by entry in the ROOT `TTree` using `RAWData` and each hit in the  
 1597 hit list is assigned to a detector channel and saved in the corresponding histograms. In the first part  
 1598 of the analysis, in which the loop over the ROOT file's content is performed, the different steps are:

1599 **Checking of the data quality for files using the new format:** if the `QFlag` value for this entry  
 1600 shows that 1 TDC or more have a `CORRUPTED` flag, then this event is discarded. The loss of statistics  
 1601 is low enough to be neglected. `QFlag` is controlled using the function `IsCorruptedEvent()` defined  
 1602 in `src/utils.cc`. As explained in Appendix A.4.3, each digit of this integer represent a TDC flag  
 1603 that can be 1 or 2. Each 2 is the sign of a `CORRUPTED` state.

1604 **Assign the hits in the hit list to a RPC channel and control the channel:** a check is done on the  
 1605 RPC channel extracted thanks to the mapping via the method `Mapping::GetLink()`. If the channel is  
 1606 not initialised and is 0, or if the TDC channel was greater than 5127, the hit is discarded. This means  
 1607 there was a problem in the mapping. Often a mapping problem leads to the crash of the offline tool.

1608 **A `RPChit` object is created:** to easily get the trolley, slot and partition in which the hit has been  
 1609 assigned, this object is particularly helpful.

1610 **If this is an efficiency run, check if the hit is within the peak window or not:** if the peak is  
 1611 contained in the peak window previously defined in section B.6.2, the hit is filled into the beam hit  
 1612 profile histogram of the corresponding chamber, added into the list of muon hits and increments  
 1613 the counter of *in time* hits. The term *in time* here refers to the hits that are likely to be muons by  
 1614 arriving in the expected time window. If the hit is outside of the peak window and not within the first  
 1615 100 ns, it is filled into the noise profile histogram of the corresponding detector, added into the list  
 1616 of noise/gamma hits and increments the counter of noise/gamma hits. Otherwise the hit is discarded.

1617 **If this was any other type of run:** if the hit is not within the first 100 ns, it is filled into the  
 1618 noise profile histogram of the corresponding detector, added into the list of noise/gamma hits and  
 1619 increments the counter of noise/gamma hits. Otherwise the hit is discarded.

1620 **In any case:** the hit is filled into the time distribution and the general hit distribution histograms,  
 1621 and increments the hit multiplicity counter of the corresponding detector.

1622 **Finally, when the loop through the hit list is over:** in the case of an efficiency run, check if the  
 1623 muon hit list has been filled. If it has been filled, thus if there were any on time hits, the efficiency  
 1624 histogram is filled to 1 (efficient) otherwise it is filled to 0 (inefficient).



# C

1625

1626

## Structure of the hybrid simulation software

1627

### C.1 Introduction

1628

insert text here...

